UNIVERSITÀ DI PISA

FACOLTÀ DI INGEGNERIA

Corso di Laurea Magistrale in Ingegneria Aerospaziale

Static and Dynamic Analysis of the Aerodynamic Stability and Trajectory Simulation of a Student Sounding Rocket

Relatori

Prof. Luca D'Agostino

Ing. Christian Bach

Candidato

Lorenzo Vallini

ANNO ACCADEMICO 2013/2014

Abstract

Within the frame of the „STERN“ program by the German Space Administration (DLR), the „SMART Rockets“ project aims to develop and launch a student sounding rocket. Driven by the liquid propellant combination of ethanol and liquid oxygen (LOX), the engine produces a thrust of 500 N. During the ascent, the rocket keeps its path only through passive aerodynamic stabilization. Also during descent, when the rocket will be recovered by a two-staged parachute system, there is no possibility to actively influence the attitude or the flight path of the vehicle. Therefore the ballistic flight trajectory of the rocket has to be well known before the launch in order to fulfill the requirements set by launch site providers. These include not only the assurance of landing inside the provided area but also the margins in terms of the various types of destabilizing effects that may be present on the vehicle.

Therefore the analysis of the rocket's trajectory and evaluation of the flight stability margins are the main tasks of this thesis. After an intensive familiarization with the topic and the „SMART Rockets“ project, the aerodynamic and overall properties of the projected rocket as well as the basics of ballistic rocket flights are summarized. Various kinds of error are studied and analytically modeled in order to be able to include their presence in the following procedure for the evaluation of the rocket fight margins. The errors considered include the thrust offset, thrust misalignment, impulse and airframe errors and the presence of uncompensated wind. The analytical results are then accompanied by a full simulation with the “ASTOS” software, which is provided within the DLR STERN program. The simulation includes a parameter study regarding different wind profiles and launch conditions, and possible failure modes like thrust misalignment and parachute deployment malfunctions.

Finally the obtained results are summarized together with the most critical aspects of the projected rocket. Important conclusions for the design and future operations are concluded together with the necessary launch conditions and manufacturing precisions that allow the fulfillment of the primary requirements of the mission.

"I believe you find life such a problem because you think there are good people and bad people. You're wrong, of course."

Lord Havelock Vetinari, Patrician of Ankh-Morpork, from
the book "Guards! Guards!" of Terry Pratchett (2002).

Contents

1 Introduction

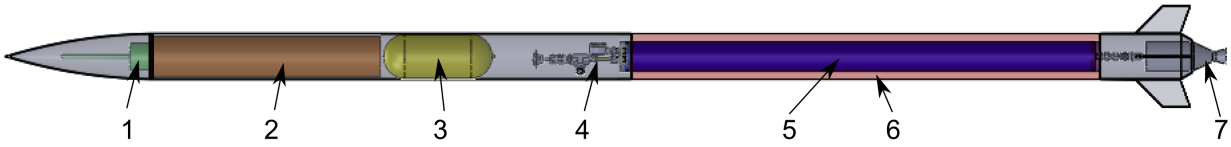

Figure 1: Current design of the SMART Rockets Project.

This thesis represents my personal contribute to the *SMART Rockets Project* (SRP) currently under development by the Technical University of Dresden (Technische Universitat Dresden, TUD). The SRP belongs to a greater initiative promoted by the German Space Administration (DLR) named *STudentische Experimental-RaketeN* (STERN) which pushes university students to design, develop and launch a sounding rocket within their academic study period. Various universities have joined the project with their own teams and relative rockets. The common choice inside the STERN project is the design of unguided models driven by solid propelled engines. The TUD group has decided on a different design strategy: the SRP rocket, or simply *SMART rocket* is going to be a liquid propelled rocket driven by a 500 N liquid oxygen-ethanol fed engine. The fig. 1 shows the actual state of the design. In the upper part of the vehicle it is shown the recovery system for the rocket safe return (2). This consists in a series of two parachutes, the drogue chute and the main chute. The first one is deployed immediately after that the vehicle has reached the culmination point while the second at an altitude of 500 m. Above the recovery system, the payload sensor and telemetry module is located within the nose cone (3). The middle portion of the body is occupied by the fuel tanks (5; 6) together with the valve system (4) and the bottle containing the driving pressurized nitrogen (4), while the engine is placed in the aft of the rocket (7). Note how the vehicle is lacking in any type of device for the active attitude control, which means that it is only passively stabilized by the presence of the fins.

Inside the SRP project my figure had a double role, on the one hand studying the aerodynamic stability of the SMART rocket with respect to (wrt) the possible disturbances it may encounter during the flight, and on the other hand analyzing the trajectory with various launch situations and both in perturbed and unperturbed conditions. The ultimate objective of these topics is the evaluation of the design and operational conditions which allow the fulfillment of the mission requirements. These can be briefly summarized as:

- the safe recovery of the rocket;
- the achievement of an altitude of at least 3 km;
- the achievement of at least sonic speed.

Between them the first is considered a primary requirements, i.e. an objective which shall be reached at all costs while the others can be seen as additional goals which do not compromise the success of the mission. The fulfillment of all the previous depends largely on the trajectory that the rocket is going to follow during its motion. The initial leaving mass, the engine thrust and the launch conditions

contribute to determine this trajectory and related altitude and velocity profiles. However this is not enough to assure the mission success. The rocket has also to be *stable* throughout the flight. But what does stable mean for a typical model rocket?

During the flight various perturbations may arise contributing in disturbing the rocket from its initial quiescent state and detaching it from the intended flight path. This perturbations can derive from inner defects of the rocket, like thrust misalignment or airframe errors, or from the external environment, like the presence of winds. When a rocket is facing such disturbances, its longitudinal axis is deflected from the original position, which corresponds to the direction of the velocity vector. The vehicle is said to be flying at an angle of attack (AoA) wrt the incoming airflow. In this situation the perturbed rocket has to be (and remain) stable otherwise the deflection of its vertical axis will continue uncontrolled resulting in a complete loss of the vehicle attitude. This will consequently induce an erratic motion of the vehicle itself which will eventually end up in a catastrophic crash on the ground. A rocket can be said to be stable until the center of pressure, i.e. the point in which the aerodynamic forces are applied, remains below the center of gravity. This is usually called the *static stability* criterion and it is relatively easy to be verified thanks to the work done by J. Barrowman in his "Calculating the Center of Pressure of a Rocket" [1]. Barrowman has applied the potential flow theory to the common design of model rockets, developing a fast and immediate method able to predict the position of the center of pressure from the knowledge of the geometry of the aerodynamics only. More specifically only the fins, nose and shoulders of the outer rocket shells are relevant according to Barrowman. Actually also the effects of the flow compressibility and the presence of the cylindrical body should be considered. In particular the body contribute can become quite relevant in the variation of the center of pressure, especially for very long and slender rockets such the SMART one. Anyway over the past fifty years the Barrowman method has been actually the only way to evaluate the stability margin of a rocket, i.e. how much stable a rocket is, and it is proved to work quite well.

Although thanks to Barrowman the aerodynamic stability can be deemed close at least from the static point of view, little information is known about the details of the process by which a stable rocket restores itself to the intended flight path once disturbed. In other words the dynamics of the aerodynamic stability has remained virtually ignored. G. K. Mandell in his "Topics in advance model rocketry" [2] has provided the main tools required to study the time evolution of the angle of attack of the vehicle for a given perturbation. Although Mandell did not correlate these perturbations with true physical errors that a rocket may present, with his work the problem of defining the dynamic behavior of the vehicle attitude would seem to be over. Unfortunately the Mandell approach although valid in general, has resulted to be inconsistent in those particular parts of the flight characterized by low vehicle velocities. These are nevertheless the moments of main interest for the stability of the rocket since as it will be shown later, its capacity to oppose the further increase of the angle of attack is directly proportional to its speed. Moreover the provider of the launch site always requires the detailed analysis of the flight margins throughout the trajectory, with particular attention to the launch phase. Since the latter is typically characterized by low velocity values, the approach described by Mandell can not in general be applied.

Therefore the first step has been to develop an alternative method enabling to assess the time varying profile of the rocket AoA even at low velocities. With such a method it has been possible to evaluate the residual stability of the rocket when it faces a disturbance at any moment of its trajectory. Before that however it has been necessary to model analytically the various types of perturbations that may affect a common model rocket during its atmospheric flight. Although this modeling is based on the previous work by Mandell, several differences can be found between the two approaches, in particular as much regards the wind effects and the presence of airframe errors. The flight margins for each of

the considered disturbance have been calculated for the actual design of the SMART rocket. Since the latter has proven to be poorly effective against the deflection caused by the possible imperfections in the manufacturing and mounting of the engine, the search for a new rocket design has started. This design should have been provided with improved aerodynamics able to increase the margin in terms of thrust misalignments and engine offsets without lowering that of the other types of disturbance.

Hence an iterative procedure based on the parametric modeling of the various quantities of interest for the aerodynamic stability of the rocket has been developed. More specifically these quantities have been defined as a function of the fin's dimensions, which have been varied in order to analyze how a rocket with different fins would have responded to the same thrust error. It results that a design with slightly bigger fins would be able to notably rise the previous critical flight margin. However the aerodynamic stability alone is not enough to ensure that the mission requirements are going to be fulfilled. The trajectory in fact depends not only on how little the rocket is deflected or how fast it restores itself. The weight of the rocket, the thrust produced by the engine, the launch angles, these and others are all quantities of fundamental importance in determining the flight path followed by an atmospheric vehicle. Therefore the trajectory of the SMART rocket has been studied in a lot of different flight conditions. Vertical and non vertical launches, ballistic motion due to possible parachute malfunctions and presence of perturbations have been all considered. Since little analytical solutions are available to the previous problem and only for a very limited number of cases, the atmospheric motion has been mainly studied by numerical analysis by means of dedicated software. These are the *Aero- Space Trajectory Optimization Software* (ASTOS), which is provided by the European Space Research and Technology Center (ESA/ESTEC) within the STERN project, the *Openrocket* and the *Rocksim* program, which are known among model racketeers and are available online [3, 4]. The use of analytical solutions to compare the numerical results has been made whenever possible. The new SMART design with the improved aerodynamics has been also verified against the original one with and without the presence of disturbances.

The objectives of this work are the evaluation of the obtained results with conclusions on the final design and future operation of the SMART rocket. These results should be attained both analytically and numerically by means of the available software. The allowable margins in terms of the modeled perturbations have to be provided together with the suitable launch conditions able to ensure the achievements of the previous requirements. In particular the most critical aspects of the model have to be highlighted together with the related solutions. More generally this work has to develop and document relatively easy, yet reasonably accurate methods for the calculation of the fundamental aerodynamic properties of model rockets. The dynamics governing the flight stability of the vehicle and that related to the trajectory have to be detailed in order to put the basis for a following deeper study of the SMART rocket. Strong emphasis should be placed on the intrinsic correlations between the two aspects so that the impact on the overall mission of any future design decision that may have to be taken with regard to an eventual issue can be immediately assessed.

This thesis deals first with the analysis of the aerodynamic stability and later with the study of the rocket trajectory. Since the two topics are far from being independent from each other, the various chapters should be always read "together", as a whole rather than single individual parts. For the same reason sometimes cross-references to subsequently parts of the text can be found. In this case no surprise if the argument referred is not immediately evident, it will be once continued the reading.

The second chapter of this paper summarizes the starting point from which it has been begun attacking the problem. It starts with a brief description of the equations of the rocket's motion together with the detailed presentation of the current design of the SMART rocket. A short mention to the previously

cited books is also made because of their importance in the rest of the analysis. The third chapter deals with the modeling of the various perturbations while the fourth applies the previously to the current design of the SMART rocket in order to evaluate the related flight margins. The improved method to keep into account for the low-speed's portions of the flight is also developed and verified here. The next chapter describes the iterative procedure adopted to design the new aerodynamics of the rocket. This is presented here together with the resultant flight margins. The last section collects the results obtained from both the simulations and analytical solutions as much regards the trajectory of the rocket. First the ideally unperturbed trajectories are considered both for vertical and non-vertical launches, then the presence of perturbations is kept into account. Therefore the conclusions of all the work are exposed, immediately followed by the bibliography. All the documents and sources used throughout the paper have been indicated case-by-case and reported here. In the very end the appendixes can be found. These contain the equations and numerical data that have been omitted in the dedicated section for practical reasons.

It is anticipated that although this paper is focusing on the SMART rocket, most of the analytical methods developed for the analysis of the aerodynamic stability and the equations related to the vertical flight analysis complete of the controlled descent part are of general use and can be applied to any model rocket.

2 Basics of Model Rocket Flight

In the first section of this chapter the general equations regarding the motion of a rocket during its atmospheric flight are presented together with the current design of the SMART rocket and its related characteristics. In particular the geometries of the various aerodynamic parts composing the outer shell of the vehicle are described with the help of detailed draws. Then in the second section the drag force developing on common model rockets is analyzed in each of its different components. At the end of this section an analytical method able to predict the drag coefficient as a function of relevant parameters is presented. The last part of this chapter deals with the topic of the aerodynamic stability of passively stabilized vehicles from both the static and dynamic point of view. A short mention to the case of rolling rockets is presented too. The very end of the chapter faces up with the problem of the variation in the position of the center of pressure as the rocket flies at a non-zero angle of attack.

2.1 Problem Statement

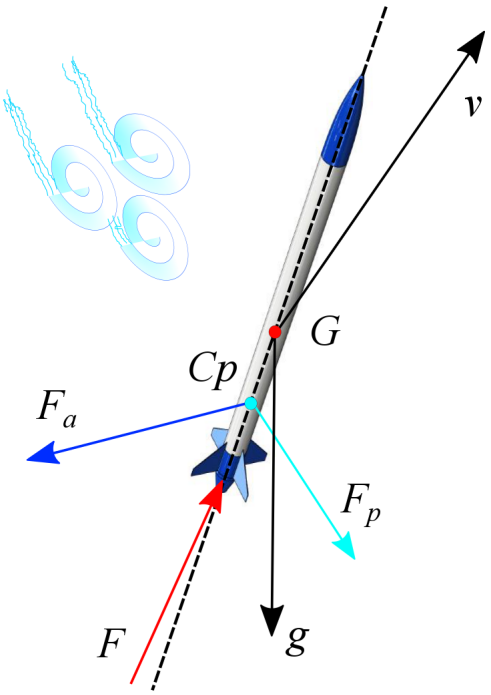

Figure 2: Sketch of the SMART rocket during the atmospheric flight.

The figure above represents the current design of the SMART rocket under the effect of the various forces faced during the flight. To fully describe the motion of the vehicle both the rigid-body and center of mass dynamics has to be known. In general however the equations governing the rotational behavior of the rocket cannot be separated from those describing its motion as a simple mass point. They are intrinsically correlated because of the presence of coupling terms that affect both types of

dynamics. For example the rotational state of the vehicle vertical axis directly affects the thrust vector and the related acceleration imparted to the vehicle center of mass. On the other side the aerodynamic forces are generally applied in a point different from the center of mass and so they generate a moment affecting the rocket rigid-body rotation. If it could be possible to eliminate these coupling terms, the rigid-body dynamics of the rocket could be studied independently from its trajectory and vice versa. As it will be subsequently shown, this separation is possible under certain circumstances that make one problem only slight dependent from the other, which is to say that the two dynamics are *weakly coupled* together. Fortunately if the rocket has been well-designed this assumption is not far from the true. The equations governing the motion of the rocket's center of mass, or center of gravity (CG), can be defined in vector form wrt an inertial reference system according to:

$$m\overrightarrow{a} = \overrightarrow{F} + m\overrightarrow{g} + \overrightarrow{F_a} + \overrightarrow{F_p} \tag{1}$$

where $\overrightarrow{F}$, $\overrightarrow{F_a}$ and $\overrightarrow{F_p}$ are respectively the thrust vector, the aerodynamic force vector and the generic perturbing force vector.

The general three-dimensional angular motion of a rigid body in response to general applied moments can be studied by means of the Euler's dynamical equations. These are easily expressed when referring the rotations of a body principal-axis reference system, whose origin lies in the body CG wrt an inertial reference frame. Assuming the$\{x_b y_b z_b\}$-body axis shown in fig. 3 and considering the radial symmetry typical of most model rockets, they can be written in the following simplified form:

$$\begin{aligned} M_x &= I_R \frac{d\Omega_x}{dt} \\ M_y &= I_L \frac{d\Omega_y}{dt} - (I_L - I_R)\,\Omega_x \Omega_z \\ M_z &= I_L \frac{d\Omega_z}{dt} - (I_L - I_R)\,\Omega_x \Omega_y \end{aligned} \tag{2}$$

where I, Ω and M are respectively the moment of inertia (MoI), the angular velocity and the external moment either along the radial or longitudinal directions.

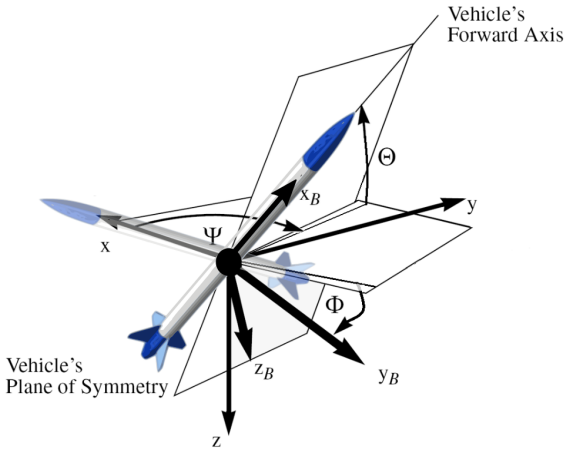

Figure 3: Definition of the body reference system.

The body rotations about the$\{x_b; y_b; z_b\}$ are commonly named as roll, pitch and yaw angle, respectively indicated as ϕ, Θ and ψ. However it is also useful to define the orientation of the body reference system relative to the velocity direction. This is typically done by means of the sideslip angle β and the angle of attack α (AoA), which are respectively the angle between the velocity vector of the vehicle relative to the fluid measured outside and inside the vehicle plane of symmetry, as shown below.

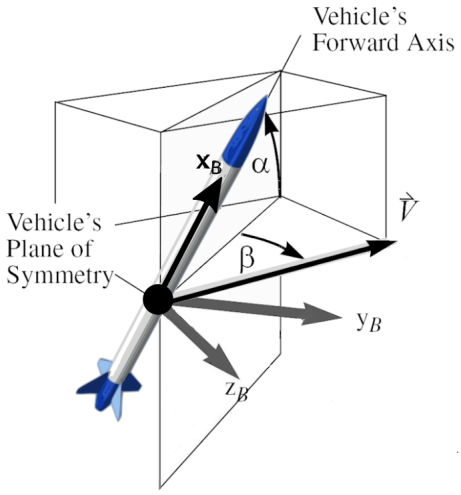

Figure 4: Definition of the angle of attack and sideslip angle.

Since the previous equations need to be applied to the specific case of the SMART rocket, the main characteristics of the current design are reported in the table below. These are the initial estimations given at the beginning of the project and should not be intended as the definitive values of the final configuration. In fact it is most likely that most of them will have to face small or large variations in order to solve the various problems that will inevitably arise during the advancement of the project.

Initial mass $[kg]$	Burnout mass $[kg]$	Total length $[m]$	Body radius $[cm]$	Burning time $[s]$	Thrust $[N]$
25	20	3	12	20	500

Table 1: Main characteristics of the current SMART rocket.

The aerodynamic effective outer shell of the rocket is divided into the nose cone, the cylindrical body, fins and a boat tail (see fig. 2). These parts will be manufactured in aramid, Glass-Reinforced Plastic (GRP) or Carbon-Fiber-Reinforced Polymer (CFRP), depending on functional and structural reason, like crash performance for the nose cone (aramid, GRP) or high specific strength for the fins and other structural parts (CFRP). The chosen shape for the nose cone is the ogival one, because it is easy to manufacture and provides low drag at the expected subsonic velocity. The preliminary geometry of the design is shown below. The dimensions are expressed in millimeters.

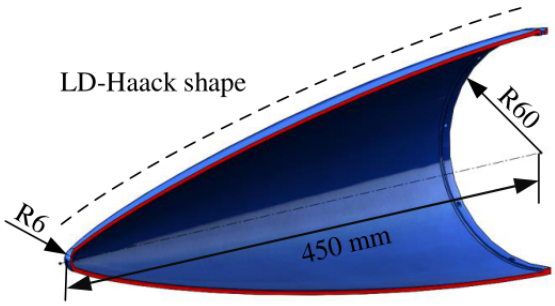

Figure 5: Nose cone preliminary design.

Common sounding rockets have 3 or 4 fins per rocket stage. The second configuration enables to use fins with a smaller exposed semi span and is a good compromise between aerodynamic and aeroelastic properties too. The selected shape is the clipped-delta fins because as it is shown in the next section it ensures the minimum induced drag. Simple flat cross sections should be preferred because of the simple manufacturing. The thickness of a fin is about 4 mm to prevent the flutter during the flight. The preliminary design of the fins is depicted in the figure below together with the related dimensions (mm).

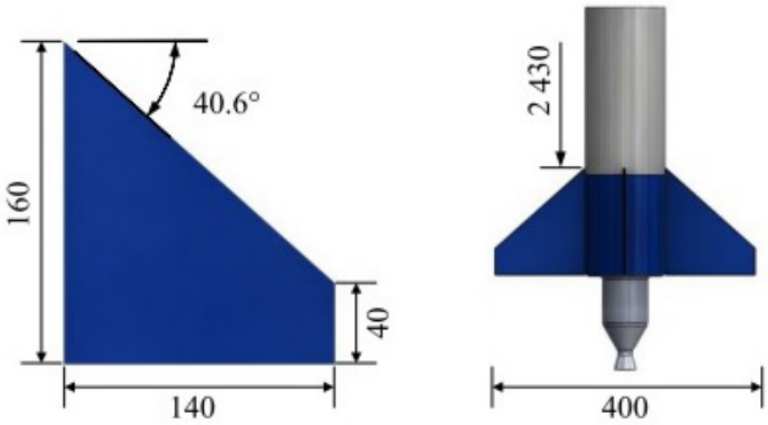

Figure 6: Fins preliminary design.

The advantages in using a boat tail was confirmed by the previous work of M. Brandt [5], but the shape suggested results incompatible with the actual size of the combustion chamber. Since the engine has to be accommodated according to fig.(7), the boat tail has been scaled to the new dimensions reported below. The design criterion adopted is detailed subsequently when dealing with the base drag.

Forward diameter $[cm]$	Aft diameter $[cm]$	Boat tail length $[cm]$	Boat tail angle $[^\circ]$
12	3.3	12	20

Table 2: Boat tail preliminary design.

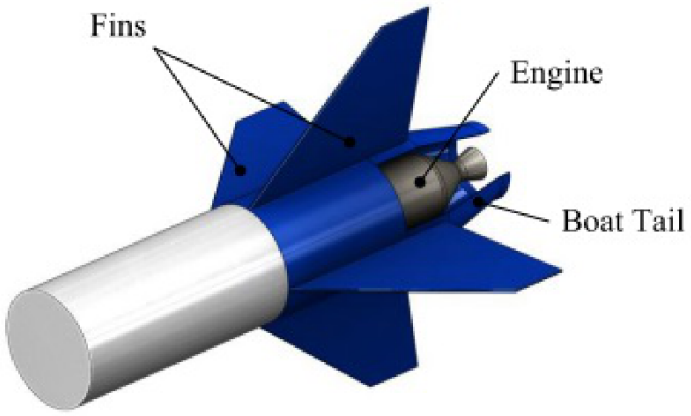

Figure 7: Aft section of the SMART rocket.

2.2 Drag Analysis

The drag is the only component of the aerodynamic force vector present in eq. 1 if the rocket is flying at zero AoA and it is a direct consequence of the relative motion of the vehicle inside the atmosphere. It is fundamental in the analysis of the vehicle performance in terms of maximum altitude and velocity and it is usually divided into viscous drag and pressure drag.

The viscous, or frictional drag derives from the flow viscosity inside the boundary layer developed as the air flows around the vehicle. The pressure drag comes from the projection along the velocity direction of the outer air pressure and can be further divided into forebody drag, base drag and parasitic drag. The latter is due to the presence of protrusions such as launch lugs and non-streamlined fins. Additional source of drag includes the induced drag generated when flying at an angle of attack and the interference drag. This is the due to the disturbances produced in the flow around the body by the presence of the fins and vice versa. The various drag components previously cited are all depicted in fig. 8. In the following they are first detailed and then an analytical method for the prediction of the overall drag coefficient is presented at the end of this section.

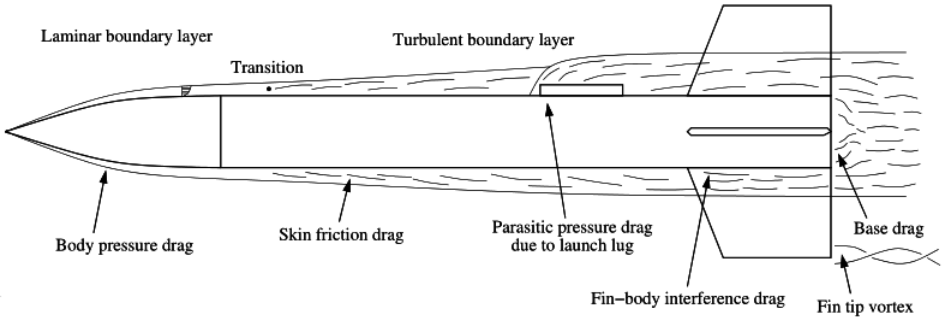

Figure 8: Drag components on a model rocket.

Viscous Drag. This is one of the most relevant component of drag in a common model rocket. It is caused by the viscous effects of the airflow moving around the vehicle. According to the boundary layer theory these effects are confined inside a thin flow region in contact with the outer surface of the body. The thickness of this region depends on the flow fashion and it also determines the severity of the resultant friction. The two possible types of boundary layers are the laminar and the turbulent one, depending on the local value of the Reynolds number $Re_y = \frac{vL}{\nu}$. At low speeds the flow is typically laminar while it turns turbulent as the Reynolds number increases beyond a critical value. The first is characterized by typical low viscous drag wrt the second because of the more ordinate pattern of the flow velocity field. The drag coefficients $C_D = \frac{D}{\frac{1}{2}\rho v^2 A_{ref}}$ for the respectively laminar and turbulent case over a flat plate wet on both sides are given by the expressions below [2]. The assumed reference area corresponds to the body cross sectional area.

$$C_{D-lam} = \frac{1.328}{\sqrt{Re_y}} \tag{3}$$

$$C_{D-turb} = \frac{0.074}{Re_y^{\frac{1}{5}}} \tag{4}$$

The second expression assumes a fully-turbulent boundary layer throughout the whole length of the plate. However since the transition from laminar to turbulent is not immediate, the previous assumption would result in a considerable overestimation of the viscous drag. The range of Reynolds numbers in which transition usually shows up is typically between $3 \cdot 10^5$ and $3 \cdot 10^6$ for a flat plate. Common model rockets fly just inside the previous so that it will be more likely that the flow along the rocket body will be partly turbulent and partly laminar.

The drag coefficient is then evaluated by defining a fictitious coordinate $\tilde{x}_{cr}$ measured on the external surface against which the boundary layer is considered fully laminar or fully turbulent respectively before or after $\tilde{x}_{cr}$. This coordinate depends on the critical Reynolds number at which the transition is assumed to occur impulsively. For a typical model rocket $Re_{y-cr} = 5 \cdot 10^5$ [2]. The drag coefficient therefore becomes:

$$C_D = \frac{0.074}{Re_y^{\frac{1}{5}}} - \frac{B}{Re_y} \tag{5}$$

where $B = 1700$ for the assumed Re_{y-cr}.

Pressure Drag. As the rocket is flying through the atmosphere the air particles are moved apart by its passage and can return to their original position only after that the vehicle has passed by. From the point of view of the rocket the airstream is flowing along the external surface in either a laminar or turbulent boundary layer fashion, depending on the Reynolds number. If the flow finds an obstacle along its path, it may not be able to reattach to the vehicle surface after that the obstacle has been overtaken. A vortex is then formed which leads to a local flow accumulation that on the other hand increases rapidly the thickness of the boundary layer. The latter becomes in fact so thick that it cannot be anymore considered as a true boundary layer. It is said that the flow has separated from the surface. Beyond the separation point the resultant vortexes produce a relatively low-pressure area that tends to retard the motion of the rocket. Therefore it is simply necessary to avoid the separation of the boundary layer in order to limit the pressure drag. Although this is perfectly possible for the forebody drag, it may be not so easy for the base and parasitic drag. The forebody drag is in fact given by the eventual separation on the nose cone and fins of the vehicle. In this respect the nose cone should have a smooth transition into the body tube and both the leading and trailing edge of the fins should be streamlined according to fig. 10. It will shortly shown that the lateral fin edge has little role in generating pressure drag but it is substantial when dealing with the drag developed at a non-zero AoA. On the other side the base and parasitic drag are hardly reduced because they depend respectively on the presence of a truncated aft section and launch lug. According to the STERN handbook [6], the rocket is going to be probably launched from the Esrange Space Center, which is located in northern Sweden above the Arctic Circle. It has been choice since many other sounding rockets promoted by Moraba have been already launched there. The Esrange requires the presence of launch lugs as interfaces with the rails of the launcher (see fig. 9). Their presence is not to be underestimated since it can amount up to the 35% of the total drag of the model. Unfortunately only empirical data valid for the specific cases are available. A dedicated analysis for the SMART rocket should be conducted.

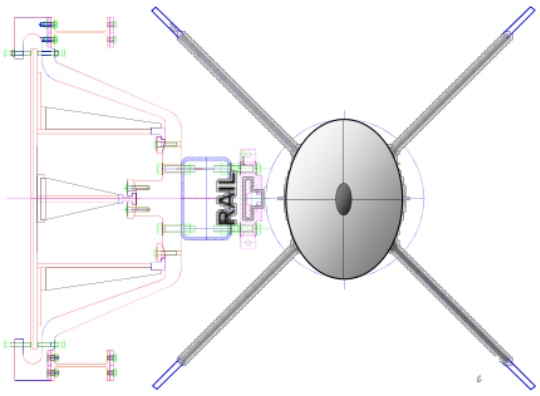

Figure 9: Esrange launch rail front view.

The base drag derives from the boundary layer separation which occurs at the rear of the rocket. As the air flows around the end of the vehicle, the blunt trailing edge prevents the boundary layer to remain

attached to the surface. Therefore it separates creating a so-called "dead air" region, where the fluid is entrapped at relatively low-velocity. From now on the next incoming air will just lap around this region without entering it. However little by little the enclosed fluid is captured and carried away by the externally flowing stream. Since no new particles are provided, this results in a pressure reduction which tends to retard the motion of the vehicle.

Actually the boundary layer acts as an insulating sheet between the outside flow and the stagnating one. Therefore increasing the thickness of the boundary layer lowers the reduction of base pressure, which on the other hand results in less base drag. An empirical formula which considers the positive effect of the boundary layer on the base drag is given below [2].

$$C_{D_{base}} = \left(\frac{D_{base}}{D_{ref}}\right)^3 \frac{0.029}{\sqrt{C_{D_{body}}}} \tag{6}$$

where $C_{D_{body}}$ is the frictional drag coefficient of the body given by either eq. 3, 4 or 5.

Actually the situation is further complicated by the flow disturbances due to the presence of the fins and by the jet exhaust gases. The latter help in supplying new particle to the dead region hence raising the pressure and lowering the base drag. Additional studies are needed to account for these effects.

Another common technique for reducing the base drag is the use of a boat tail. This allows to better direct the flow toward the dead air region. Moreover the base drag is further reduced by the pressure recovery along the boat tail and by the lowered rear surface section. Lengthening the rocket in order to provide longer boat tail reduces more the base drag but on the other side increases the overall drag because of the greater skin friction. Therefore if a given rocket design allows the use of a boat tail, the total length of the model with a boat tail should never exceed the expected original length.

Ref.[7] suggests to move forward the fins wrt the base of the rocket of one body diameter in order to reduce the interference drag. This is due to interruption of the boundary layer over the body by the presence of the fins and vice versa. By shifting the fins forward the flow is able to smooth out along the residual body aft section. Since for the SMART rocket the begin of the boat tail is supposed to coincide with the trailing edge of the fins, this results in a boat tail length of about one body diameter. Another way to reduce the interference drag is to round each body-fins intersection point by means of proper fillets. These should not be too thick in order not to increase the surface area and so the viscous drag.

Drag at a non-zero AoA. As it will shown subsequently, when a stable rocket is flying at an angle wrt the flow direction, a corrective moment will be produced in order to restore the unperturbed flight configuration. This moment is given by the force generated in the perpendicular direction wrt the body vertical axis. The presence of a non-zero AoA causes this normal force to have a component in the opposite direction wrt the velocity vector. Therefore the induced drag can be reduced by lowering the normal force generated by the rocket. However this leads to a longer restoration time of the AoA and so longer presence of the induced drag on the vehicle. Hence it is better to have a well-stable rocket able to respond quickly and strongly to any perturbation altering its attitude rather than a low-stable vehicle which will be flying at a non-zero AoA for the most of its trajectory. Moreover the aerodynamic stability is directly connected with the intensity of the corrective normal force so that by reducing it the rocket may get too close to the unstable condition for a given disturbance.

The fins are the aerodynamic component which produce typically most of the overall normal force of the vehicle. The amount of induced drag developed is directly related with the shape of the fin's

planform area. The clipped delta is the one exhibiting the best efficiency in terms of lift-to-drag ratio together with the elliptical fin. The latter however is much more complicated to be manufactured and so it has been discharged. Moreover the fins are also responsible for another contribute to the overall induced drag produced by the model. This is directly connected with the way through which a fin is producing lift. In fact as the flow faces the inclined fin, normal force is generated thanks to the pressure difference between the upper and lower side. At the same time the high pressure spills over the fin tip in an attempt to relieve the low pressure on the other side. This creates a span-wise flow over the entire fin, more noticeably near the fin tip. Because the air is also flowing backward over the fin surface, the result is the creation of a helical motion of the air known as a fin-tip vortex (see fig.(10)). Energy is required to create and maintain this vortex, and this energy loss shows up as induced drag. The smaller and weaker the tip vortex, the less the induced drag.

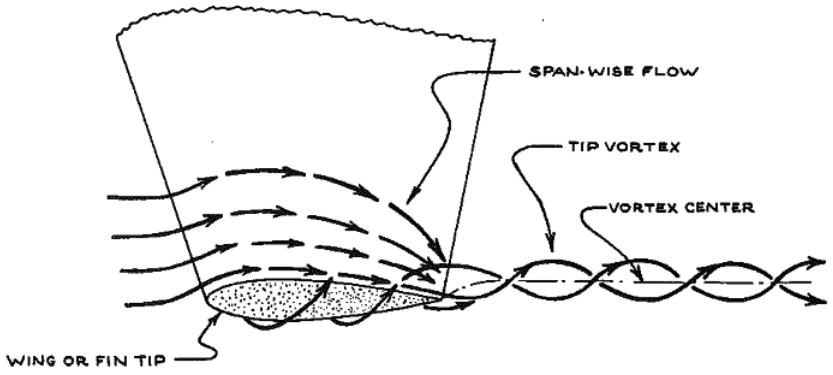

Figure 10: Tip vortex on a fin generating lift.

The generation of these trailing vortexes can be inhibit by placing an additional tip plate over the tip of the fin to keep the air from spilling over. Anyway this concept requires very careful design trade-offs so that the reduction of induced drag is greater than the additional friction drag of the plate and the interference drag at the joint of the fin tip and the tip plate. The simplest way to reduce the tip vortex and the induced drag is to shape the fin tips properly. Data coming from wind tunnel tests shows that the most effective shapes are the square and sharp lateral edge (see fig.11). The first is preferable because of the simple manufacture.

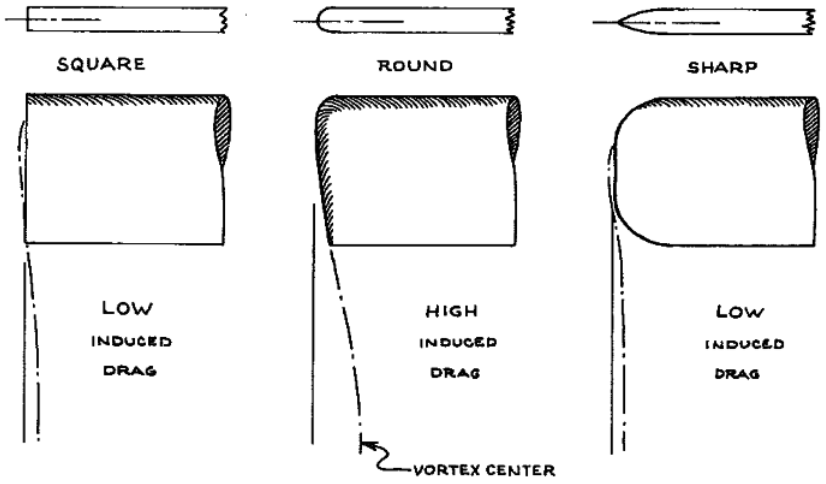

Figure 11: Induced drag on different fin's lateral edge.

The Datcom Method. The *Datcom method* (DATa COMpendium) is an analytical method derived from the United States Air Force Stability and Control Datcom able to predict the drag coefficient as a function of the Reynolds number. It has been already successfully applied by G.M. Gregorek on missiles and by W.P. Bengen on model rockets [2].

This method keeps into account for the viscous, base and interference drag but it neglects the presence of induced and parasitic drag due to lugs and other protruding elements. Therefore it can be applied only to rocket flying at zero AoA. The viscous drag is obtained from the equations developed for a plat plate in the previous section with a slight correction in order to keep into account for the 3-d effects present on a real body. These correction factors are reported below for both the rocket body and fins, which are not thin enough to be considered as flat surfaces. They have been obtained empirically from experimental results over several model rockets.

$$K_{body} = \left[1 + 60\left(\frac{D_{ref}}{L_{body}}\right)^3 + 0.0025\frac{L_{body}}{D_{ref}}\right]\frac{S_w}{A_{ref}} \tag{7}$$

$$K_{fins} = 2\left(1 + 2\frac{\hat{t}}{\hat{c}}\right) \tag{8}$$

where S_w is the wet body surface, $\hat{t}$ and $\hat{c}$ the mean thickness and mean chord of the fin respectively. According to the Datcom method the drag coefficient of a model rocket is given by:

$$C_D = C_{D_{body}}K_{body} + C_{D_{fins}}K_{fins}\frac{S_p}{A_{ref}} + C_{D_{base}} \tag{9}$$

where S_p is the total planform area of all the fins.

The interference drag is integrated inside the fin's drag through the definition of the total planform area, which correspond to the actual area of one fin plus its imaginary extension into the body tube. For most common fins, it can be simply obtained by prolonging the leading and trailing edge until they intersect the vertical body axes (see fig. 12). In other words the Datcom method models the interference drag as an extra frictional drag given by the fictitious extension of the fin's area inside the body. Clearly this is an approximation that tries to make up for the lack of information about the interference drag for common model rockets.

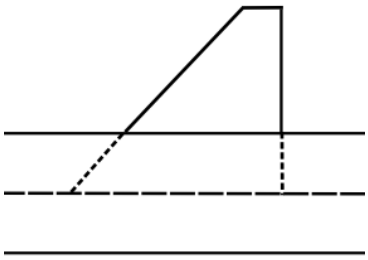

Figure 12: Definition of the total planform area of a fin.

For the clipped delta fins the total planform area is given by:

$$S_p = \frac{n}{2}\left(c_t + c_t + \frac{D_{ref}}{2}\tan\zeta\right)\left(S + \frac{D_{ref}}{2}\right)$$

where n is the number of fins and ζ the sweepback angle (40.6° from fig. 6).

Assuming a critical Reynolds number equal to $5 \cdot 10^5$, the drag coefficient given by eq. 9 has been evaluated for the original design of the SMART rocket. The boundary layer around the body is calculated from eq. 5 while that on the fins from eq. 3. This implies the assumptions of partly laminar-turbulent flow for the body tube and only laminar for the fins. The previous assumptions are confirmed by the velocity profiles obtained in section 6.2. The result is shown below for the range of Reynolds number covered by the model from the launch until the engine burnout.

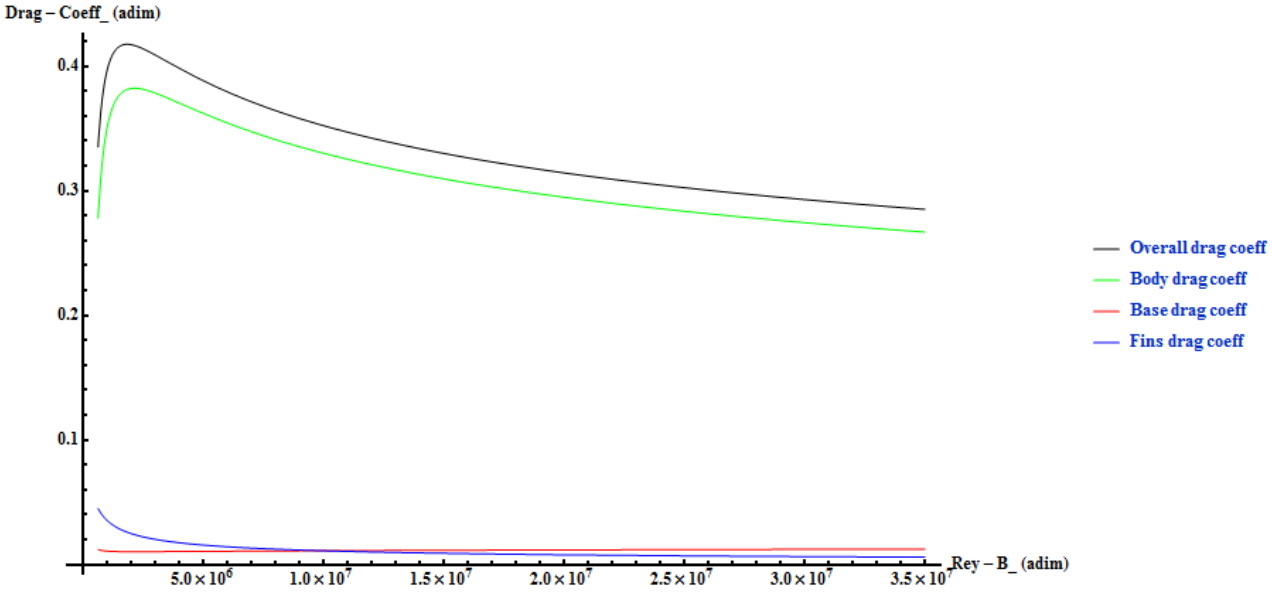

Figure 13: Drag coefficient of the SMART rocket.

From the previous figure it can be seen how the body contribute is the most relevant in determining the overall drag coefficient of the model. The fins are less important because of their small dimensions compared to the body length. Notably the base drag contribute is proportional to the fins one, even slightly greater at higher Reynolds. This is due to the reduction of boundary layer thickness at higher speeds, which reduces the shielding effect between the dead-air region at the aft section and the outer flow. The body drag coefficient exhibits a peak at the point in which the boundary layer turns from being partly laminar and turbulent into a fully-turbulent one. In fact the rocket is so long that the flow will become turbulent somewhere along the body length since the very beginning of the flight. Initially however the increase in skin friction due to the growing of this turbulent region is overcoming the reduction in both the laminar and turbulent boundary layer thickness because of the inverse dependance of C_D from eq. 5 with the Reynolds numbers. However after that the Reynolds has become greater than about $3 \cdot 10^6$, the boundary layer has turn fully-turbulent and further increase in the Reynolds results only in a decrease of the body drag coefficient.

Eq. 9 has been used to evaluate the drag acting on the rocket when flying at zero AoA, which assumes the following form:

$$D\left(Re_y\right) = \frac{1}{2}\rho v^2 A_{ref} C_d = \frac{1}{2}\rho A_{ref}\left(\frac{\nu}{L_{tot}}\right)^2 \left(Re_y^2 C_d\right) \tag{10}$$

The density and viscosity in the previous equation can be assumed equal to the mean atmospheric values in the altitude range covered by the rocket. However for common model rockets it is possible to consider the ground-level values without committing notable errors because of the relatively low apogees. For the SMART rocket case this results in a slightly drag increase of about 5% only. The previous equation can be greatly simplified by defining a suitable mean drag coefficient C_{D_0}, which

allows to consider the drag force to be only velocity dependent. This will be very useful for the analytical evaluation of the altitude and velocity performance of the rocket. The drag of the SMART rocket obtained from eq. 10 is plotted below together with the constant drag coefficient profile. The latter is obtained with a C_{D_0} equal to 0.3. This should be increased to about 0.4 to account for the presence of the launch lugs.

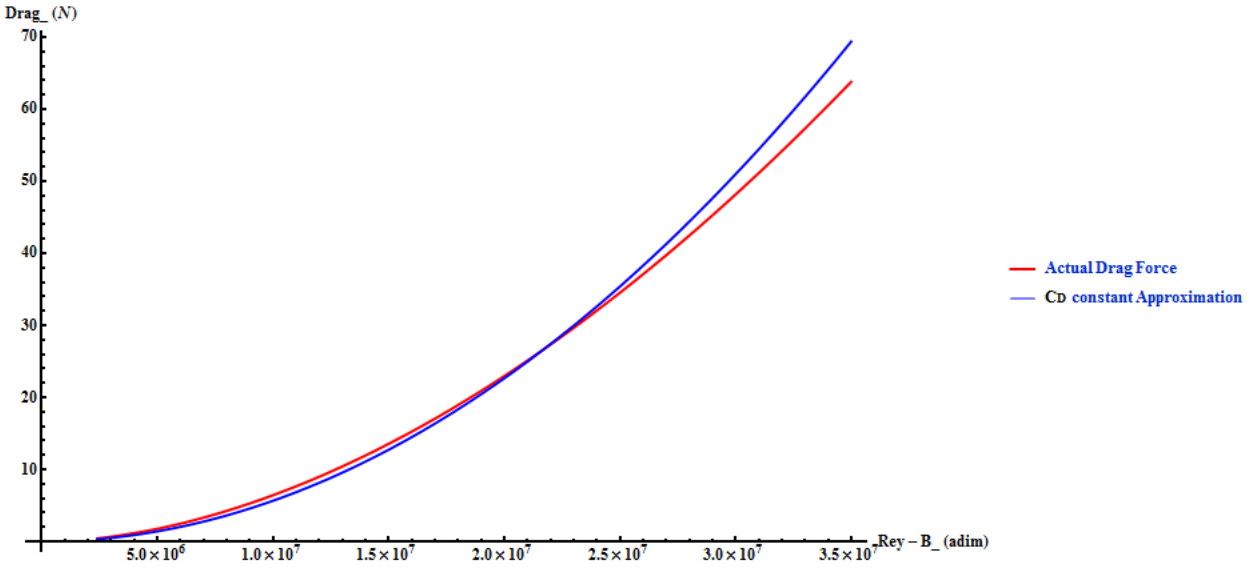

Figure 14: Drag force vs Reynolds number with constant and variable drag coefficient.

At very small Reynolds numbers the quadratic proportionality in eq. 10 keeps the drag force low, even if the frictional coefficients are very high. With increasing Re_y the drag increases correspondingly but it is still well-approximated by the curve with constant C_{D_0}.

2.3 Aerodynamic Stability

In the previous section the drag force acting on the vehicle as it flies with zero AoA has been analyzed. Unfortunately during the flight there are several disturbances of different nature that contribute to deflect the rocket vertical axis from the velocity direction. When this happens the rocket is said to be flying at an angle of attack. In this case the aerodynamic vector can not be decomposed in the drag force only. Other components will arise tending either to stabilize or destabilize even more the vehicle. Typical model rockets are only passively stabilized by means of fins which correct the angle of attack caused by any disturbances producing an opposite aerodynamic moment wrt the center of gravity of the vehicle. More properly this moment is generated by the normal force developed by the flow not only around the fins but also around any other aerodynamic surfaces of the rocket while flying at an AoA. Depending on their shapes there could also be destabilizing parts of the vehicle, i.e. parts which produce moment in the same direction of the perturbing one and so contributes even more in increasing

the AoA. The most common potentially destabilizing elements are the boat tails and forward fins wrt the vehicle center of gravity.

The effect of the various normal forces can be combined into a single one, whose magnitude is given by the sum of the separate terms and which results in moment equal to that of the separate forces. The point on which the total force acts is defined as the center of pressure (Cp) of the rocket. As can be seen from fig. 15, the moment produced attempts to correct the rocket's flight only if the Cp is located aft of the CG. If this condition holds, the rocket is said to be statically stable. A statically stable rocket always produces a corrective moment when flying at a small angle of attack. The argument for static stability above may fail in two conditions: the normal forces might cancel each other out exactly, in which case a moment would be produced but with zero total force. Second, the normal force at the Cp might be in the wrong direction yielding an non-corrective moment. However we shall see that the only component to produce a downward force is the boat tail with an intensity proportional to its length, which is usually low wrt the whole body. Therefore the total force acting on the rocket cannot be zero nor in a direction to produce an non-corrective moment when aft of the CG. The stability margin of a rocket is defined as the distance between the Cp and CG, measured in calibers, where one caliber is the maximum body diameter of the rocket. A rule of thumb among model racketeers is that the Cp should be approximately 1-2 calibers aft of the CG. However, the Cp of a rocket typically moves upwards as the angle of attack increases. As we will later verify, the effect of the Cp shift is much more felt for very slender rockets and cannot be neglected.

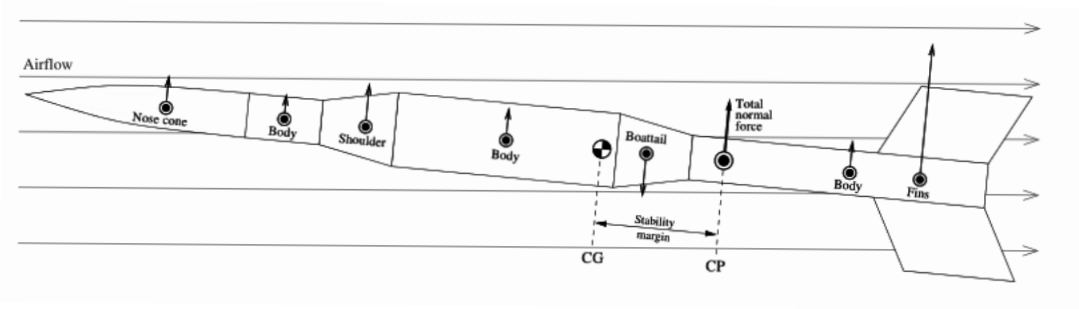

Figure 15: Normal force components.

As you can see from fig. 2 if we neglect any possible perturbation, the only forces that contribute to the angular momentum of the rocket are the aerodynamic one. In fact the weight is always applied in the center of gravity and the thrust is aligned with the vertical axis if the rocket engine is well-mounted. The aerodynamic forces are usually split into components for further examination. In order to have independent force components, it is necessary to define pairs in which each component is always perpendicular to the other. Two such pairs are the normal-axial forces and the lift-drag forces shown in fig. 16. The two pairs reduce to the drag only if the angle of attack is zero.

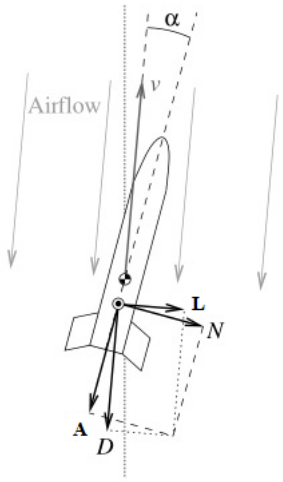

Figure 16: Perpendicular component pairs of the total aerodynamic force.

Despite static stability criteria is a simple but effective tool that tells us whenever our rocket is stable or not, it gives us any information neither about the time required to restore the AoA within a certain threshold nor about the intensity of deflection when a perturbation of given intensity is applied. That's something inherent with the *dynamical stability* of rockets, or the time evolution of the rocket attitude response when facing a perturbation. This topic has been well depicted by G. K. MANDELL and it is fully described in ref [2]. The basic idea is that if the rocket is aerodynamically well designed and the intensity of the perturbation not too high, it will rotate by small angles of attack so that it is going to be quickly restored to its previous intended flight path as the perturbation dies to zero. The *rotodynamic* response, i.e. the rigid-body dynamics of the rocket can be considered relatively fast wrt to the ballistic dynamics of the velocity vector that the averaged flight path direction is almost equal to the main intended one. Furthermore if the rocket velocity is sufficiently high, the time evolution of the dynamic stability response will be much faster than the time-change of velocity so that the two set of equations 1-2 are essentially independently from each other. As it is further shown, this assumption is inconsistent in some situations of particular interest for the design, such as at launch, and therefore the development of new approach have been necessary.

Non-Rolling Rockets In general we should refer the rotation of the body axis wrt an inertial system in order to be able to use the previous eq.s 2. However if the decoupling between the dynamics describing the CG motion and the rotodynamic problem of the rocket attitude holds, the angular momentum of the system calculated in the CG coincides with the inertial angular momentum [8]. Hence the absolute rotodynamic motion of the rocket is equal to the one which could be seen as if we were moving together with the CG, i.e. at a velocity equal to the speed of the rocket itself. In other words any reference system centered in the CG and moving together with it will always see the same angular displacement as if it was observing the body from an inertial point of view. Therefore any angular displacement of the body axis can be referred wrt the rocket velocity direction, whose

orientation requires just the knowledge of the angle of attack α and side angle β defined in fig. 4. Eq.s 2 for a non-rolling rocket ($\omega_R = 0$) can be then rewritten as:

$$M_x = I_R \frac{d^2\omega_R}{dt^2} = 0$$

$$M_y = I_L \frac{d^2\alpha}{dt^2} \tag{11}$$

$$M_z = I_L \frac{d^2\beta}{dt^2}$$

The previous set of eq.s is valid every time that the rigid-body dynamics can be considered uncoupled wrt the CG motion and vice versa. There are however situations where the previous assumption is invalid, for example when the time variation of the deflected axis of the rocket is comparable with the variations of the velocity vector. Typically this happens at launch where the low rocket speeds make the aerodynamic corrective forces small wrt the external perturbations. Therefore the maximum deflection from the original configuration and the required time required to restore it are not negligible. Despite eq.s 11 are not strictly applicable during the launch phase it will shown later that a similar approach can still be adopted in the analysis of the very initial transient response of the rocket.

Clearly in eq.s 11 there is no net distinction between the rotational response about either the y- or the z-axis because of the symmetry of the rocket and the non-rolling assumption. Hence in the following part the perturbing moments are considered to be applied along one body axis only. The angular deflection is going to be referred to simply as α. The combined response in presence of disturbances acting on several directions can be simply obtained by superpositions. Note that the terms on the left side comprise both the external perturbing and the internal restoring moments. In general a rocket subjected to an angular acceleration responds by generating two types of corrective moments, one dependent on the angular displacement, called *corrective moment*, and the other one proportional to the angular velocity, the *damping moment*. The first one is directly related to the normal force generated by the various components when flying at an AoA different from zero while the other is connected with the lateral motion of the rotating vehicle at an angular rate different from zero: this motion involves a lateral component of velocity proportional to the distance from the CG and to the rate of rotation. On the other hand this velocity induces an additional drag exerted by the flow that has to move aside as the rocket is rotating, as it is shown in fig. 17.

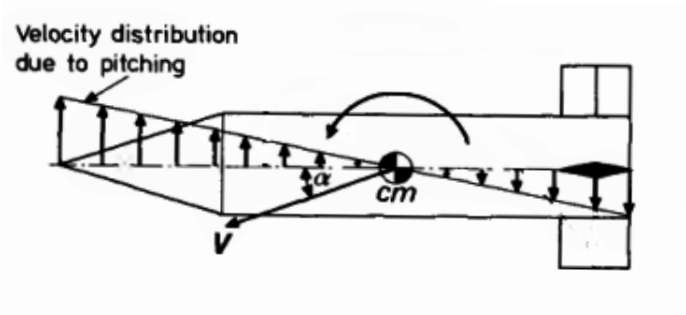

Figure 17: The lateral motion originating the damping moment.

These corrective terms can be easily modeled as soon as we remain inside the linearized theory developed by J. S. Barrowman, see [9], which predicts a linear dependance of the previous corrective and damping moment on respectively the angular displacement and velocity. This theory is based on the potential flow theory applied to rockets of common shape and it remains valid for small AoA, typically less than 0.225 rad (about 12°). Under these assumption the previous moments depend only on the geometry of the rocket's components, the velocity wrt the fluid and the angular deflection and rate of deflection accordingly to:

$$M_{corr} = \frac{1}{2}\rho A_{ref} v^2 C_{na} \left(X_{Cp} - X_G\right) \alpha \tag{12}$$

$$M_{damp-aero} = \frac{1}{2}\rho A_{ref} v \left[\Sigma C_{na_i} \left(X_{Cp} - X_G\right)^2\right] \frac{d\alpha}{dt} \tag{13}$$

where $C_{na} = \Sigma C_{na_i}$ is the sum of normal force coefficients of each component, Cp_i and Cp are respectively the center of pressure of each part and of the overall rocket.

Mandell assumed that the Cp position remains constant throughout the rotodynamic response of the rocket but this is not totally true. The Cp moves toward the CG as the rocket is flying at an AoA, hence reducing the stability margin and the value of corrective moment developed by the normal force. This happens because when flying at an AoA, the effects of body lift neglected by Barrowman are not negligible wrt the normal forces developed by the other components, even if the AoA is small. If the shift is notable, the rocket could also turn unstable during the flight even if it has sufficient stability in the original configuration. This problem is better described subsequently; for now it is sufficient to say that the Mandell approach is still valid once means to quantify this shift and the relative reduction in stability are provided. According to Barrowman, the Cp position is given by the moment average of the normal force coefficients. As its position is known the stability margin of the rocket in calibers can be calculated at once according to:

$$X_{Cp} = \frac{\Sigma C_{na_i} X_{Cpi}}{C_{na}} \tag{14}$$

$$SM = \frac{X_{Cp} - X_G}{D_{ref}} \tag{15}$$

As can you see from eq. 12 the corrective moment is sensible on whether a component is stabilizing or destabilizing the vehicle, as the C_{na} can be either positive or negative. Moreover the position of every component relative to the CG is important too, as for example a pairs of fin forward can greatly reduce or even turns the corrective moment to negative values (i.e. a destabilizing moment). Instead the damping moment is independent on the position of the component, either forward or rearward the CG, but still dependent on the sign of the normal force. These coefficients together with theCp_i can be calculated directly from the Barroman theory [9] and are only dependent on the geometry of each component. Actually an additional damping term comes courtesy of the rocket nozzle exhaust and it is referred to as *jet damping moment*. As the thrust of a rocket relies on the physical principle that the total linear momentum of the system comprising the vehicle plus the exhaust mass is conserved, the principle of conservation of angular momentum ensures the presence of the jet damping term. When the vehicle rotates in pitch or yaw during motor firing, the angular momentum imparted to the exhaust gases opposes to further deflections of the rocket. In fact as the rocket is rotating, the exhaust plume

possesses also a lateral component of velocity, i.e. an angular momentum of opposite sign to the one of the vehicle itself. Clearly this extremely useful side-effect ends as the engine reaches burnout. This damping due to the exhaust jet can be written as [2, 10]:

$$M_{damp-jet} = \dot{m} \left(L_{tot} - X_G\right)^2 \frac{d\alpha}{dt} \tag{16}$$

so that the overall momentum damping becomes:

$$M_{damp} = M_{damp-aero} + M_{damp-jet} = \left[\frac{1}{2}\rho A_{ref} v \left[\Sigma C_{na_i} \left(X_{Cp} - X_G\right)^2\right] + \dot{m} \left(L_{tot} - X_G\right)^2\right] \frac{d\alpha}{dt} \tag{17}$$

If the Barrowman theory holds, eq.s 11 can be rewritten as:

$$M_{pert-y} = I_L \frac{d^2\alpha}{dt^2} + C_2 \frac{d\alpha}{dt} + C_1 \alpha \tag{18}$$

$$M_{pert-z} = I_L \frac{d^2\beta}{dt^2} + C_2 \frac{d\beta}{dt} + C_1 \beta \tag{19}$$

where M_{pert} is the generic perturbing moment acting along the body y- or z-axis and:

$$C_1 = \frac{1}{2}\rho A_{ref} v^2 C_{na} \left(X_{Cp} - X_G\right) \tag{20}$$

$$C_2 = \frac{1}{2}\rho A_{ref} v \left[\Sigma C_{na_i} \left(X_{Cp} - X_G\right)^2\right] + \dot{m} \left(L_{tot} - X_G\right)^2 \tag{21}$$

C_1 and C_2 are referred to respectively as the corrective and damping moment coefficients and together with the longitudinal moment of inertia I_L, they are the most important dynamical parameters in the attitude control of a rocket. As you can see they are directly velocity dependent so that it is clear why faster rockets are typically more stable than slower one, especially as they leaving the launch rod, exposing themselves to wind or other kind of perturbations. These parameters can be rearranged defining the damping ratio ξ and the natural frequency ω_n as:

$$\xi = \frac{C_2}{2\sqrt{I_L C_1}} \tag{22}$$

$$\omega_n = \sqrt{\frac{C_1}{I_L}} \tag{23}$$

The meaning and importance of these two will be shortly clarified.

Previous eq.s 18-19 correspond to two uncoupled linear differential equations of the second order that could be easily solved if we consider the coefficients to be constant. Mandell has made this assumption throughout his study by stating that a properly designed rocket that clears the launch rod with sufficiently high velocity, when facing small external perturbations, it will be characterized by

enough quicker rotational response that the velocity has exhibited little or no variation at all during this transient. This assumption is typically verified during the high velocity portion of the flight but it results inconsistent at launch, except that for very-light, high specific thrust-powered rocket. This is not our case being the SMART engine a liquid propelled one with a thrust-to-weight about equal to 2. Therefore it is required a different approach to the problem that considers the variations of the rotodynamic coefficients with time.

If the speed can be considered constant, previous eq.s correspond to second order ODE with constant coefficients whose solution is only dependent on the initial conditions and on the type of perturbing term. If no disturbance is present, the response is different from zero only in the case in which at least one of the initial conditions is different from zero and it is called *free* or *homogeneous response*. In the case of a generic input different from zero, the so-called *forced response* can be built by simply combining the response to a few special types of input. Almost all of the common perturbations encountered by a rocket during its flight can be modeled as one of these special input. They are summarized below:

- impulse disturbances;
- sinusoidal disturbances;
- step disturbances.

The response of a second order system to this kind of perturbations are shown below. Note that only the response for the particular case of underdamped system, i.e. damping ratio $\xi < 1$ are reported. This is the only case of practical interest when speaking about passively stabilized rockets because higher value of damping means slower restoring time hence rockets flying for a large amount of time at an AoA different from zero.

Homogeneous:	$A \exp\left(-\xi\omega_n t\right) \sin\left[t\omega_n\sqrt{1-\xi^2}+\varphi\right]$	where A , φ from α_0, $\left(\frac{d\alpha}{dt}\right)_0$
Step:	$\frac{M_{step}}{C_1}\left(1-\frac{\exp(-\xi\omega_n t)}{\sqrt{1-\xi^2}}\sin\left[t\omega_n\sqrt{1-\xi^2}+\arctan\left(\frac{\sqrt{1-\xi^2}}{\xi}\right)\right]\right)$	where M_{step} step intensity
Impulse:	$\frac{H}{I_L\omega_n\sqrt{1-\xi^2}}\exp\left(-\xi\omega_n t\right)\sin\left[t\omega_n\sqrt{1-\xi^2}\right]$	where H impulse intensity
Sinusoidal:	$\frac{A_f}{\sqrt{\left(I_l\omega_f^2-C_1\right)^2+C_2^2\omega_f^2}}\sin\left[t\omega_f+\arctan\left(\frac{C_2\omega_f}{I_l\omega_f^2-C_1}\right)\right]$	where $A_f \sin\left(t\omega_f\right)$ sinusoidal input

Table 3: Standard responses of a second order system.

The rotodynamic response of the rocket depends on all the dynamical coefficients C_1, C_2, I_L, ξ and ω_n and on the type of input perturbation. Generally high values of longitudinal moment of inertia are beneficial because they reduce the first peak of the amplitude answer in case of an impulse disturbance, but too much high values can lead to models with excessively low damping and natural frequency. The first is very dangerous because if the system is subjected to sinusoidal input whose frequency is close

to the natural one of the system, the resonant response can be too much severe and the oscillations would turn out catastrophic. The reduction in natural frequency makes the system oscillation slower which implies longer time flying at an angle of attack and sensible alteration of the intended flight path. Increasing both the damping and corrective moment coefficients is beneficial from the point of view of the rotodynamics response of the rocket but it can lead to too much weight and excessive drag due to excessive fin's area. The most valuable parameters we can consider during the design are the damping ratio, the stability margin, which is directly related to C_1, and the natural frequency. The first two don't vary with the velocity while the natural frequency follows a linear variation. Mandell suggested some range within these parameters should remain to obtain a good general response without quantifying the intensity of perturbations the rocket is able to sustain for a given choice. As you can understand the design of a rocket's aerodynamics is basically a trade-off between several solutions depending on the perturbations the rocket is going to face and it is only up to the designer to choose the configuration that most suits his needs. After that the possible perturbation's shapes are defined, analytical method for the rotodynamic response of the rocket can be provided.

Rolling Rockets Rolling rockets are a particular case of common rockets and must be considered with caution. Previous assumption of small angular displacement and rate of displacement is invalid now because the roll velocity is typically very high in order to achieve a high angular momentum of the whole system which is therefore less sensitive to external perturbations. This seems to be a good reason to put all the rockets into a rolling condition, but the problem is that rolling motion is actually detrimental for the overall stability. Rolling rocket perturbed in pitch alone will face oscillations in yaw too, which result in greater time flying at an AoA and greater drag. This happens because the previous set of eq.s 2 is said to be coupled in case of a rolling rate and they cannot be solved independently. Moreover a rolling motion actually decrease the damping ratio of the system, getting its response closer to resonance when an external disturbance acts on frequencies close to the rolling natural one.

So why the rocket should rolling?

In the past it has been known that inducing a rapid enough roll rate on models which are only marginal or even slightly unstable could make them flight straight and true as if they were fully-stable designed. This is because the time growth of a perturbation in a rolling rocket is much slower than if the vehicle would not roll at all. The rate of growth is inversely proportional to the radial moment of inertia and roll rate of the vehicle so that it is clear why when a flying model is designed to roll, it is usually doing it at a very high rate. Moreover projectiles and artillery bullets, which are typically squat and short (hence with a high radial MoI), are usually flying in rolling condition: if they were flying as a common rocket does, the intrinsic negative stability margin would send them anywhere else but the target. Moreover if a non-rolling rocket can be subjected to any different kind of perturbations, a rolling body receives usually only sinusoidal inputs at a rate equal to the roll rate. This is good because sinusoidal disturbances reduce the dispersion of the flight trajectory. The flying path will be an oscillating one around the intended trajectory so that the precision of the launch, or shoot, is greatly enhanced. If we now add the greater angular momentum effect that increase the angular inertia, it is now clear why sometimes rolling rockets have been called "rolling stabilized". More information about rolling rocket and their response to any external input can be found in [2].

For us, it is sufficient to understand that if the rocket has been properly designed from the aerodynamic stability point of view since the beginning, hence with a good stability margin and dynamic response, inducing a rolling motion can only make things worse. Moreover the rolling motion is negative from the trajectory point of view too because the roll induces an additional circumferential velocity in the

flow around the body. This component thickens the boundary layer and creates an additional drag term which acts throughout the flight. Anyway we are not free to get rid of the rolling problem because there are some kind of perturbations that can produce an unwanted rolling motion during the flight. Usually when we want to make a rocket flying in rolling condition, the main strategy is actually to design the fins so that they are generating the desired rolling moment throughout the flight. The easiest way to do it is by simply rotating the fins of the same amount and in the same direction wrt the vertical body axis. However in case of airframe errors or poor manufacture the fins could present some misalignment that actually produces the unwanted rolling motion. Therefore even a non-rolling rocket can find itself rolling if its fins are not properly designed. Note that the damping terms characteristic of a pitch or yaw deflection are not present if the rocket is rolling. In other words the rolling motion can progress unconstrained in a common rocket. Therefore it is very important to ensure the required precision during the manufacture and mounting of the airframes.

The roll rate given by a set of equal canted fins is given by extending the Barrowman method according to eq. 24 [2]. This equation will be useful in calculating the roll rate given by a certain configuration of misaligned fins.

$$\omega_R = \frac{12 v A_{ref} R_{Cp} K_r}{c_r K_d S \left[(1+3\lambda) S^2 + 4 (1+2\lambda) \frac{D_{ref}}{2} S + 6 (1+\lambda) \frac{D_{ref}^2}{4} \right]} \theta \tag{24}$$

where R_{Cp} is the Cp radial position of one fin, v the velocity of the rocket, θ the fin cant angle and $K_{r,d}$ two constants depending on the geometry.

As previously stated, a rolling rocket is more likely to be perturbed by sinusoidal perturbations only so that it is useful to see how it behaves when such disturbance is arising. In the case of a rolling system the y-axis response cannot be decoupled from the z- one and vice versa. They are said to be coupled by the rolling term ω_x. A perturbation acting along the pitch axis only would results in oscillations of the rocket around the yaw axis too, even after that the disturbance has smoothed out to zero. Moreover the step and impulse perturbations commonly acting during the flight turn into sinusoidal inputs for a rolling vehicle, because their point of application rotates together with the rocket. Therefore it is reasonable to consider the response only to a sinusoidal perturbation applied both in pitch and yaw. This perturbation has generally equal amplitude in both direction and forcing frequency equal to the the one at which the rocket is rolling. The response along either pitch or yaw is equal to that of a non-rolling rocket with an output amplitude and frequency given by the equations below. The description of the dynamic response and the related solutions for rolling rockets are reported in [2].

$$\omega_{n-roll} = \sqrt{\frac{C_1}{I_L + I_R}}$$

$$\xi_{roll} = \frac{C_2}{2\sqrt{C_1 (I_L + I_R)}}$$

where ω_{n-roll} and ξ_{roll} are the *roll-coupled* natural frequency and damping ratio.

The previous coincide with the usual ω and ξ for relatively small radial MoI wrt the longitudinal one, which is the usual rocket case. Rolling response can be simply studied by considering the common form of ω and ξ of non-rolling rocket and verifying that the roll rate at which the vehicle will start spinning due to the misaligned fin will be different from the natural one.

2.4 Body Lift Effects

In general the center of pressure moves during the flight depending on the relative flow conditions. The two main factors that affect its motion are the Mach number and the AoA. Anyway the Cp movement with the Mach becomes appreciable only for high-subsonic or transonic conditions [11], which is not the case of the SMART model. Therefore only the effect of flying at an angle wrt the fluid direction will be considered. In his method Barrowman neglected the normal force developed by the cylindrical body when flying at an AoA because it seems negligible wrt the normal components developed by the other aerodynamic parts of the rocket, such as fins, nose and shoulders. Anyway as stated by R. Galejs in [12], being the normal force proportional to the AoA it is not clear when we are allowed to neglect one component wrt another, as the rocket is oscillating at such small AoA. Galejs suggested the use of a corrective term in the Barrowman eq.s to account for the presence of the body lift:

$$C_{na-body} = k_{body} \frac{A_p}{A_{ref}} \alpha \tag{25}$$

where $k_{body} = 1 \div 1.5$ need to be determined empirically.

This force is applied in the center of the planform area, i.e. the surface area of the body cut along its vertical axis, which is given by:

$$X_{plan} = \frac{\int_0^{L_{tot}} xR\left(x\right) dx}{\int_0^{L_{tot}} R\left(x\right) dx} \tag{26}$$

where $R\left(x\right)$ is the distance between the body vertical axis and the external aerodynamic surface.

Barrowman mainly neglected this term because all his analysis are based on the application of the flow potential theory which is based on assuming the flow as irrotational. The body normal force is mainly a viscous phenomena due to the development of helicoidal vortexes around the body vertical axis, which are stable and symmetrical up to relatively high AoA of 30° [13]. Up to this point, the body is contributing to the overall normal force with a component applied in the center of the planform area which is typically forward of the CG. This is because in a rocket most of the weight is located in the engine, so in the aft portion of the vehicle. Therefore this additional normal force has a destabilizing effect because it is applied forward than the original position of the center of pressure and so it contributes in shifting the latter toward the center of gravity. If the rocket is flying straight and true, the AoA is zero and this component is also disappearing, returning the Cp to the original position predicted by Barrowman. When flying at AoA higher than 30°, the symmetrical shape of the vortexes breaks up and additional perturbing moments in yaw and pitch arise from the asymmetrical configuration, see fig. 18.

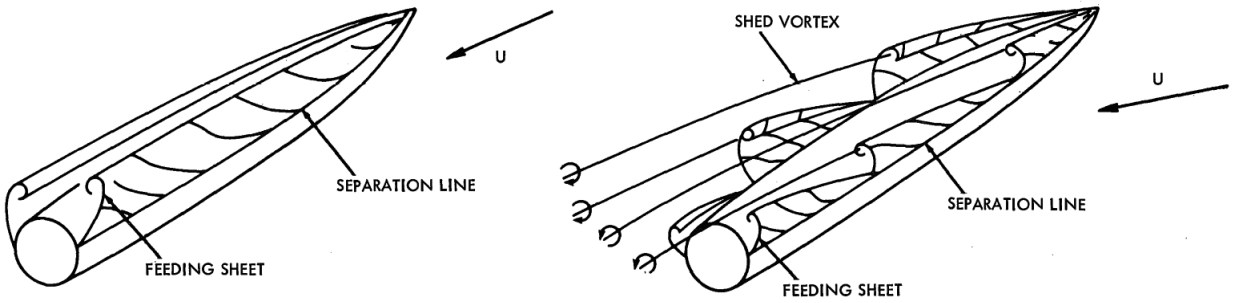

Figure 18: Symmetrical (left) and asymmetrical (right) vortex formation over a body of revolution at an AoA [14].

The Galejs approach is also partly confirmed by the work of L. H. JORGENSEN and J. H. ALLEN, [15]. They considered an additional cross flow term to the common slender-body theory for predicting the force and moment acting on bodies of revolution at an AoA. Actually the work of Galejs can be considered as the extension to the potential theory of Barrowman. Moreover the shape of the additional viscous term defined by Jorgensen and Allen corresponds with the one defined by Galejs, even if the theory of Jorgensen and Allen is invalid in the presence of fins. The normal force coefficients corresponding respectively to the Jorgensen and Galejs theories are reported below:

$$C_{n-Jorgensen} = \eta C_{d-n} \frac{A_p}{A_{ref}} \alpha^2 \tag{27}$$

$$C_{n-Galejs} = k_{body} \frac{A_p}{A_{ref}} \alpha^2 \tag{28}$$

where C_{d-n} is the crossflow drag coefficient and η the crossflow drag proportionality factor.

The crossflow drag coefficient is related to the drag developed in the vortexes around an infinite cylinder while the proportionality factor takes into account the finite length of the body. They depend respectively on the normal Mach and Reynolds number, $M_\infty \sin\alpha$, $Rey_\infty \sin\alpha$, and on the slenderness ratio $\frac{L_{tot}}{D_{ref}}$. They can be evaluated from empirical charts such as those reported below. For the actual configuration of the SMART rocket:

$$\eta C_{d-n} \simeq 0.9$$

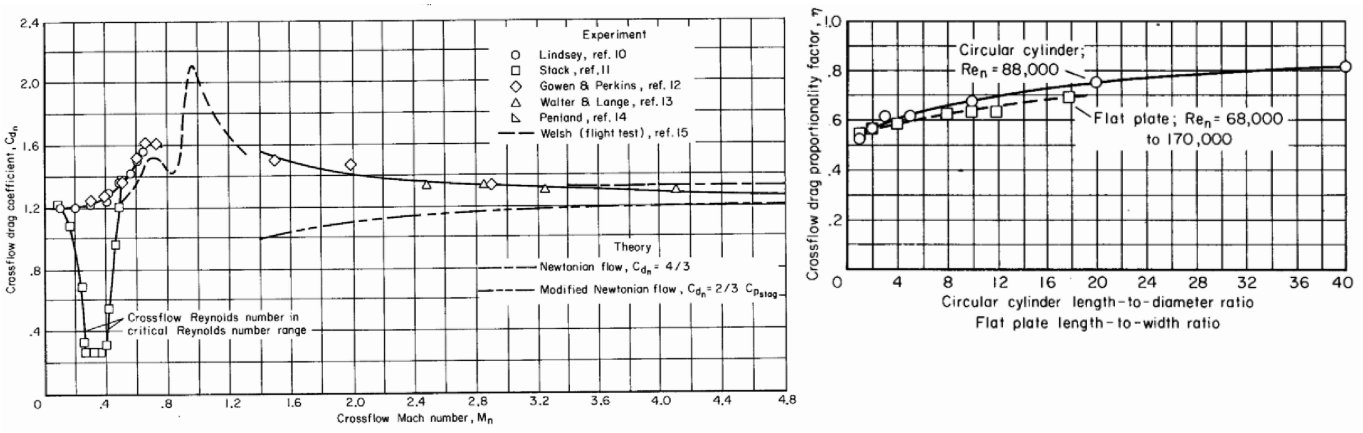

Figure 19: Crossflow drag coefficient and proportionality factor for circular cylinders [15].

To better verify the correspondence between the two methods, they are plotted below for the previous crossflow drag coefficients for the Jorgensen method and several values of the Galejs k_{body} constant.

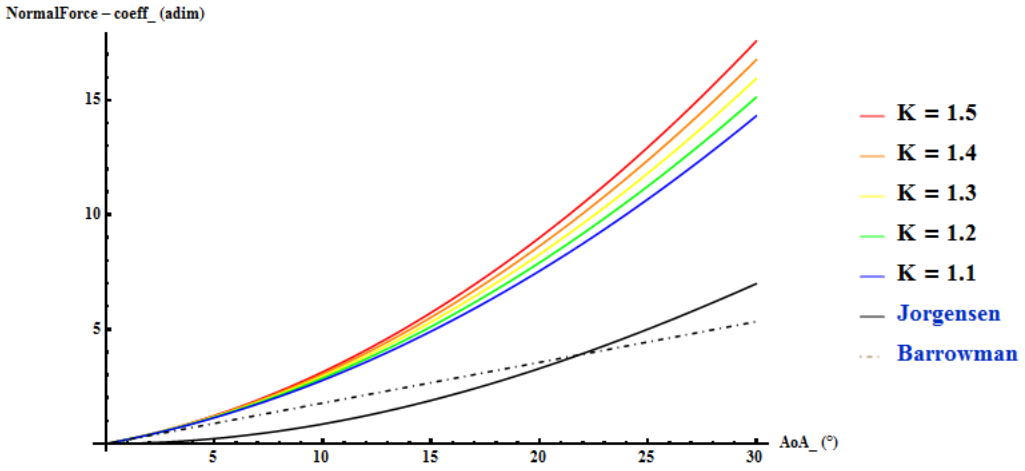

Figure 20: Normal force coefficient according to the Barrowman, Jorgensen and Galejs method.

The body term introduced so far is much more detrimental for very slender body, i.e. body whose slenderness ratio is high. Unfortunately our rocket falls in this category so that the max AoA that the actual design can sustain without reaching the marginal stability condition is very low. This is because as the rocket flight at an angle, the normal force developed by the body is quite relevant wrt the others and being this force applied forward than the CG, its effect is to move the Cp much closer to the CG hence reducing the Barrowman stability margin and so the corrective moment.

The stability margin and corrective moment accounting for the body lift are reported below. Their variation with the AoA is plotted in fig. 21-22.

$$SM = \frac{\overline{X}_{Cp} - X_G}{D_{ref}} = \left(\frac{\sum C_{na-barr_i} C_{p-barr_i} + C_{na-body} X_{plan}}{\sum C_{na-barr_i} + C_{na-body}} - X_G \right) \frac{1}{D_{ref}} \tag{29}$$

$$M_{corr} = \frac{1}{2} \rho A_{ref} v^2 \left[C_{na-barr} + C_{na-body} \right] \left(\overline{X}_{Cp} - X_G \right) \alpha \tag{30}$$

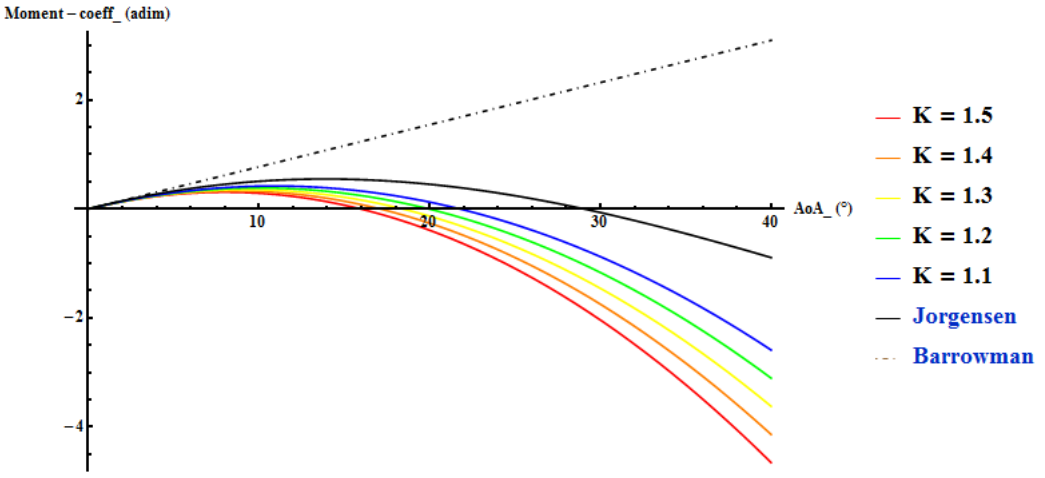

Figure 21: Corrective moment coefficient according to the Barrowman, Jorgensen and Galejs method.

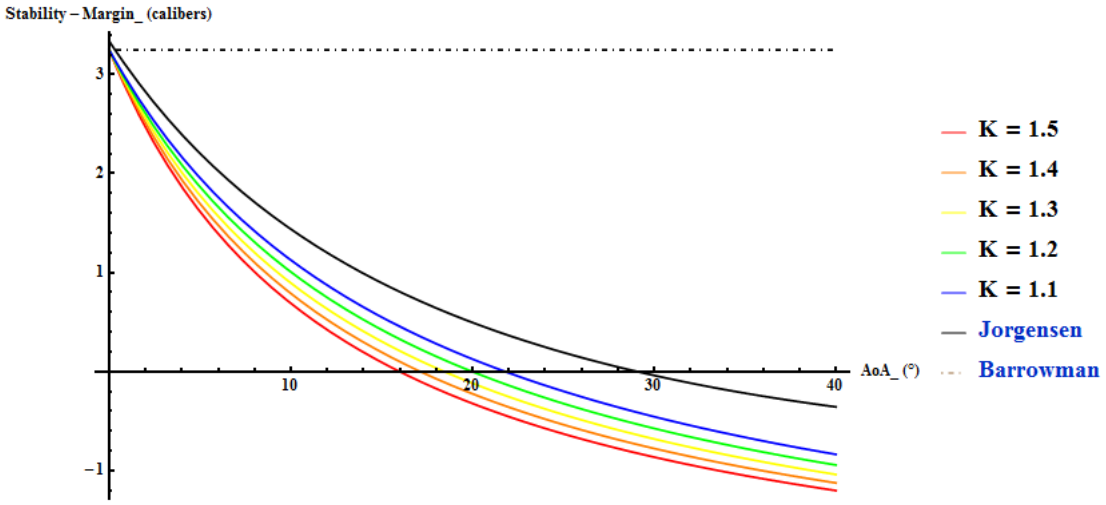

Figure 22: Stability margin according to the Barrowman, Jorgensen and Galejs method.

The requirements impose us a minimum stability margin during each phase of the flight, especially when flying at an AoA. The Mandell analysis of previous chapter always assumed that the Cp position was fixed during the rotational response of the rocket but as we have seen that it is far from being true. As the rocket deviate from the vertical in the presence of a disturbance, the Cp will start shifting toward the CG, i.e. reducing the stability margin possessed by our rocket. Nevertheless the normal force coefficient is increasing also because of the extra normal force given by the body, so that for small AoA the resulting corrective moment is growing too. This lasts up to the point at which the reduction in stability margin is too elevated for the corrective moment to continue increasing, even if the normal force actually does. From now on any further increase in AoA will result in a reduction of both the stability margin and the corrective moment. When the critical deflection angle producing the marginal stability condition is reached, the moment generated by the rocket reverses its sign, turning from positive to negative. The vehicle has now crossed the stability edge and it will not return anymore in the original unperturbed configuration.

Neglecting the movement of the Cp when flying at an angle inevitably produces an overestimate of the stability response of the rocket and this error is much more intense the higher are the vehicle slenderness ratio and the AoA. To obtain a more precise estimation of the real performance of the model in facing an external perturbation, we can consider the AoA reached at the very maximum peak of response and check what is the margin left when flying at such AoA: actually the real maximum AoA reached by our rocket will be higher due to the fact that the corrective moment decreases as the AoA increases. If we ensure that the stability margin calculated as if the Cp was supposed to remain constant is sufficiently high, the actual AoA reached by the rocket will still be sustainable. Until the corrective moment remains positive, i.e. stabilizing the vehicle, we can approximate eq. 30 by neglecting the $C_{na-body}$ wrt the usual Barrowman's terms. In other words we are assuming that the moment is varying only because of the Cp motion (see fig. 23) while we neglect any increase in normal force coefficient. This allows us to study the stability response of the system in dependance of the Cp position only.

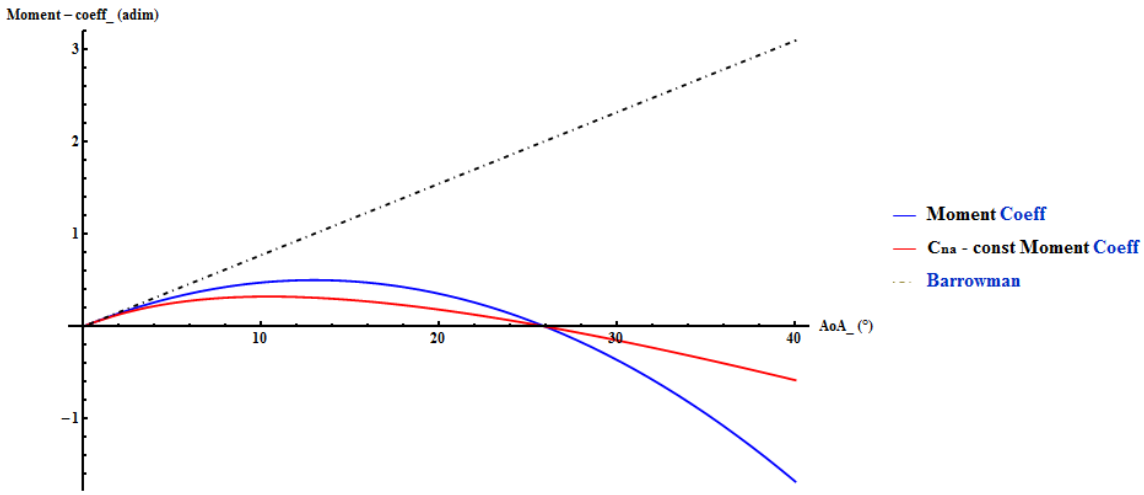

Figure 23: The corrective moment coefficient according to the Galejs method and the approximation with constant C_{na}.

According to eq.s 12-13 the dynamical coefficients depend on the position of the center of pressure wrt the gravity center, in particular the corrective moment whose variation is given by previous graphs. The damping moment does not exhibit great change when the body term is considered. The solution to the rotational problem is obtained for a given perturbing term from eq.s 18-19 once the position of the Cp has been defined. However as the rocket flies at an AoA different from zero, the center of pressure shifts towards the gravity center hence reducing the stability margin and worsening the rotodynamic response of the system. Considering a time varying Cp would increase too much the complexity of the problem so that it is easier to assume different constant values of the its position and evaluate the related response. If it is assumed that the Cp remains in the initial zero-AoA position, the rocket will be deflected up to a maximum angle which is actually lower than the true one because the corrective moment and stability margin have been overestimated. However by evaluating the shift given by the previous maximum deflection, it is possible to update the Cp position to a new minimum value. The related rotational solution will result in another maximum angle of attack reached during the response, which is in general higher than before. The effective AoA reached by the rocket will be equal to a value lying somewhere in the middle between these two maximum. Actually it will be closer to the lower border because considering only the variation of the center of pressure without the extra body normal force results in an underestimation of the corrective moment, as can be seen from the figure above. Therefore in the subsequent rotodynamic analysis a mean stability margin will be considered, given by the average between the initial and the shifted Cp position.

3 Modeling of the Perturbations

The various type of perturbations that the rocket is going to face during its flight are now defined from the analytical point of view. Although any kind of perturbation can be modeled as a combinations of step, impulse and sinusoidal inputs, most of the common disturbances faced during the flight are peculiar and affect the rotational motion of the rocket in their own particular way. For example a wind layer of constant velocity can be seen as a step input only during the very initial transient of the rocket response, over time on the order of a few tenths of a second. Therefore the disturbances have not been organized according to the shape of the response they impose to the system but instead in dependance of their relative origin. The disturbances originating from the rocket engine are considered first followed by those given by airframe errors and presence of wind. The results of this section close the problem of the rocket rigid-body motion and allow us to obtain analytical solutions to the previous eq.s 18-19. This method will be applied to the current design of the SMART rocket in the next part.

3.1 Thrust Errors

The thrust errors group all those disturbances that are directly originated from the rocket engine. They can be summarized as thrust vector misalignment, engine offset and combustion instabilities. The first two terms depend on imprecision in the engine mounting or poor manufacturing. The last comes from temporary instabilities inside the combustion chamber that are able to temporary deviate the thrust vector from the vertical body-axis direction. All of them generate a moment wrt the center of gravity and therefore contribute to deflect the rocket from the original zero-AoA flight configuration. Depending on the time at which they start affecting the flight they are more or less detrimental for the overall performance of the mission. Clearly if the engine is not well-mounted or the nozzle not perfectly aligned, the thrust errors will arise since the very beginning of the flight and remain active throughout the powered phase of the rocket. For this reason they can be effectively modeled as step input from the point of view of the rigid-body dynamics and represent the most critical disturbances that can affect the rocket stability. In fact during the launch the corrective capability of the vehicle is minimal because of the minimum speed (see eq.s 12-13). From this point of view, the instabilities disturbances are less critical because they can happen at any time during the engine burning and typically for a much shorter interval. They are described as impulse disturbances and they will also be thought to act during the launch phase in order to appreciate the different sensibility of the rocket to the various thrust errors.

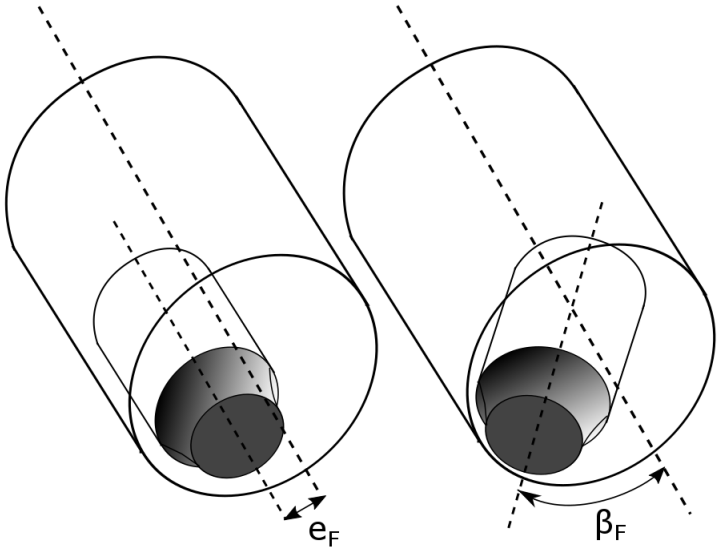

Figure 24: Sketch of a thrust misalignment and engine offset.

Thrust Vector Misalignment and Engine Offset. The thrust vector misalignment and thrust offset are two of the most detrimental disturbances that can affect the rocket during the flight. They are thought to be applied since the launch where the velocity is minimum and so the deflection induced in the rocket's attitude is very high. This could lead to excessive shift of the Cp and negative stability margin. Therefore it is necessary to carefully predict the time behavior of the AoA for a perturbation of given strength, with particular care of the maximum peak reached during the deflection. The intensity of the disturbance depends on the level of precision present in the engine. A non-perfectly symmetrical nozzle leads to a misaligned ejection of the gases out of the rocket which in turn results in a lateral component of thrust wrt the vertical body axis. The resulting moment deflects the rocket from the initial zero-AoA condition. Something similar happens if the engine axis does not coincide with the vertical body axis. The thrust vector will then be shifted from the intended position by some offset, as shown in fig.(24).

The disturbances due to thrust vector misalignment and thrust offset can be modeled respectively as:

$$M_{F-mis} = F \sin \beta_F \left(L_{tot} - X_g \right) \tag{31}$$

$$M_{F-off} = F e_F \tag{32}$$

where e_F is the thrust offset, β_F the thrust misalignment angle and $\sin \beta_F \simeq \beta_F$ for small angles.

The step solution is obtained by solving either one of eq.s 18-19 once that the direction along which the perturbing moment is applied has been defined. Again for symmetrical reason there is no difference in considering either the body y- or z-axis. The initial conditions are assumed to be both equal to zero, i.e. the rocket is in a quiescent state before the disturbance arises. The time evolution of the response is reported in table 3 and correspond to the blue curve depicted below.

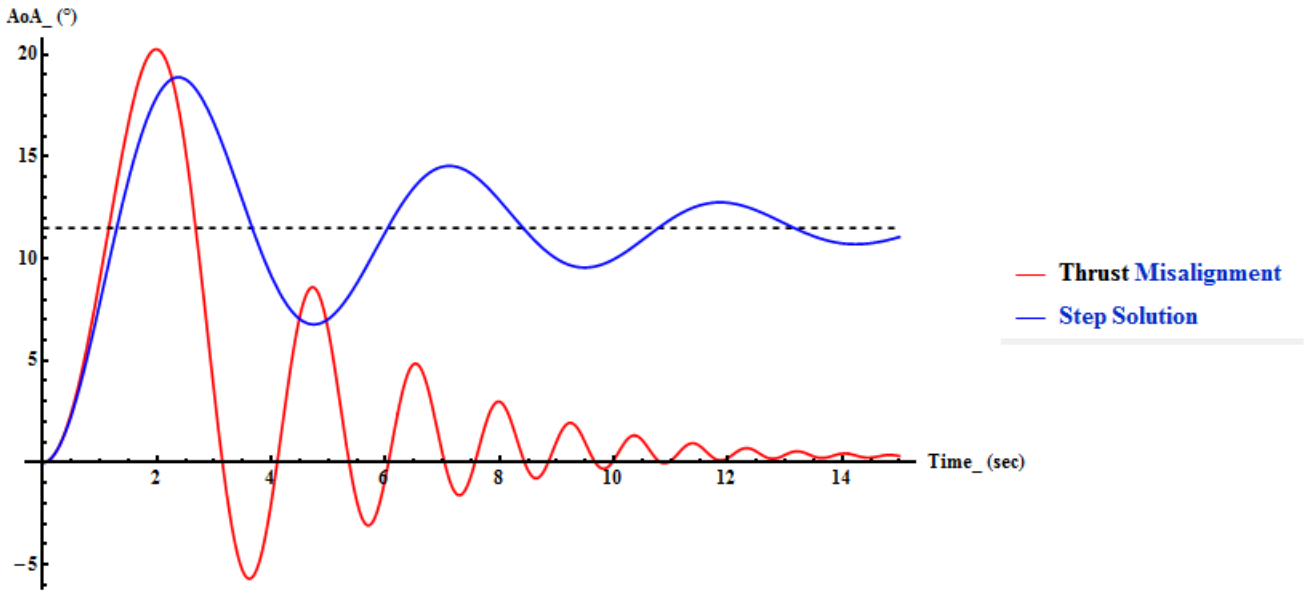

Figure 25: AoA profile in case of thrust misalignments and offsets.

From previous figure it can be seen how the time evolution of the AoA is a damped sinusoid asymptotically stabilizing about a constant value equal to:

$$\alpha_\infty = \frac{M_F}{C_1} \tag{33}$$

which is reached at the typical setting time of the system, equal to $t_{sett} = \frac{3 \div 4}{\xi \omega_n}$.
Now being the corrective moment quadratically growing with the velocity, as this is increased during the powered phase, the AoA at which the vehicle is flying will be reduced. In other words the normal force developed by the fins grows together with the speed of the rocket and so the minimum amount of deflection required to correct a given constant perturbation decreases. The true profile of the AoA will be therefore more like the red curve in fig. 25. However we are much more interested in evaluating the maximum α reached by the rocket, which corresponds to the first peak of the response. This is the design parameter which defines whenever a perturbation of known intensity is sustainable by the vehicle without turning unstable. The maximum value of the AoA according to the blue solution is given by:

$$\alpha_{1st-peak} = \alpha_\infty \left[1 + \exp\left(-\pi \frac{\xi}{\sqrt{1-\xi^2}} \right) \right] \tag{34}$$

which is obtained at $t_{1st} = \frac{\pi}{\omega_n \sqrt{1-\xi^2}}$.
It would seems easy to obtain the maximum AoA from the previous by substituting the given perturbation strength and the rocket dynamical coefficients evaluated at the launch conditions. However

in doing so the current SMART rocket resulted to be deflected up to 150° for just 1° of thrust vector misalignment! That is clearly unphysical. The reason of such overshoot is that the overall rotodynamic analysis fails when the velocities of the rocket are not enough high to ensure a rapid enough rigid-body dynamics wrt the CG variations. Remember that eq.s 18-19 have been obtained from the assumption of weakly coupled dynamics. This implies that the velocity vector remains almost unchanged as the rocket deflects, which on the other side guarantees that the dynamical coefficients $C_1$and C_2can be considered almost constant. If the rocket speed is low, the corrective forces will restore the original attitude over time scale which are comparable to the burning time of the engine! Clearly the time variation of the velocity vector is not negligible on such interval. Therefore at low speeds the two dynamical problems are strictly correlated each other and the previous solutions are not applicable anymore. Another model able to take into account the velocity variation in the very initial part of the response has been developed and it will be fully described in the next section.

Combustion Instabilities. As stated before the instabilities that may arise due to temporary variations during the combustion process can be considered as impulsive disturbances. In general the impulsive phenomena arises not only from combustion instabilities but also during the rocket staging separation and from the interference with the rails during the launch. The latter can be neglected because if the launch tower is properly designed it will not develop any remarkable force at the moment of release. Staging is not present in our configuration and it will not be considered. As for the thrust misalignment we are much more interested in the amplitude of the first peak rather that the time behavior of the response, which is anyway damped out toward zero as time increases. This is because the generic solution for a second order system with impulsive inputs is equal to the homogeneous response of the same system with a particular set of initial conditions, shown below:

$$\left\{ \begin{array}{c} \alpha_0 = 0 \\ \left(\frac{d\alpha}{dt}\right)_0 = \frac{H}{I_L} \end{array} \right\}$$

The initial angular displacement is equal to zero while the angular velocity depends on the strength of the impulse, named H. In other words any second order system reacts to an impulse as if it was suddenly altered from the initial quiescent condition (zero angular displacement and velocity) to another one where the first derivative of its state variable, i.e. the rate of change is now different from zero. The time evolution of the impulse solution is reported in table 3 and plotted below for the current SMART design affected by an arbitrary impulse:

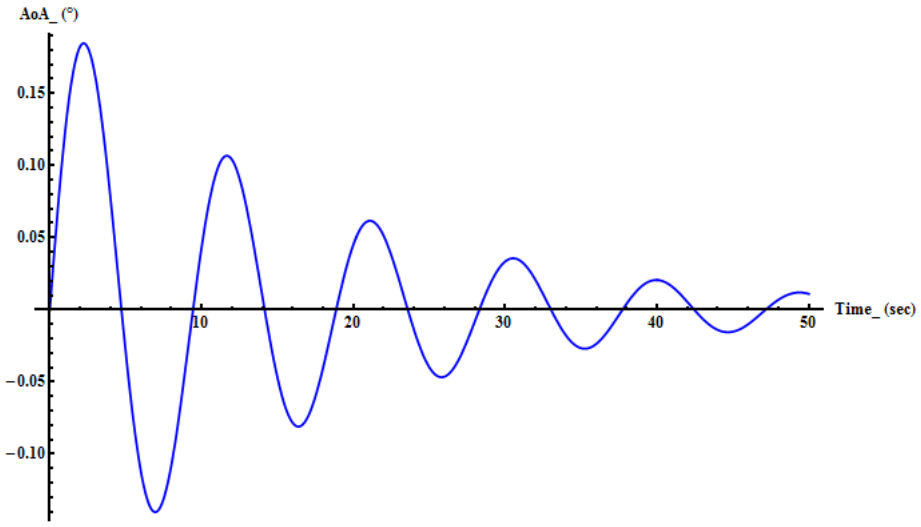

Figure 26: AoA profile in case of combustion instabilities.

For an impulsive disturbance due to combustion instabilities the intensity depends on the amount of lateral thrust actually produced by the engine times the interval during which this instability subsists. The latter can be assumed equal to the residence time of the propellant inside the combustion chamber, i.e. the time required for a particle to move throughout all the engine. This assumption has been validate by comparison with the impulse strength considered by Mandell [2]. Therefore the impulse strength H can be modeled as:

$$H = \epsilon F \left(L_{tot} - X_g\right) t_{ch}$$

where $\epsilon \in (0;1)$ is an ignorance factor accounting for the fraction of total thrust contributing in the disturbance and τ_{res} is given by [16]:

$$\tau_{res} = L^* \frac{a_c}{RT_c}$$

where a_c, T_c and $L^*$are respectively the sound speed, the temperature and the characteristic length of the combustion chamber, given by the ratio of chamber volume over nozzle throat area.

The first peak of the response is directly obtained from the previous complete solution (see table 3):

$$\alpha_{1st-peak} = \frac{H}{I_L \omega_n} \exp\left[-\frac{\xi}{\sqrt{1-\xi^2}} \arctan\left(\frac{\sqrt{1-\xi^2}}{\xi}\right)\right] \tag{35}$$

which is obtained at $t_{1st} = \frac{\xi}{\sqrt{1-\xi^2}} \arctan\left(\frac{\sqrt{1-\xi^2}}{\xi}\right)$.

Since previous equation applies for those situations where the rotodynamics is much faster than the CG motion, it is again useless at launch or generally when the rocket is not flying at sufficiently high

speed. Therefore as for the thrust vector misalignment and offset it is required a new method able to predict the response in the case of a non-constant velocity vector. It will presented subsequently together with the one valid for the thrust step perturbations.

3.2 Airframe Errors

There are two types of most common airframe errors in a model rocket. The first is the presence of one or more misaligned fins. This induces aerodynamic moments to the vehicle even if it is not flying at an angle of attack. In fact the improper fins see an incoming flow with a non-zero incident angle, which results in the development of forces normal wrt the body vertical axis. Different types of disturbances arise depending on the number and relative orientation of the misaligned fins. The other error related to the aerodynamics of the vehicle is the susceptibility of the fins to flutter. This happens when the vibrations induced by the flow over the fins are not anymore damped out by the fins material itself. In this condition the fin will start oscillating according to its natural frequency and the surrounding flow conditions. The onset of the fluttering phenomena can be controlled by providing enough rigidity to the structure while the problem of misalignment is easily overcome by increasing the precision during the manufacture and mounting of the fins.

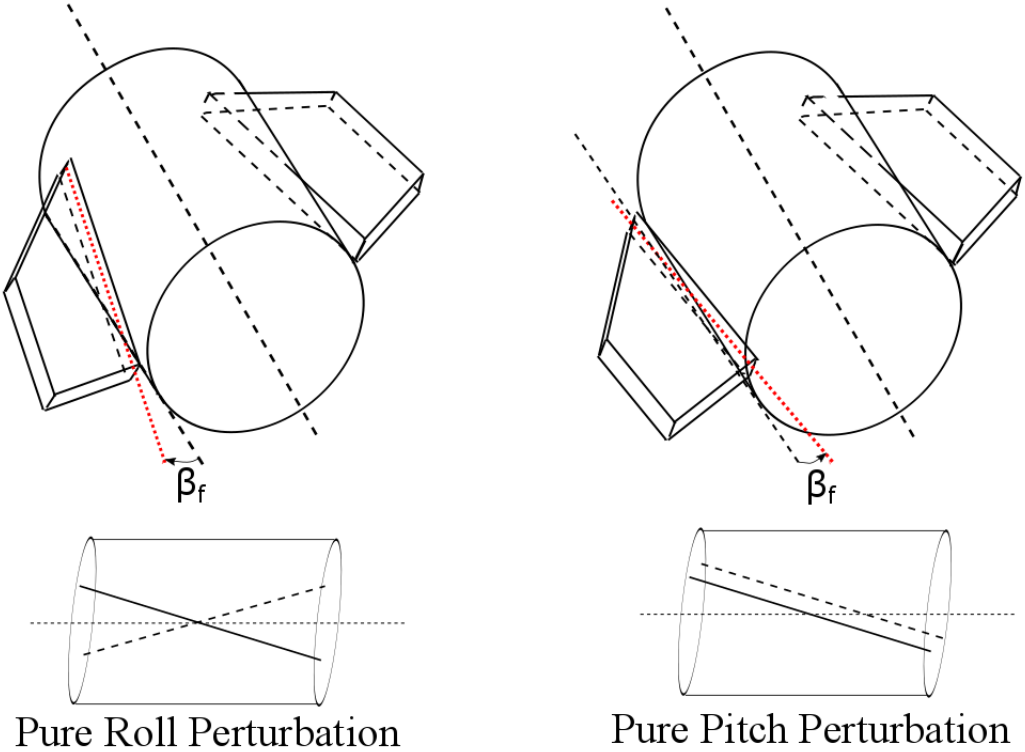

Figure 27: Example of possible fins misalignments.

Fins Misalignment. Depending on the number of misaligned fins and the relative orientation between them, different perturbing moments can arise. If just one fin is not aligned, the resulting disturbance will be given by a rolling moment together with a pitch or yaw moment, depending on the position of the fin relative to the body axis. To obtain a perturbing term in pitch or yaw only it is necessary that two opposite fins present the same misalignment in the same direction (see fig. above). On the other hand if the couple is misaligned but in the opposite direction, only a rolling term will arise. There are other possible configurations which anyway produce a perturbing moment equivalent to one of the previously described.

Let us consider for now the case of opposite fins misaligned in the same direction, i.e. only pitch or yaw moment acting on the vehicle. This perturbing moment acts since the rocket has been launched and makes it fly at an AoA different from zero throughout the flight. This happens because the airframe errors develop a side force even if the rocket is flying at no incidence wrt the fluid. As the vehicle clears the launch rod, it starts feeling the perturbing moment given by the misaligned fins. Thus it starts rotating in the opposite direction wrt the fin's misalignment angle, i.e. the rocket rotates in order to reduce the yet destabilizing fin's moment. In doing so, the AoA of the entire vehicle is increasing and the other components of the rocket start to produce a normal force too. This opposes to the perturbing one given by the fins, which is already reducing because of the decreasing AoA seen by the fins. Moreover in this particular configuration the center of pressure coincides initially with the Cp of the fins because only them are producing normal force at zero AoA. While the rocket is rotating, the overall Cp shifts towards the CG because of the additional terms coming from body, nose and shoulders, if any. From the static stability point the view, the only possible equilibrium is when all the moments acting on the body are zero. However being all the moments of aerodynamic origin, they can be thought as the sum of several normal forces all applied in the overall Cp of the vehicle. Therefore the static equilibrium is ensured when the overall normal force is zero, i.e. the destabilizing force given by the fins is balanced by the other terms. The AoA at which this equilibrium is reached can be obtained from:

$$\left(C_{na-nose} + C_{na-boat} + C_{na-body}\right)\alpha - C_{na-fins}\left(\beta_f - \alpha\right) = 0 \tag{36}$$

where β_f is the fins misalignment angle.

Previous eq is valid only for $0 \leq \alpha \leq \beta_f$, i.e. the fins are acting as a destabilizing component, hence the minus sign before the $C_{na-fins}$ coefficient. Substituting the body term according to eq. 25 and solving:

$$\alpha_1 = \beta_f$$

$$\alpha_2 = -\left(\frac{C_{na-fins}}{k_{body}\frac{A_p}{A_{ref}}} + \beta_f\right)$$

The second expression doesn't belong to the acceptable solution interval and must be discarded. Note that the following simplification $C_{na-nose} \simeq -C_{na-boat}$ has been used, which is peculiar of the current rocket configuration. In general the AoA will stabilize itself about a value dependent on the relative importance between the fin's perturbing term and the other corrective terms, but it won't never be higher than the fin's misalignment angle. In fact when the rocket oscillates beyond this value, the

fins start now to collaborate with the other stabilizing elements in restoring the attitude toward AoA equal or lower than β_f. Clearly this is strictly valid only if the Cp is still aft than the CG when the β_f angle is reached, otherwise the rocket will turn unstable. Therefore the best way to minimize the problem connected with the fin's misalignment is obviously to keep the misalignment angles smaller as possible.

From the dynamical point of view the AoA can reach higher values during the initial transient of the response, depending on the damping of the system. Again it is important to quantify this overshoot in order to ensure that the stability margin of the system can sustain it. For a preliminary analysis we can assume that the initial time behavior of the AoA is described by the following:

$$\alpha_{1st-peak} = \beta_f \left[1 + \exp\left(-\pi \frac{\xi}{\sqrt{1-\xi^2}} \right) \right] \tag{37}$$

which corresponds to the first peak of a second order system with a step input and that is going to asymptotically stabilize about β_f.

Actually the previous equation implies the validity of the weakly-coupling assumption which is not appropriate during the launch. However the perturbing moment due to misaligned fins has the good feature of being velocity dependent too, i.e. when the velocities of the rocket are low, the disturbance is small too and vice versa. Therefore the perturbing moment is growing together with the corrective and damping terms so that this particular response is not expected to be critical for the rocket stability. This is the main difference wrt the thrust errors, which are much more serious just because they can reach very severe values independently from the rocket velocity. Providing that the maximum misalignment angles are not high enough to drive the rocket towards instability, we can evaluate the maximum AoA from eq. 37, where the damping ratio is calculated with the initial stability margin of the rocket. This because as the Cp shifts when flying at a non-zero AoA, the damping ratio increases thus reducing the overshoot of the response. The corrective coefficient is typically lowered at a faster rate than the damping one, hence resulting in greater system damping. By considering the minimum damping corresponding to the zero-AoA stability margin we obtain a conservative estimation of the first peak.

The previous solution is valid in the very special case in which two pair of opposite are misaligned exactly of the same amount, which is a rather strong assumption in presence of poor aerodynamics. It will be more likely that all the fins present different misalignment angles, so that the overall effect on the system is quite hard to predict. Anyway we can still assume that the misalignment angle of each fin doesn't exceed a certain threshold so that the total misalignment is within a certain range. Moreover we assume that eq. 24 for rolling rocket is still valid even if the fin canting angle is now given by the combination of the various misalignments. For example consider a rolling rocket with a given cant angle, which actually correspond to a situation in which all the fins are misaligned of the same amount and in the same direction. If the relative orientation of one of these fins is varied wrt the other, the result will be a reduction of the overall cant angle together with the generation of some perturbing moment, whose direction is not easy to determine. It depends on the specific fin configuration of the rocket together with the actual rolling state. However as long as the rocket starts to roll, the moment arising due to any possible configuration is seen as a sinusoidal input for the rolling rocket with a frequency equal to the rolling one. The most important point for a second order system facing a sinusoidal perturbation is to keep the natural frequency of oscillation far from the typical forcing frequency in order to avoid resonance. In fact when an external sinusoid acts on frequencies

which are close to the natural one of the system and the damping factor is below$\sqrt{2}/2$, the amplitude of the response will increase considerably. The system is said to enter in resonant conditions, which from the flight point of view corresponds to violent oscillations of the rocket vertical axis and consequently high AoA. The problem of resonance is commonly encountered in designing rolling rockets, where the desirable roll rate is elevated. This allows to better exploit the benefits coming from the rolling conditions but imposes that somewhere during the flight the rocket natural frequency will be reached (and overcome) by the roll frequency. If a sinusoidal perturbation is acting during this time interval and the damping of the system is too low, the resonant behavior can really compromise the overall flight. Instead for a non-rolling rocket it is sufficient to keep the natural frequency of the system far from the expected roll frequencies that may be induced in the rocket. If a set of equally misaligned fins in the same direction is equivalent to a rolling configuration, it is reasonable to assume that if one or more of these fins is not exactly "canted" as the others, the resulting rolling frequency provided to the rocket will remain below the one given by the fully canted configuration. Therefore it is sufficient to ensure that the roll-coupled natural frequency of the system ω_{n-roll} will remain above the roll frequency given by eq. 24, where the fin cant angle θ is now given by:

$$\theta = (\beta_f)_{max} \tag{38}$$

where$(\beta_f)_{max}$ is the imposed maximum misalignment angle of a single fin.

Note that for a common rocket the radial moment of inertia is much less than the longitudinal one so that ω_{n-roll} actually coincides with ω_n.

Flutter. In non-rolling rockets sinusoidal perturbations arise during the flight only if the fins are subjected to flutter. When a structure, like a fin, is placed in a flow of sufficiently high velocity, there is the possibility that the vibrations induced by the flow over the surface couple the elastic modes of the fin such that the vibrating structure will start extracting energy from the airstream. If the extracted energy is dissipated by the internal damping, or friction of the structure, the coupled vibration modes will be eventually damped out. However as soon as the extracted energy equals the amount of energy that the structure is capable of dissipating, neutrally stable vibration will persist. When this happens it is said that the "flutter" speed of the structure has been reached. This depends not only on the flow conditions but also on the geometry and material of the fin. At higher speeds, the vibration amplitude will diverge and the structure will quickly collapse. To prevent the fins from fluttering it is sufficient to provide enough structural rigidity during the design so that they will not encounter the characteristic flutter speed throughout the flight of the rocket.

However the flutter speed is not easy to be determined. In this work the approach developed by D. J. Martin [17] has been used. This method extended the empirical expression for heavy, high-aspect-ratio wing's flutter speed to low-aspect-ratio fins, accounting for eventual tapering and presence of sweepback angle too. The critical flutter mach is given by:

$$M_{fl-cr} = \frac{G_E}{X_{fl}\left(\frac{\lambda+1}{2}\right)\frac{p}{p_0}} \tag{39}$$

where G_E is the effective shear modulus of the fin, $\lambda = \frac{c_t}{c_r}$ the taper ratio, $\frac{p}{p_0}$ the pressure ratio and X_{fl} a non-dimensional geometry-dependent parameter.

The latter can be obtained as a function of the mean thickness ratio $\frac{\overline{t}}{c}$ and fin-aspect ratio $\frac{\overline{S}}{c}$ from fig. 28. If the geometry is fixed, the flutter velocity depends only on the material and flow pressure. The most likely material to be used is the Carbon-Fiber-Reinforced Polymer (CFRP), because it offers the optimum compromise between high specific strength and light weight. The shear modulus of the 45° inclined-fiber version corresponds to 33 Gpa [18]. The denominator in eq. 39 can be evaluated once decided the pressure ratio, which depends only on the flight instant considered. From the left plot in fig. 28 it is possible to check where the calculated quantity is placed wrt the continuous line at the shear modulus of the given material. If the point lies below this empirical line then fluttering should not be expected for the actual flight configuration.

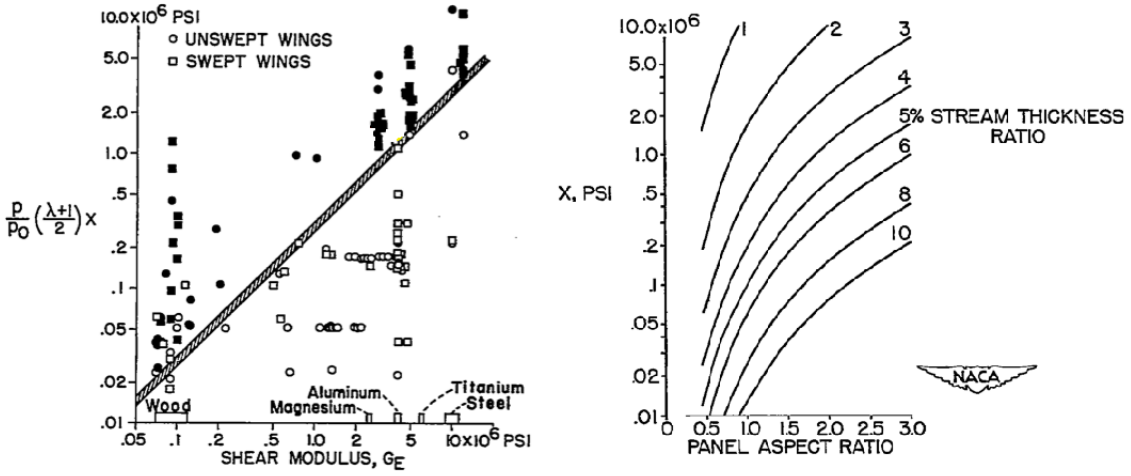

Figure 28: Composite chart for bending-torsion flutter [17].

3.3 Wind

The main environmental threat for the rocket flight is the presence of wind. If a passively stabilized vehicle flies through the atmosphere in windy condition the dynamics imposed by the interactions with the moving airstream can only be marginally governed. Moreover the presence of wind on the launch pad can seriously affect the stability and the subsequent path of the vehicle. Only the presence of horizontal wind blowing at constant speed is assumed in this paper. In doing so the free turbulence naturally presents inside the flow field is neglected, together with the possible vertical motion due to thermals. However if the airstream is not too much chaotic it is always possible to define an average direction of motion with a suitable mean velocity. This is usually done immediately before the launch in order to verify if the atmospheric conditions are suitable for launching. From this point of view it is desirable to design the rocket to be as much flexible as possible in terms of weather condition acceptable for the flight. In fact it is most likely that the provider of the launch site will allow a maximum launch delay only of a few hours because of the high number of rockets participating the project and so the tight schedule.

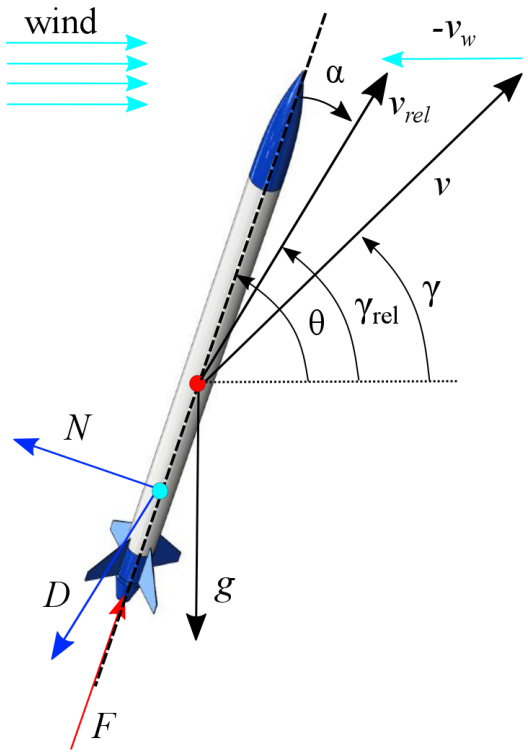

Figure 29: Wind superposition.

When an horizontal wind is acting on the rocket, the wind speed superimposes on the velocity that the flow would have if only the rocket was moving. Therefore the flow velocity vector seen by the vehicle has changed as soon as the rocket enters the region where the wind is blowing. The overall effect is a change of the flow velocity vector seen by the rocket, both in modulus and in direction (see figure above). Hence the rocket is deceived to be flying at a non-zero AoA wrt the fluid. The corrective normal forces are so generated in order to reduce this angle wrt the fluid and reach the stable zero-AoA flight configuration. This is only possible when the rocket vertical axis is aligned with the *relative* velocity wrt the fluid, whose direction constantly changes because the rocket velocity does. Actually this means that the rocket trajectory is bending into the incoming wind direction, i.e. upwind. This behavior is commonly called *weathercocking* by model racketeers. Depending on the moment of the flight at which the wind shows up, the rocket may be detached from the intended flight direction of a considerable amount. The various effects on the trajectory will be detailed in section 6.4. For now it is sufficient to say that to minimize the impact of the turn due to wind of a given intensity, both excessive fins area and stability margin should be avoided. In doing so we are minimizing the overall corrective moment and so the rotation imparted to the body vertical axis. Even if the weathercocking can not be prevented, we can slow down the turn and so the detachment of the rocket from the intended flight path. Note that as the rotation is retarded and the velocity of the rocket is increased, the relative importance of the wind speed when superimposed decreases. Therefore a high specific thrust rocket with the minimum stability margin acceptable is much less sensitive to weathercocking wrt a slower

overstable rocket flying through the same wind layer. However the stability margin and the fins area are directly related with ability of the rocket to sustain the other perturbations that may affect its flight. Flying with a too low stability margin can make the Cp shift beyond the CG even if only a minimal disturbance affects the rocket. On the other side overstable rockets can accept high margin regarding possible manufacturing imperfections but they are going to be highly deflected even if a light breeze blows on the launch site. Therefore an unavoidable tradeoff is required between the wind sensitivity and the stability response to thrust or airframe errors when designing the aerodynamics of the vehicle.

From the point of view of the aerodynamic stability it is important to ensure that the AoA encountered by the rocket as it deflects in the wind will not invalidate the minimum requirement in terms of stability margin. According to the definition of the AoA as the angle between the body x-axis and the flow velocity direction relative to the vehicle, the time evolution of this angle will be a damped sinusoidal motion which starts from a non-zero initial value. As the wind velocity superimposes to the original flow field, the velocity vector of the airstream undergoes an abrupt change which results in an impulsive variation of the rocket AoA, even if the vertical axis is remained unchanged. This time evolution can be suitably described as the homogeneous response of one of the previous eq.s 18-19 with a particular set of initial conditions given by:

$$\left\{ \begin{array}{c} \alpha_0 = \alpha_w \\ \left(\frac{d\alpha}{dt}\right)_0 = 0 \end{array} \right\}$$

where α_w is the initial AoA, which is also the maximum deflection reached by the rocket during the response. The latter is reported below and represented in fig. 30:

$$\alpha\left(t\right) = \alpha_w \frac{\xi}{\sqrt{1-\xi^2}} \exp\left(-\xi\omega_n t\right) \sin\left[t\omega_n\sqrt{1-\xi^2} + \arctan\left(\frac{\sqrt{1-\xi^2}}{\xi}\right)\right] \tag{40}$$

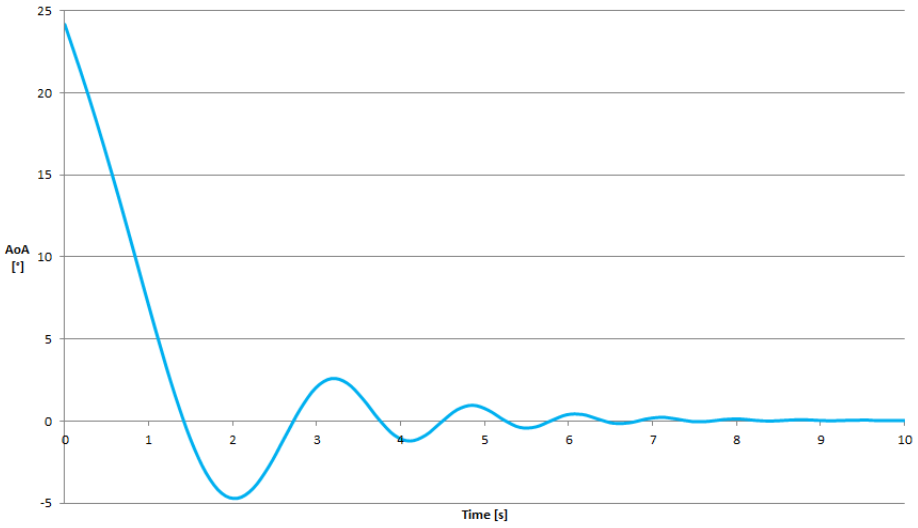

Figure 30: AoA profile in case of constant horizontal winds.

where α_w depends from both the wind and rocket speed and their relative orientation at the moment the wind starts to affect the vehicle.

Again the most dangerous situation for the rocket stability is during the launch. However this time this is due to the fact that the minimum rocket velocity results in a greater initial AoA as the wind speed is superimposed. The orientation of the launch tower is also important because it determines the subsequent orientation of the rocket velocity vector relative to the wind. Differences arise if the rocket is launched vertically or at an angle wrt the ground, the so-called launch angle γ_L. In the last case it is important also to specify if the launch vector lies on a plane parallel or perpendicular to the wind direction. The initial AoA resulting from each of the previous situations are identified as α_{w-1d}, α_{w-2d} and α_{w-3d} respectively for the vertical, inclined on a parallel and inclined on a perpendicular plane wrt the wind (see fig. 31). They can be obtained from the following relations.

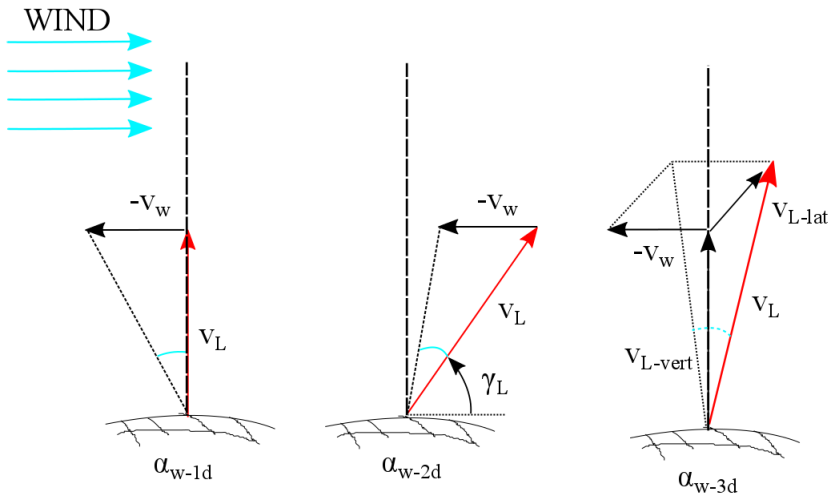

Figure 31: Initial AoA for different launch directions in windy conditions.

$$\alpha_{w-1d} = \arctan\left(\frac{v_w}{v_L}\right) \tag{41}$$

$$\alpha_{w-2d} = \arctan\left[\frac{v_w}{v_L}\left(\frac{\sin\gamma_L}{1-\frac{v_w}{v_L}\cos\gamma_L}\right)\right] \tag{42}$$

$$\alpha_{w-3d} = \arctan\left(\frac{v_w}{\sqrt{v_{L-lat}^2 + v_{L-vert}^2}}\right) = \arctan\left(\frac{v_w}{v_L}\right) \tag{43}$$

where v_L is the launch velocity, γ_L can vary between 0°and 180° and it is less than 90° if the rocket is launched upwind, i.e. against the direction of the incoming wind.

The previous relations are still valid if the wind shows up at a generic time instant during flight. It is simply necessary to substitute the actual velocity modulus and flightpath angle at the given time.

The main difference wrt the previous perturbing terms is that the maximum AoA does not depend on the aerodynamics. It is just a function of the velocities and relative orientation of the rocket and the wind. There is actually no difference between a perfectly one-caliber stability rocket and a highly overstable one: both of them are facing the same initial deflection when the wind shows up. Differences arise later on as the rocket axis is deflected and the flight path detaches from the intended one. This part will be described subsequently when dealing with the trajectory simulation. From the aerodynamic stability point of view it is sufficient to notice from previous eq.s that the initial AoA can be reduced in any case if the launch speed is increased or the wind reduced. This makes the overall velocity vector less sensitive when the additional wind component is superimposing. In the third case of rocket launched crosswind there are actually no differences wrt a vertical launch. Instead if the rocket is launched at an angle in the same plane of the wind, proper orientation of the launcher is able to reduce the initial angle faced by the rocket. As it will be shown later this has a great impact on the trajectory followed by the vehicle too. The initial AoA for an inclined launch in the wind plane is plotted below for several combinations of launch angles and wind velocities.

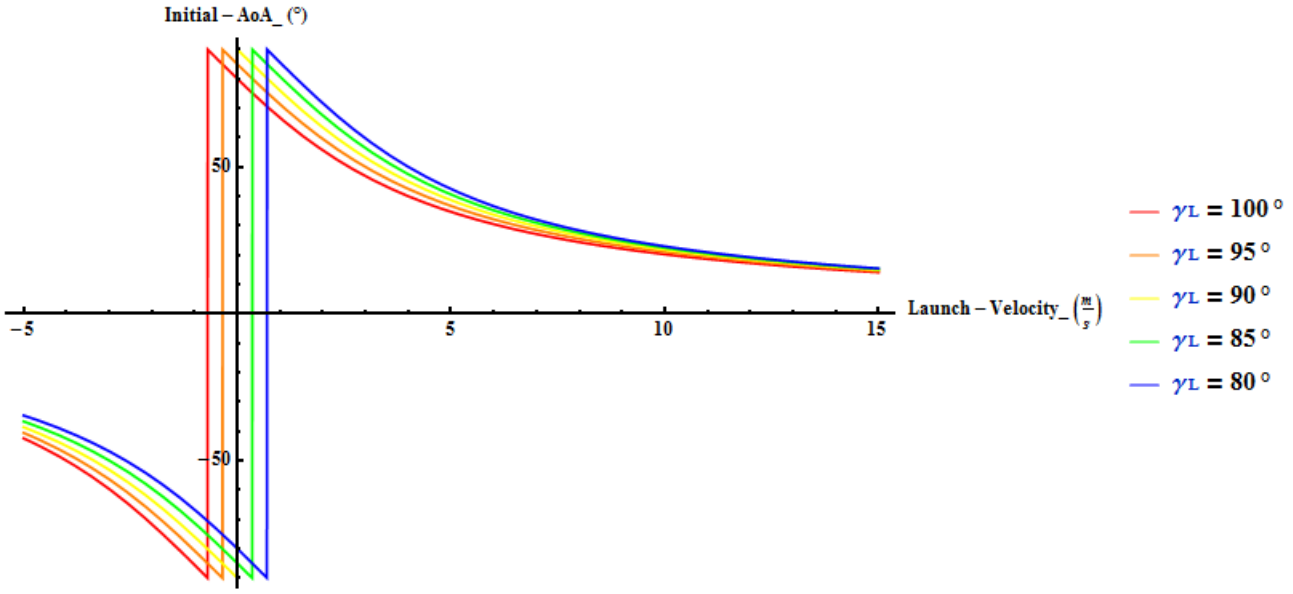

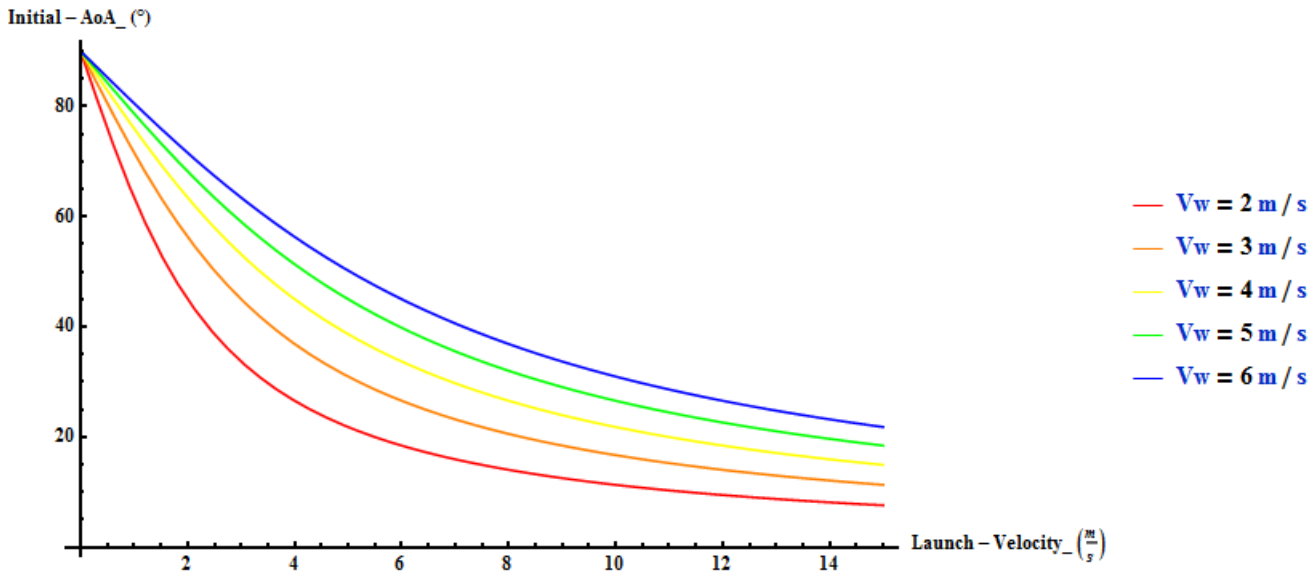

Figure 32: Sensitivity charts for the initial AoA with different launch and windy conditions.

In general launching downwind, i.e. with launch angles greater than 90°, reduces the initial deflection angles while launching upwind increases them. However these variations are minimal if compared to those exhibited by changing either the launch speed or the wind intensity. The table below gives an idea of the sensitivity of $\alpha_w$with the previous parameters:

$v_L = 13^{\mathrm{m}}/_{\mathrm{s}}$	γ_L	[°]	70	80	90	100	110
$v_w = 6^{\mathrm{m}}/_{\mathrm{s}}$	α_w	[°]	27	26	25	23	21

$\gamma_L = 90°$	v_L	$^{\mathrm{m}}/_{\mathrm{s}}$	11	12	13	14	15
$v_w = 6^{\mathrm{m}}/_{\mathrm{s}}$	α_w	[°]	29	27	25	23	22

$\gamma_L = 90°$	v_w	$^{\mathrm{m}}/_{\mathrm{s}}$	8	7	6	5	4
$v_L = 13^{\mathrm{m}}/_{\mathrm{s}}$	α_w	[°]	32	28	26	21	17

Table 4: Variations of the initial AoA as a function of the launch conditions for in-plane wind.

As an example note that a vertical launch at about 13m/s with a 6m/s wind results in about 25° of initial AoA. In order to reduce it to 23° it is necessary to rotate the launch tower of about 10° downwind. On the other side we obtain the same result by slightly increasing the launch speed (about 1m/s) or even more easily by decreasing the wind intensity.

In conclusion to ensure the aerodynamic stability when flying in windy conditions it is enough to provide that the rocket is able to sustain the maximum AoA faced when the wind shows up without turning unstable. Eq.s 41-42-43 allow to calculate this value once the velocity modulus and orientation relative to the wind at the time the wind starts to blow are known. The most critical part of the

trajectory is again the launch so in the next design procedure the previous eq.s are going to be solved wrt the launch velocity and the launcher orientation. In order to reduce the initial AoA it is either possible to increase the launch speed or rotate the launch tower in the downwind direction, i.e. the same direction towards which the wind is blowing. Longer launch rails are beneficial too because they increase the release speed of the rocket.

4 Aerodynamic Stability Analysis

In the previous sections the various disturbances that can affect the rocket during the flight have been analytically determined. For each perturbation a corresponding method to predict the time evolution of the rocket AoA has been developed. The aerodynamic stability is ensured if the maximum AoA reached during the response remains below the value required to shift the Cp beyond the position which provides the minimum stability margin. The latter depends on the requirements which have been imposed to the rocket. This requirements are now defined in order to validate the current SMART design to the previous perturbations. Although most of the previous solutions are applicable to the specific problem, those related with the thrust errors result to be inconsistent so that it has been necessary to look for improved methods. These are described in the second part of this section. In the end the validity of such methods is compared with the data coming from dedicated ASTOS simulations. The ASTOS results for the current design in terms of thrust errors are reported too.

4.1 Current SMART Design Validation

The main requirements to be fulfilled by any STERN rocket are defined in first place by the German Space Administration (DLR), which is the promoter of the project itself. Afterward there is the provider of the launch site, which is most likely going to be the Esrange Space Center. The specifications imposed by the National Association of Rocketry (NAR) has been considered too. All of them can be found in [6, 19, 20, 21] and are listed below:

- Adequate static stability margins at an angle of attack of 15 degrees; the DLR recommends a minimum stability margin of about 1.5.
- The maximum static stability margin as predicted by Barrowman analysis must be equal to 4 calibers at an airspeed corresponding to the lowest forward velocity at which the rocket is expected to leave the launcher guidance.
- Angle of fins must fall within a plus or minus 2° variation.
- Rockets must be guided until they have attained a forward velocity of at least 4 times the velocity at which the wind is blowing or gusting at the launch site.
- Launch should not be conducted in winds above than 9 m/s.
- Rockets must be launched within 20° from the vertical.

The first requirement simply states that the rocket should not in any case get too much close to the marginal stability throughout the flight. This could be easily fulfilled by increasing the fins size and moving the Cp further towards the aft of the rocket. The configuration thus obtained would be much more stable against thrust errors but also too much easily affected by weathercocking in the wind. Therefore there it goes the second requirement that puts a limit to the maximum allowable margin, which can not overcome the 4 calibers when calculated according to eq. 15. These two points alone fix the upper and lower limit of the stability margin, even if the lower bound is not completely defined. In fact it is not clear how much stable a rocket should remain when deflected, but this also depends on the amount of imposed deflection. On the other hand this is strictly connected to the intensity of the perturbation which the vehicle has to face. Although the maximum fins misalignment and windy

conditions acceptable for the flight are defined by the previous, there is no specification about the threshold in case of a thrust error. Therefore in the following analysis two possible maximum AoA were considered: the first one, $\alpha_{1.5}$ is the value required to reduce the stability margin up to the 1.5 calibers suggested by DRL, the second, α_{max} is the AoA at which the marginal stability condition is reached. Clearly the second corresponds to a much more extreme situation wrt the first. If a rocket is flying at its α_{max} that means that its Cp already coincides with the CG, i.e. the overall corrective moment is equal to zero. Flying in this condition is almost like flying unstable, with random motion of the vehicle without any aerodynamic control. Therefore if the marginal stability is obtained for a given disturbance we should either change the design or reduce the allowable maximum intensity of such disturbance, if it is possible.

The subsequent perturbation analysis has been applied to the current design of the SMART rocket at the moment it clears the launch rod. This because all the previously studied disturbances are much more critical when the vehicle velocities are low. The flight portion near the culmination could also be sensitive to any perturbing terms. However after the burnout the only relevant disturbance left is the possible presence of wind at high altitude, which anyway is not a great issue as the ascending trajectory of the rocket is almost over. Moreover in the actual mission configuration the parachutes are designed to deploy immediately after that the culmination has been reached. Therefore there is no need to preserve the rocket attitude throughout the descend too. The main parameters of interest in the analysis are listed in table 5 together with the maximum AoA previously defined. The latter are calculated from eq. 29. The launch speed has been evaluated considering a time-varying thrust rather than a constant value. The profile used corresponds to the one obtained from the *Graphit-Brennkammer-5* test of the 24/09/2014 shown in fig. 33. The experimental blue curve has been scaled to the fictitious red one having an average value equal to the desired 500 N thrust. The detachment has been assumed to be at 10 m altitude, corresponding to the launch tower provided by Esrange.

X_G $[m]$	I_L $[kg \cdot m^2]$	I_R $[kg \cdot m^2]$	v_L $[\frac{m}{s}]$	C_{na} $[-]$	SM_L $[calibers]$	ξ_L $[-]$	$(\omega_n)_L$ $[\frac{rad}{s}]$	$\alpha_{1.5}$ $[°]$	α_{max} $[°]$
1.87	12.8	0.045	13	10.1	3.2	0.1	0.6	9	26

Table 5: Main dynamic parameters for the current SMART rocket.

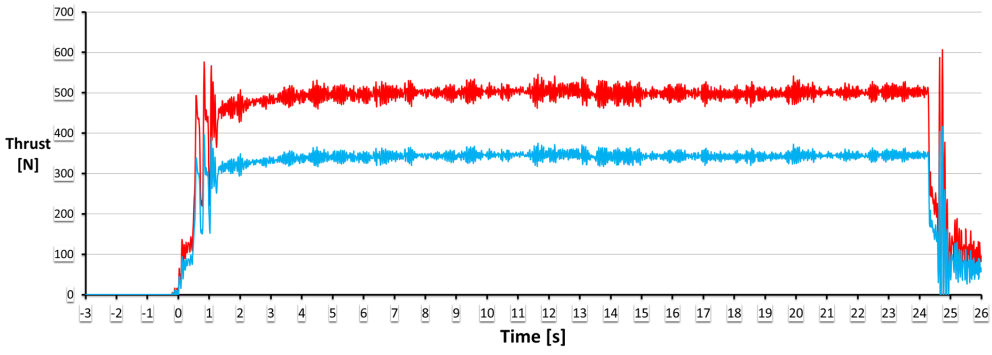

Figure 33: Experimental thrust profile used for the evaluation of the launch speed.

Thrust Errors

Thrust Vector Misalignment and Engine Offset. Neither the DRL nor the Esrange have provided a precise limit defining the amount of thrust vector misalignment and offset acceptable on a STERN rocket. Therefore the values required to drive the rocket towards the instability have been evaluated. Eq. 34 gives us the maximum AoA once the intensity of the error, the damping ratio and the C_1 coefficient are known. The last can be evaluated from eq. 20 while the damping ratio is shown above in table 5. The perturbing term is evaluated as the one necessary to obtain from eq. 34 the previously defined maximum angles $\alpha_{1.5}$ and α_{max}. The results are shown below:

β_F $[°]$	e_F $[mm]$	$\alpha_{1st-peak}$ $[°]$	SM $[calibers]$
0.015	1	26	$SM = 0$
0.008	0.2	9	$SM = 1.5$

Table 6: Max thrust misalignment angles and offsets.

Previous results are too low to be accepted as true physical solution for the previous problem: a misalignment angle of about $0.015°$ is actually $0°$, so that the current rocket would be in any case unstable in flight! The real problem is that the adopted eq. 34 is invalid for the current rocket design. The low launch velocity results in a too slow rigid-body motion so that the initial weakly-coupling assumption fails. For example consider the time required to get to the first peak of the response, given by $t_{1st} = \frac{\pi}{\omega_n\sqrt{1-\xi^2}}$. By substituting the launch parameters from table 5 the $\alpha_{1st-peak}$ would be theoretically reached after about $5s$. Clearly assuming a constant velocity equal to the launch one throughout this time interval is not acceptable. Therefore another method to predict the maximum AoA in the presence of a thrust error is required. It should be able to take into account the variation of the velocity vector during the time evolution of the rotodynamic response. The development of this method and its results are described in the next section.

Combustion Instabilities. The allowable intensity of the combustion instability has been calculated as for the previous case because no indication was provided from the above requirements. Eq. 35 together with table 5 were used to obtain the impulse strength necessary to reach the $\alpha_{1.5}$ and α_{max} angles. The results are shown below:

ϵ $[-]$	H $[N \cdot m \cdot s]$	$\alpha_{1st-peak}$ $[°]$	SM $[calibers]$
12	4	26	$SM = 0$
4	1.4	9	$SM = 1.5$

Table 7: Max combustion instabilities.

In the case of combustion instabilities it is not possible again to consider acceptable the results given by eq. 35 for exactly the same reason of before: the time of maximum peak is actually about equal

to 2.5 s. So the velocity variation during the time evolution of the rigid-body motion of the rocket is appreciable and must be considered. Therefore even in this situation an improvement in the model is required. Anyway this time the results seemed to be much more reliable than before. The ϵ parameter assumes values even greater than 1 for both $\alpha_{1.5}$ and α_{max}, which actually means that in order to reach the critical AoA a combustion instability should produce a lateral component of thrust greater than the total thrust itself! Clearly this is unfeasible. The reason why this happens is that the longitudinal moment of inertia is so high that the rocket is not easily deflected by impulsive disturbances. It will be shown that even the updated results show little variations wrt the previous.

Airframe Errors

Fins Misalignment. From the above requirements the maximum fins misalignment angle allowed is 2° in either direction wrt the x_b-axis of the rocket (see fig. 27). The angle can be measured by using an approved fin alignment guide, such as the KSSTAC10 [21]. Once the β_f angle is known, the maximum deflection imparted to the rocket at launch is obtained from eq. 37 and it is shown below:

β_f [°]	$\alpha_{1st-peak}$ [°]
1	1.8
2	3.5

Table 8: Max AoA for the fin misalignments provided by NAR.

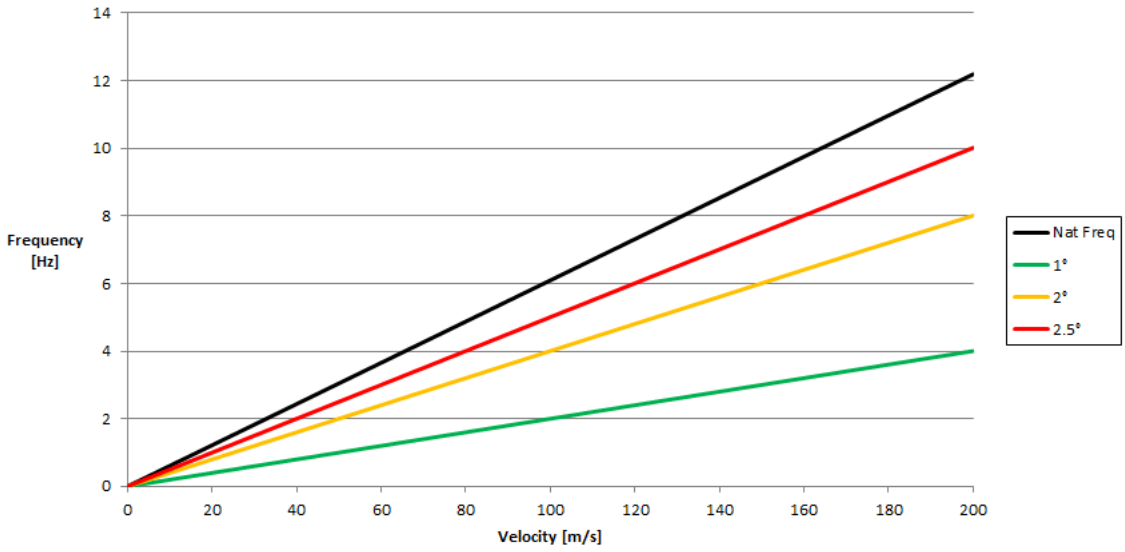

Figure 34: Induced roll frequencies for a given fin misalignment vs pitch natural frequencies.

As stated before in the case of a fin misalignment, the roll frequency induced to the rocket should also remain far from the natural frequency range covered during the flight. Fig. 34 shows both the previous as a function of the velocity of the rocket. Note that both ω_n and ω_R exhibit a linear variation with the velocity according to eq.s 23-24.

Although the first peak reached during the response remains sufficiently low for the given maximum fins misalignment, the natural frequency of the rocket is too close to the induced rolling frequency. From the plot above it can be seen how the roll frequency line related to 2.5° of misalignment is dangerously approaching the natural frequency one. For slightly greater β_f angle of about 3°, the two lines almost coincide.

Flutter. The flutter validation follows the procedure described in the previous section. Ground-launch conditions were considered because they offer the worst possible value in terms of pressure ratio. Moreover a security factor equal to 2 for the X_{fl} parameter has been considered. According to these assumptions X_{fl} is about equal to $0.8 \cdot 10^6 psi$ resulting in a mean thickness of 3.5 mm. The actual 4 mm fully satisfied the flutter safe condition. The related procedure is plotted below; note that the stream thickness ratio from below does not coincide in general with the actual fin mean thickness.

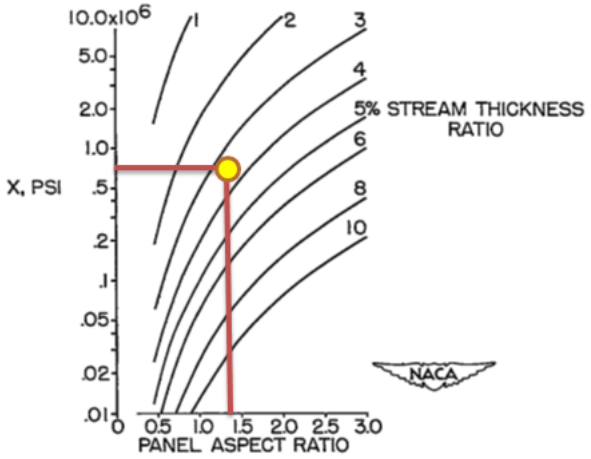

Figure 35: Mean thickness ratio for flutter safe condition.

Wind

Constant-Velocity Horizontal Wind. The fourth requirement presented before states that the rocket should leave the launch rod with a forward velocity of at least 4 times the wind speed at the launch site. This is equivalent to say that for a vertically launched rocket the initial AoA in windy conditions can not overcome 14°. Actually a model with sufficiently high stability margin is able to sustain higher angles (and so higher wind velocities) without getting too close to the marginal stability condition. However the weathercocking resulting from such greater deflection at launch will seriously compromise the subsequent trajectory. As it will be shown later in the second part of this

paper, the weathercocking can be effectively controlled by an accurate calibration of the launch angle for a given windy condition. In model rocketry this may not always be achieved because it requires precise measurements of the wind intensity and direction, so NAR has established the previous over-conservative requirement. Within the STERN-programm such measurements are mandatory in order to run the simulations required by the pre-launch test campaign, which are mainly aimed to define the launch angle and direction. These simulations are those which will decide if the initial AoA faced by the rocket at launch is acceptable from both the aerodynamic stability and trajectory point of view. In the followings only the verification of the aerodynamic stability of the rocket has been analyzed so that it should not surprise if AoA greater than 14° have been considered as acceptable. The next wind weighting study will confirm or not the possibility of such a launch configuration.

Moreover the wind and launch conditions defined by Esrange has been assumed rather than those provided by NAR in the last two requirements. Accordingly to [19] over the course of the year typical wind speeds vary from 1 m/s to 6 m/s, rarely exceeding 11 m/s. The highest average wind speed of 4 m/s (gentle breeze) occurs around March 17, at which time the average daily maximum wind speed is 6 m/s. The lowest average wind speed of 3 m/s occurs around August 5, at which time the average daily maximum wind speed is 5 m/s (see fig. 36).

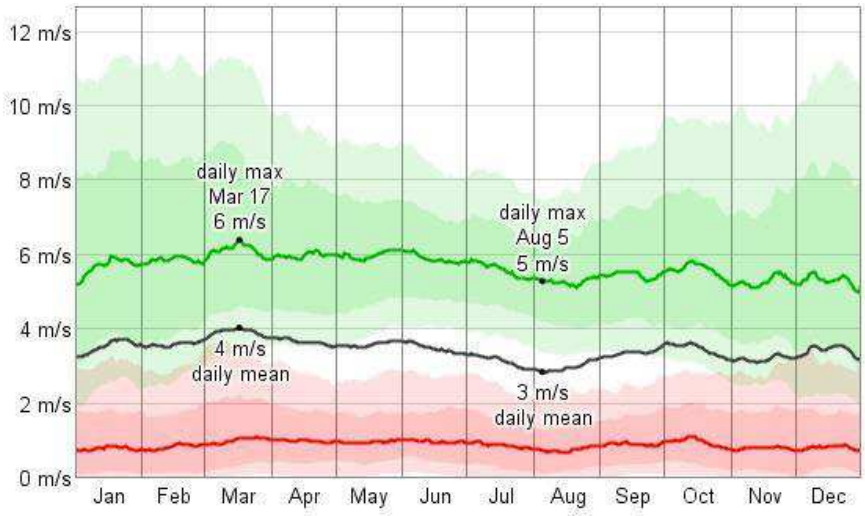

Figure 36: Esrange wind profile.

Eq.s 42-41 allow us to calculate the initial AoA for a given wind intensity once that the launch angle has been fixed. Generally Esrange allows maximum angles up to 89° but for the STERN project it is just 80° because of the experimental nature of the project itself. The various possibilities of upwind, vertical and downwind launch have been considered and the respective results in terms of α_w are shown below. The presence of crosswind is equivalent to the vertical case.

$\gamma_L = 80^\circ$	v_w	m/s	3	4	5	6
	α_w	[°]	14	18	22	26

$\gamma_L = 90^\circ$	v_w	m/s	3	4	5	6
	α_w	[°]	13	17	21	25

$\gamma_L = 100^\circ$	v_w	m/s	3	4	5	6
	α_w	[°]	12	16	20	23

Table 9: Max AoA for launch in windy conditions.

From the previous results it is clear that the actual SMART design is too much close to the marginal stability when facing winds of about 5-6 m/s. Moreover this is only an average value of a wind profile able to reach peaks up to 11 m/s, which will inevitably instabilize the flight. Therefore the launch can not be realized in such windy conditions for any type of launch angle. This is due to the low launch speed at which the vehicle leaves the tower.

4.2 Thrust Errors Analysis

The too low allowable margin in terms of thrust errors obtained from the previous results has revealed the weakness of the method developed in section 4.1. It is necessary to find another solution in order to be able to close the aerodynamic stability analysis of the rocket. In the following a possible approach is defined for the case of thrust vector misalignment and offset and then extended to the case of combustion instabilities. Throughout the following the disturbances are assumed to be applied either along the y_b- or along the z_b-axis only so that there is no distinction between the pitch or yaw response of the rocket. The validity of these new approaches will be discussed in the next section.

Thrust Vector Misalignment and Engine Offset. The method to be developed should be able to encompass the variation of the velocity vector in the rotodynamic problem. In particular it should consider its time growth under the action of the rocket thrust. A first approach was to include a properly defined velocity profile inside the previous solution, as it is shown below:

$$\alpha(t) = \frac{M_F}{C_1(v)} \left(1 - \frac{\exp\left(-\xi(v)\,\omega_n(v)\,t\right)}{\sqrt{1-\left[\xi(v)\right]^2}} \sin\left[t\omega_n(v)\sqrt{1-\left[\xi(v)\right]^2} + \arctan\left(\frac{\sqrt{1-\left[\xi(v)\right]^2}}{\xi(v)} \right) \right] \right) \tag{44}$$

where ω_n, ξ and C_1 are now function of the velocity $v(t)$.

Once assigned a velocity profile $v(t)$, the previous can be numerically solved to obtain the time evolution of the AoA. Although immediate the previous is basically *wrong*. In fact when the velocity of the rocket is too low, the rigid-body motion can not be decoupled from the CG dynamics so that eq. 2 should not be written in the form of eq. 11. The rotation of the $\{x_b y_b z_b\}$-body reference frame is not anymore definable wrt the velocity vector because the latter is now changing on time scale comparable with those of the vehicle rotodynamics. Therefore it is mandatory to return to the very foundation of the problem.

Let us consider the case of a vertically launched rocket with a given thrust misalignment angle. The disturbance is assumed to arise as the rocket clears the launch rod in order to neglect possible interactions with the launch tower. In this situation the rocket vertical axis is deflected up to a certain AoA which prompts the fins to produce the corrective moment necessary to balance the perturbing moment. As shown before the asymptotic value required is decreasing in time because of the increasing velocity. Depending on the amount of misalignment angle it will be eventually reduced to zero after a certain time. However during this interval there will be a significant deviation from the intended vertical trajectory because of the lateral component of thrust. Therefore the velocity vector is subjected to a considerable rotation, in particular it will be deflected in the same direction of the vehicle turn. Anyway if the launch speed is enough elevated and the misalignment angle not too high, it is reasonable to assume that this rotation will remain small at least in the initial part of the response. This is however what the aerodynamic stability analysis is interested in because the maximum AoA coincides with the very first peak of the response. Hence it is still possible to describe the rotation of the body frame wrt an inertial reference system with an axis coincident with the assumed-constant initial velocity direction. So eq. 2 can be written again in the previous form of eq. 11 where now the velocity has to be intended as a constant-direction vector with an increasing modulus. Assuming that the aerodynamic coefficients can still be described according to eq.s 12-13, the rigid-body motion in presence of thrust errors is given by the following:

$$I_L \frac{d^2\alpha(t)}{dt^2} + C_2(v(t)) \frac{d\alpha(t)}{dt} + C_1(v(t))\alpha(t) = M_F \tag{45}$$

This is a second order non-homogeneous linear equation in the independent variable t with non-constant coefficients $C_1$and C_2. The latter are known as a function of time once a profile for the velocity modulus $v(t)$ is assigned. The chosen profile should remain the closer it can to the actual variation of the rocket speed in the early part of the trajectory. In doing so the precision of eq. 45 in predicting the AoA is enhanced. Neglecting the drag effect, the velocity profile can be effectively approximated as a linear one:

$$v(t) = v_L + \left(\frac{F}{m} - g\right) t \tag{46}$$

This is valid until the speed has reached a sufficiently high value that the drag becomes comparable with the weight of the rocket. For the current SMART design this happens after about 5 s with a speed around 50 m/s. It will be demonstrated that this time interval is large enough to enclose the first peak of the AoA. Actually the center of gravity shifts towards the nose of the rocket as the engine is burning. However this effect can be neglected because it increases the moment arm of both the perturbing and corrective moment. The mass variation is also negligible on time-scale comparable to the first AoA peak. Note that the previous approach is valid even if the rocket is launched at an angle wrt the vertical. In this case it is necessary to verify that the velocity turn due to gravity is also negligible in the early portion of the flight. Previous assumption holds if the specific-thrust ratio of the rocket is sufficiently high.

Previous eq. 45 has been numerically solved for the given velocity profile and zero initial conditions by means of the Mathematica 9.0 software [22]. This is a computational software used in many fields and based on symbolic mathematics, which can be user defined through a simplified GUI. The result is reported below for an arbitrary misalignment angle together with the standard step solution given by fig. 25.

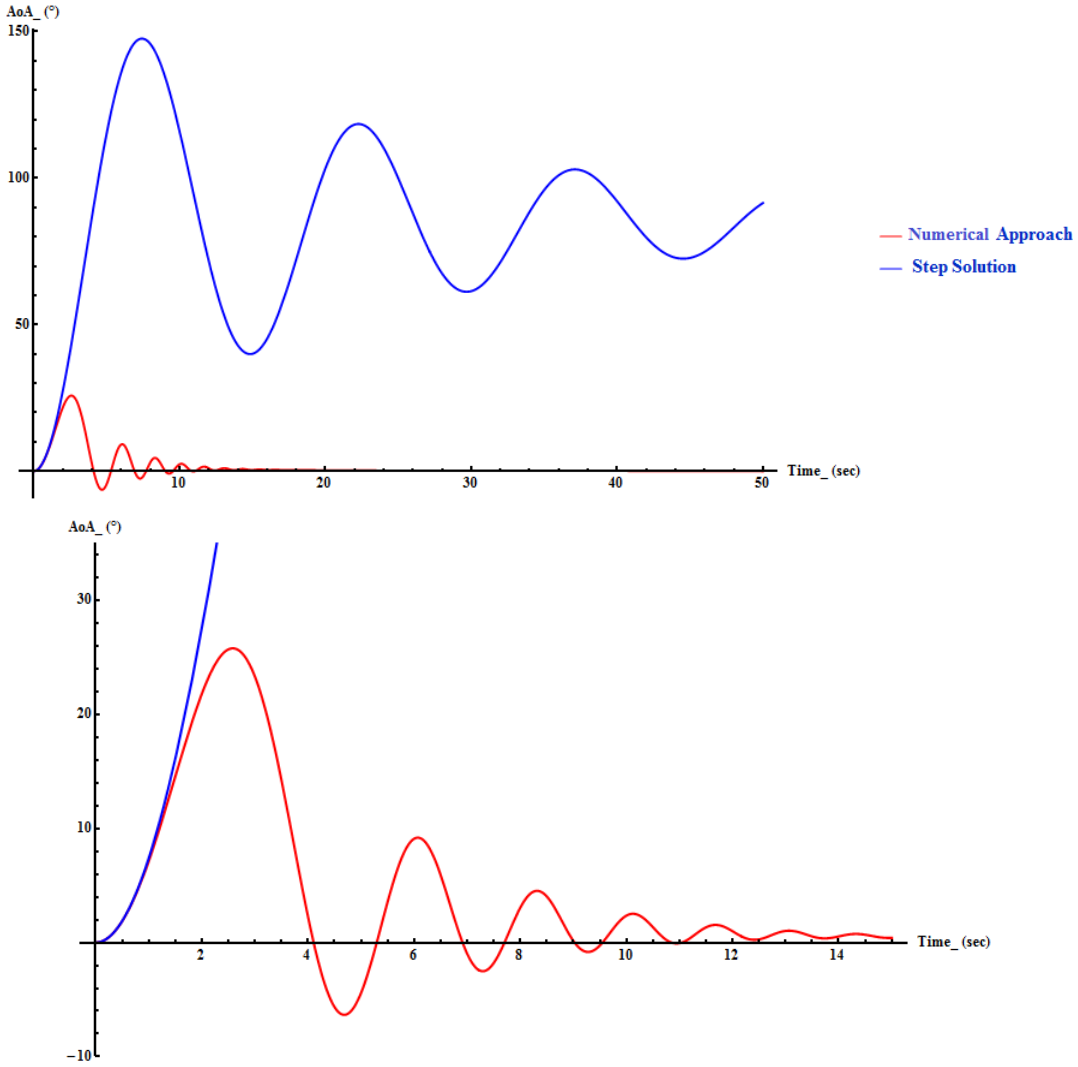

Figure 37: Numerical approach vs standard step solution for thrust misalignments and offsets.

The differences between the two approaches are evident. Note how the step solution greatly overestimates the AoA wrt that given by the numerical one. This is due to the assumed constant launch speed. The numerical profile tends to settle about a time-decreasing AoA as expected. The latter should be considered accurate only until both the drag is negligible and the velocity direction constant. As soon as one of the previous fails, the real solution starts to detach from the analytical one.

Note that the previous approach neglects the shift of the Cp as the rocket flies at a non-zero AoA. Only the velocity variation is included in the C_1 coefficient so that eq. 45 is solved every time with a constant stability margin. However the Cp movement can still be considered by running the model defined inside Mathematica several times with different stability margins. In particular if the AoA

required to obtain a given final margin is known from eq. 29, we can substitute the mean between the original and the final inside eq. 45 and check for which value of the perturbing term we recover the same AoA. By applying this procedure to the current SMART design for the previous $\alpha_{1.5}$ and α_{max} angles, the corrected maximum misalignment are shown below:

β_F [°]	e_F $[mm]$	$\alpha_{1st-peak}$ [°]	SM $[calibers]$
0.35	7	26	$SM = 0$
0.15	3	9	$SM = 1.5$

Table 10: Corrected max thrust misalignment angles and offsets.

Once the maximum misalignment angle is know, the offset necessary to produce the same AoA can be obtained by simply equating the eq.s 31-32. Note the evident difference between this and the results of table 6. The validity of this method will be verified in the last part of this chapter.

Combustion Instabilities. The approach developed before can still be applied to the case of combustion instabilities. Providing that the direction of the velocity vector can be assumed constant at least until the first peak of the response, the general equation describing the rigid-body motion of the body frame is equivalent to the homogeneous version of eq. 45 and is reported below. The solution is again computed numerically with the typical impulsive initial conditions and it is plotted in fig. 38.

$$I_L \frac{d^2\alpha(t)}{dt^2} + C_2[v(t)]\frac{d\alpha(t)}{dt} + C_1[v(t)]\alpha(t) = 0 \tag{47}$$

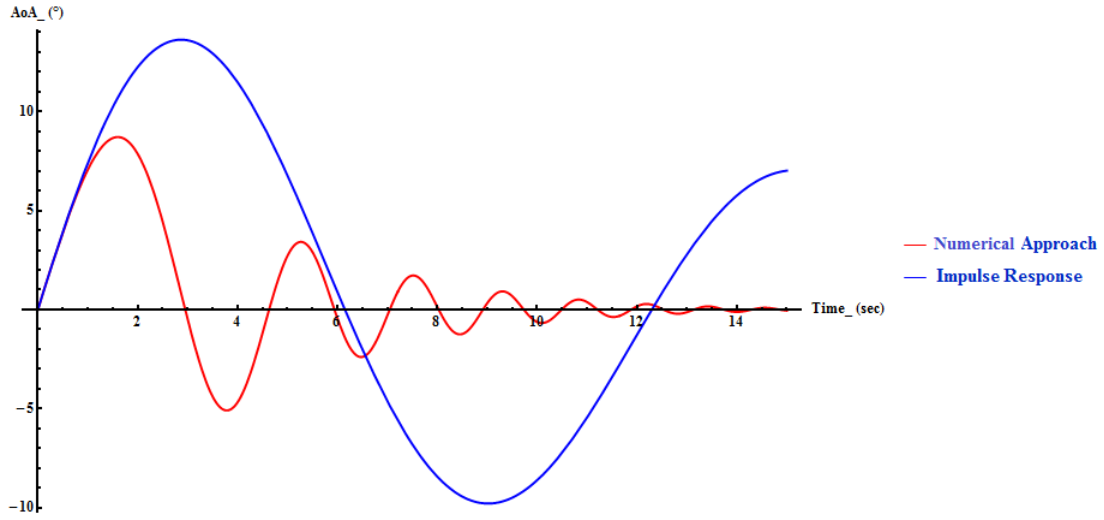

Figure 38: Numerical approach vs standard impulse solution for combustion instabilities.

The results can be considered accurate only up to the point in which the drag is negligible and the velocity direction constant. Taking the Cp shift into account as before, the maximum combustion instabilities provided by this method applied to the current design are reported below:

ϵ $[-]$	H $[N \cdot m \cdot s]$	$\alpha_{1st-peak}$ $[^\circ]$	SM $[calibers]$
16	5	26	$SM = 0$
6	2	9	$SM = 1.5$

Table 11: Corrected max combustion instabilities.

Note that the differences wrt the previous table 7 are negligible. As before ϵ overcomes the unity in order to reach the given maximum AoA. As it will be shown in the next section, the analytical approach developed for thrust misalignment and offset results in a conservative overestimation of the AoA reached by the rocket during the response. Since the method is almost identical it is reasonable to assume that the same conclusions hold for the impulse case too. This means that the real values of the ϵ parameter required to obtain the $\alpha_{1.5}$ and α_{max} angles are even higher than those calculated above. Therefore the impulse response of the current rocket is not critical from the aerodynamic stability point of view again because of its very high longitudinal moment of inertia.

4.3 Thrust Errors Verification

The methods developed in the previous section need to be verified before continuing the validation of the current design in the presence of thrust errors. The ASTOS software has been adopted because it allows to simulate the presence of a lateral component of thrust. The description of the data used during the simulations is detailed in section 6.1. For now it is sufficient to say that the mass properties, geometries and aerodynamic coefficients provided to the software coincide with those of the current SMART design. Note that even ASTOS is not able to consider the shift of the Cp when flying at an AoA. However the scaling feature included in the aerodynamic modeling environment permits to adjust the stability margin without the need to define a new aerodynamics at each simulation. Once the first has been run with the original Cp position, the maximum AoA obtained is used to calculate the minimum stability margin. The mean between this value and the original is then used for the subsequent simulation. The true behavior of the rocket lies between these two results.

The ASTOS solutions for vertical launch are plotted below together with the numerical one. The thrust misalignment considered is equal to 0.35°, i.e. the maximum according to the analytical model. In the legend it is shown the stability margin used for each simulation. They are expressed in percentage wrt the original value reported in table 5. The 70% corresponds to the mean value calculated according to the method previously described.

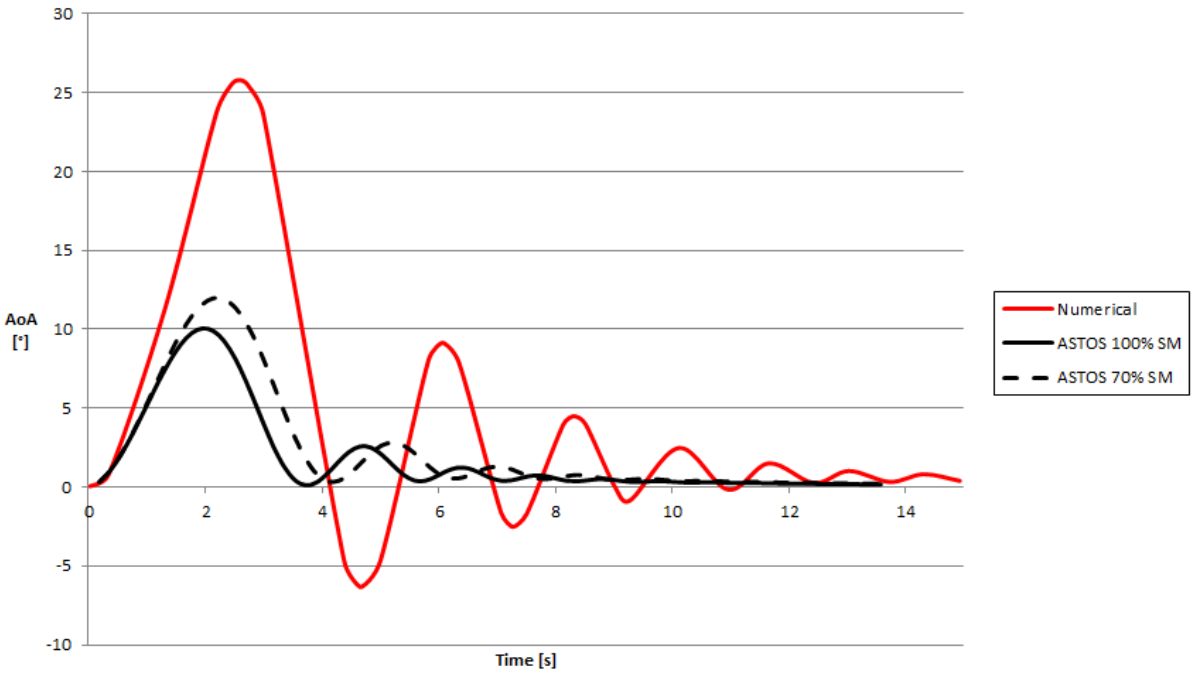

Figure 39: Numerical approach vs ASTOS solutions for a 0.35° thrust misalignment.

From the previous figure it can be seen how the numerical method overestimates the AoA faced by the rocket during the response. In particular the first peak is almost doubled wrt the real one, which lies somewhere between the continuous black and dashed curves. This difference is due to the fact that the assumption of constant-velocity direction is invalid for the current SMART design. The main responsible is the too low velocity at which the rocket is leaving the launch tower. As soon as the body vertical axis is deflected, the developed lateral component of thrust creates a lateral velocity component, which is comparable to the vertical one. Therefore the resulting vector is rotated from the original direction since the very beginning of the flight. In particular since both the vertical axis of the vehicle and the velocity vector have rotated in the same direction (see figure below) the overall effect is a reduction of the initial AoA. This is confirmed by the plot below which represents the time profile of the flightpath angle and pitch angle of the rocket defined in fig. 77. It has been obtained from the ASTOS solution relative to the 70% mean stability margin. From the enlargement it is clear how the rotation of the velocity vector (red curve) is significant on the time scale of variation of the body vertical axis (blue curve). The numerical model does not consider this rotation therefore by referring the AoA to the original vertical direction it eventually results in greater angles wrt the real case.

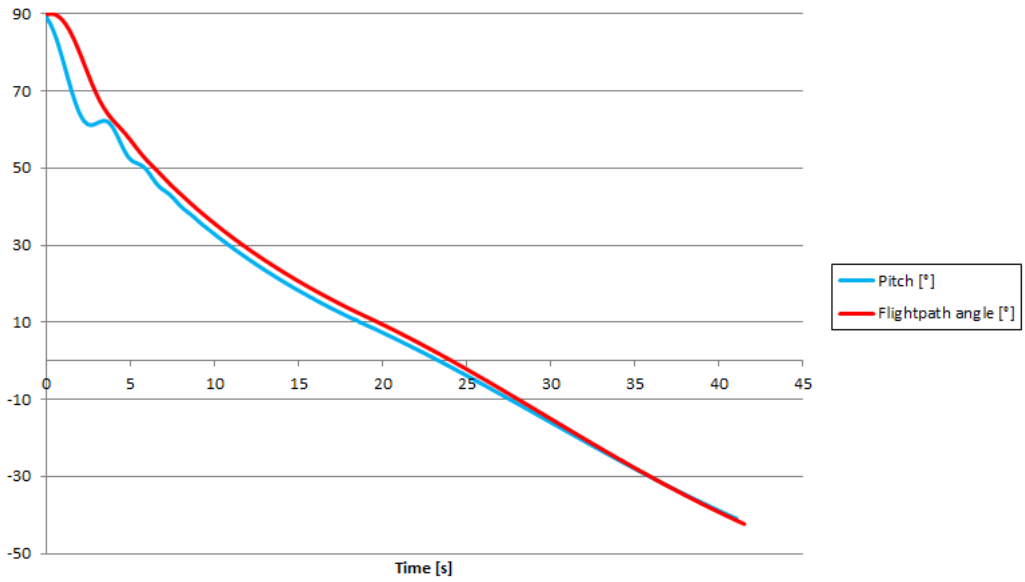

Figure 40: Flightpath angle and pitch angle for a 0.35° thrust misalignment.

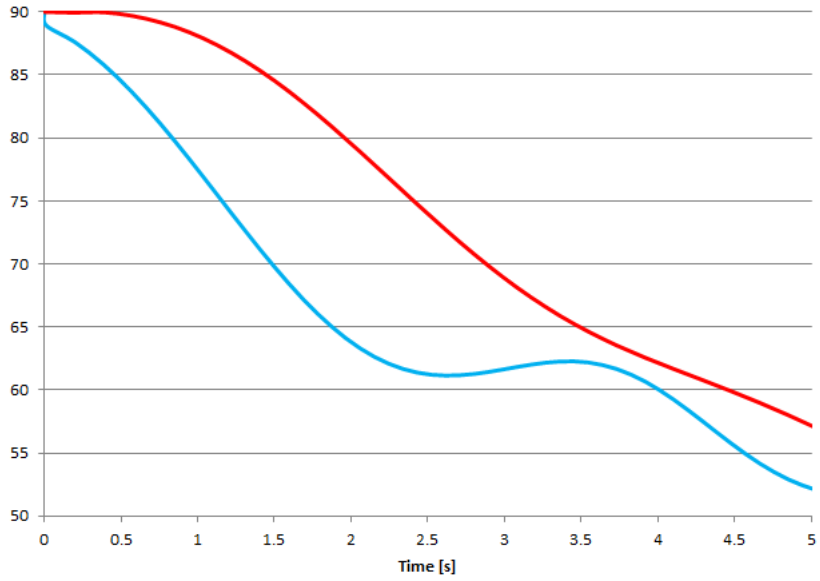

Figure 41: Enlargement of the previous.

Although this velocity rotation is positive from the point of view of the aerodynamic stability because of the reduction in AoA, it has a highly detrimental effect on the trajectory. In fact as the velocity

vector detaches from the vertical, the gravity continues to rotate it in a fashion called *gravity-turn*. As it will be shown later when dealing with the trajectory simulation, this effect can greatly penalize the maximum altitude reached by the rocket. Moreover the lower the thrust-to-weight ratio, the much more intense the g-turn is going to be. Being the current rocket characterized by a very low specific-thrust ratio of about 2, this turn represents a serious problem. To further validate the numerical approach a different test case should be considered. In particular a model characterized by higher launch velocities and specific-thrust ratios would make the simulated and numerical results better fit each other. In those conditions the initial velocity turn would be less severe and its time evolution would proceed at a much slower rate. Hence the oscillations of the vertical body axis would remain closer to the original vertical direction.

Several simulations have been run with different thrust misalignment angles in order to evaluate those necessary to reach the previously defined $\alpha_{1.5}$ and α_{max}. The final result for the current design are shown below. The shift of the Cp has been taken into account as it has been done in the numerical approach.

β_F [°]	e_F [mm]	$\alpha_{1st-peak}$ [°]	SM [$calibers$]
0.6	12	26	$SM = 0$
0.25	5	9	$SM = 1.5$

Table 12: Max thrust misalignment angles and offsets obtained from ASTOS.

Although the margin in terms of offset can be considered acceptable, the maximum misalignment angle that the rocket is able to sustain without exiting the minimum 1.5 calibers stability prescribed by DLR is about 0.25°. This happens because the $\alpha_{1.5}$ angle is too low for the actual rocket configuration. Higher margin in terms of manufacturing and mounting precision would be desirable. This can be obtained by either achieving higher launch velocity or designing new aerodynamics able to provide better response in terms of thrust misalignment. The first may not be increased too much at this state of the project because the order of magnitude of the rocket final mass and the performance of its engine have been already established. Therefore the current aerodynamics has to be changed without compromising the response to the other kind of perturbations, which was about satisfactory. The procedure followed is detailed in the next chapter.

5 Design of the Aerodynamics

In this chapter the aerodynamic properties of the rocket is parametrized wrt the fins geometry in order to define a new aerodynamics. Only the parametric plots are reported here while the analytical expressions can be found in appendix 8.1. The new configuration should be able to better withstand the perturbations due to thrust vector misalignment. Therefore in the second part the response to the latter has been studied as a function of the previously defined parameters. Another design for the rocket aerodynamics is then chosen and its new flight margins to the various perturbations are presented. This updated design will be considered as a reference in the subsequent trajectory analysis by means of ASTOS. In the last part of the chapter the variations of the stability margin and damping ratio with the mass properties are analyzed in order to keep into account for the eventual change of the rocket inner subsystems as the project proceeds toward the final SMART configuration.

5.1 Parametric Analysis

The best way to reduce the maximum response in presence of thrust misalignment is to increase the corrective coefficient C_1. This can be done either by increasing the overall normal force developed by the rocket or by moving the Cp further away from the CG. In the current configuration the normal forces are produced by the nose, the boat tail, the body and the fins. The contribute from the first two terms is however negligible wrt that provided by the fins and the body. The latter induces a normal force only when flying at an AoA, a condition that should be avoided. Therefore design a new aerodynamics is actually equivalent to design new fins for the rocket. Nevertheless the original shape of the planform area is maintained. In fact the clipped-delta exhibits the highest efficiency in terms of induced drag, i.e. the extra drag developed when the fin is producing lift (see section 2.2). Another possible choice was the elliptical shape but it has been discarded because of the more complex realization. The number of fins is not changed too in order to preserve the overall symmetry of the rocket. Thus if the C_1 coefficient needs to be increased by varying the fins, the simplest way to proceed is to make them bigger or move them further aft from the CG. The latter is impractical in the current design because the fins are already placed almost at the bottom of the rocket, as it is shown in fig. 2. Moving them further down implies that they have to be mounted on the boat tail, where the combustion chamber is going to be placed. The engine scaffold may interfere with the mounting tabs of the fins hence complicating the final assembling. Therefore the fins have to be enlarged, but how much?

When increasing the fin planform area, the higher normal force produced will move the Cp further away from the CG, hence increasing the stability margin. This is beneficial for the response to most of the perturbations but it also raises the sensibility of the rocket to weathercocking. Moreover the bigger the area, the more drag will be produced penalizing both altitude and velocity performance. There must be an ideal size that guarantees the required stability margin with the lowest possible drag coefficient. To get as close as possible to this optimum a parametric analysis considering all the involved properties of the rocket has been developed. The first thing to be done is to describe the fin planform area as a function of a proper set of geometrical dimensions. The actual sweepback angle of 40° previously evaluated by Brandt [5] has been maintained because it maximizes the lift produced by the clipped-delta airfoil. This is also confirmed by Y. Liu, L. Zuoand and J. Wang [23]. With these assumptions two quantities are enough to fully describe the dimensions of the generic fin. The span S and a k parameter have been chosen, where k is the ratio of the actual planform area to the original one. Both of them are proportional to the normal force produced by the fin. Moreover the k

parameter is directly connected with the variation of the skin friction drag developed during the flight. Actually this choice leaves out from the analysis the fin thickness. However this can be defined from the no-flutter condition once the fin area is known, as it will be later shown.

The root and tip chord are plotted below as a function of the previous. Their analytical expressions can be found in appendix 8.1 together with those of the other properties plotted here.

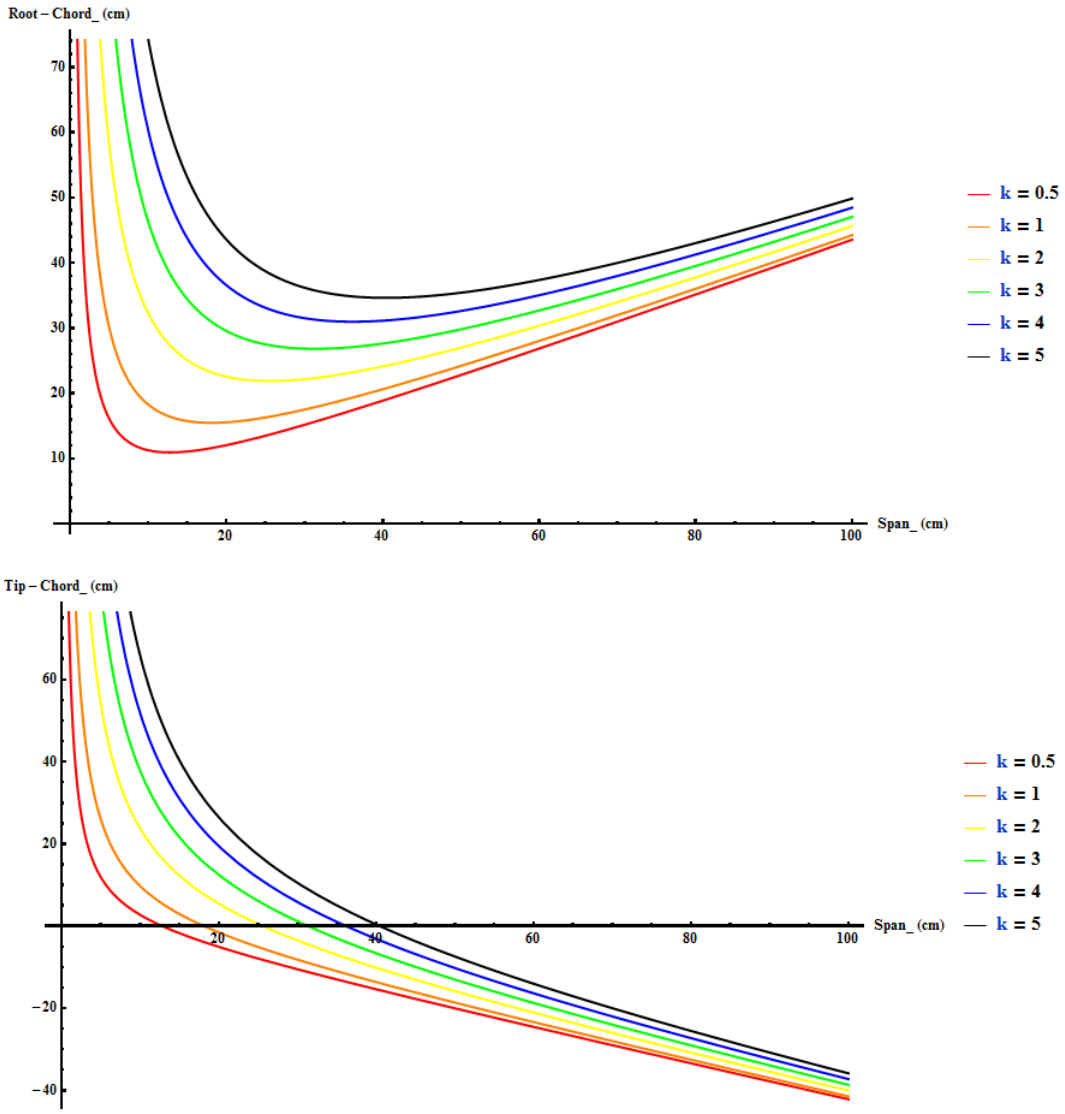

Figure 42: Fin root and tip chord as a function of the fin span and non-dimensional area.

For a given span both the root and tip chords increase with the fin area, i.e. the k parameter. On

the other hand enlarging the span reduces both the chords in order to keep the area constant. This holds until the tip chord decreases below zero for too high S value. From this point the root chord grows again together with the span because the fictitious negative area given by the tip chord keeps the k parameter constant. Clearly the real rocket can not present negative dimensions. Therefore combinations of $(S;k)$ lying in this region should not be considered neither here nor in the followings graphs.

The fin drag coefficient at zero AoA is given by the second term in the right side of eq. 9. Its dependance is depicted below for the thickness of the original design.

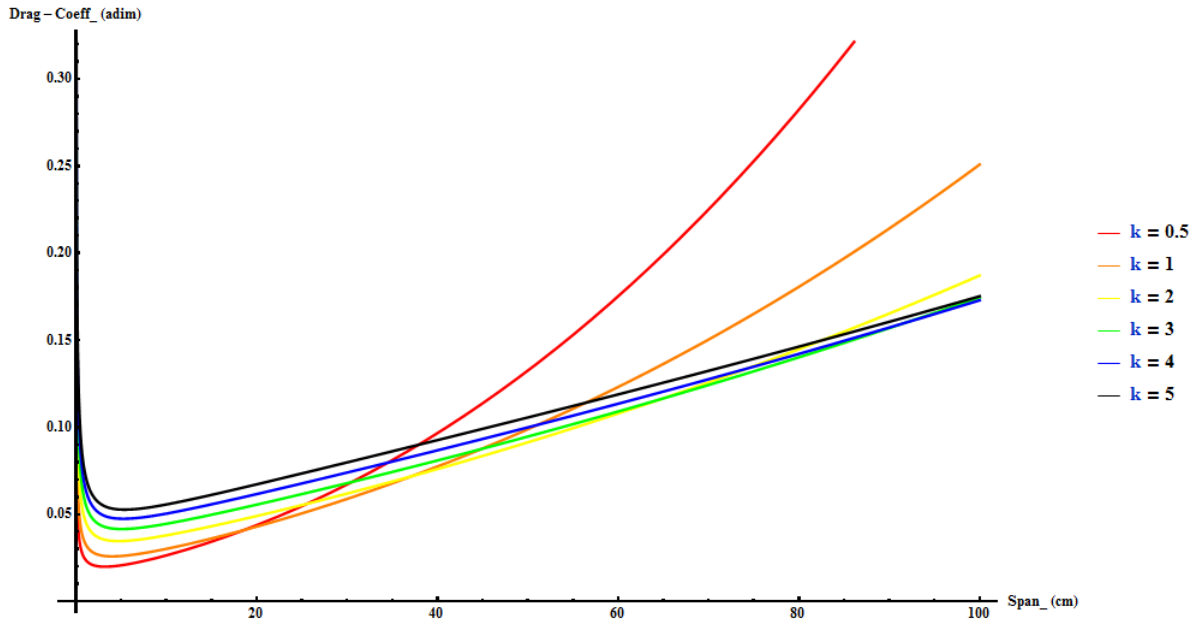

Figure 43: Fin drag coefficient as a function of the fin span and non-dimensional area.

As expected the drag coefficient is lowered for decreasing k and S. Moreover the minimum thickness required to ensure the no-flutter condition decreases too as the span is reduced. This further lowers the drag coefficient.

Substituting the previous $(S;k)$ parameters in the Barrowman eq.s, the resulting variations of the normal force coefficient and Cp position wrt the nose of the rocket of the fins are shown below:

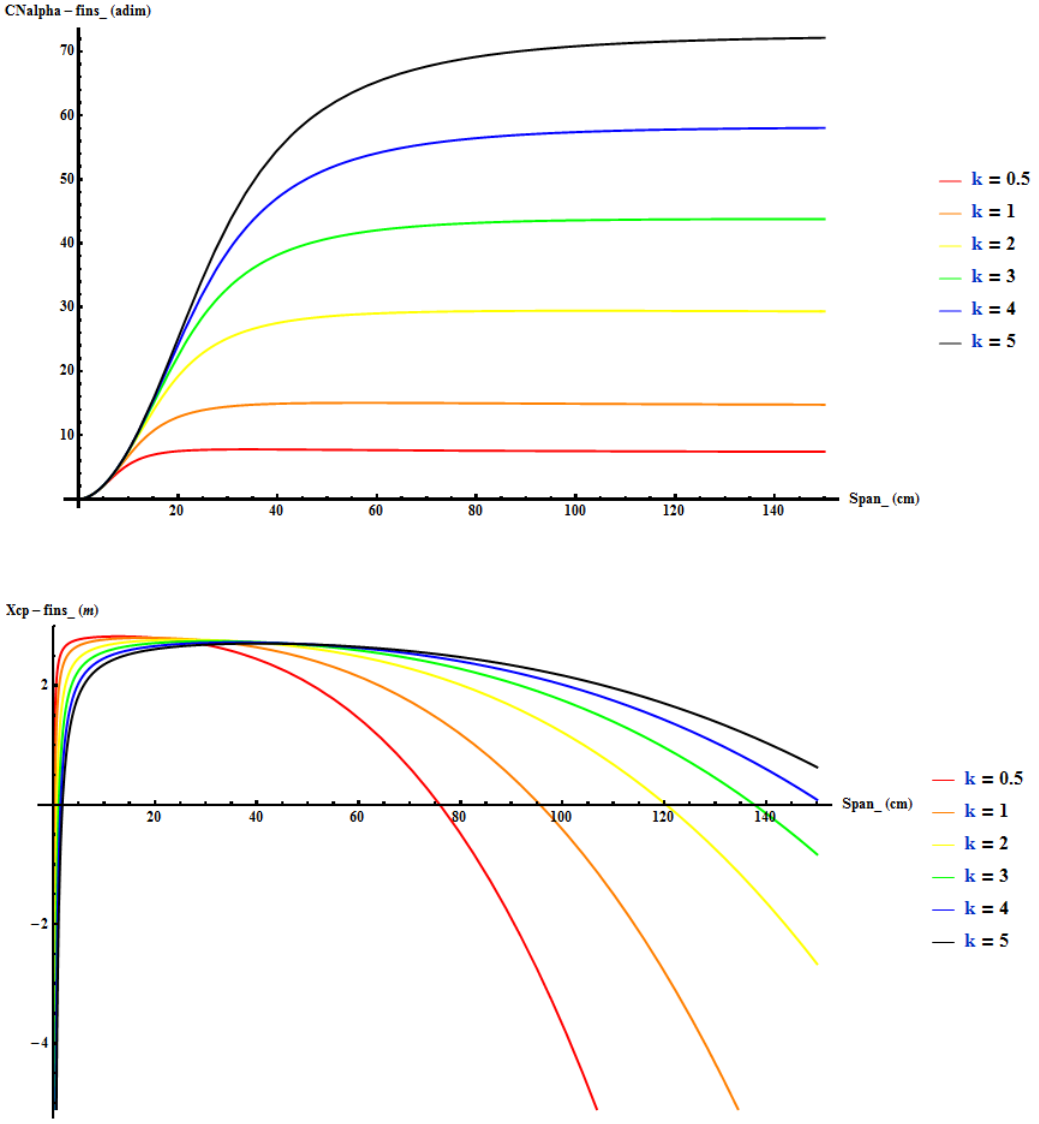

Figure 44: Fin normal force coefficient and center of pressure as a function of the fin span and non-dimensional area.

The normal force produced by the fins grows with the span and the planform area but only up to the point beyond which the tip chord turns negative. The Cp of the fin presents a maximum and then starts to decrease as the span is enlarged. The decreasing rate depends on the area of the fin: the bigger, the more the Cp will remain far from the CG. Remember that this distance corresponds to the moment arm of the corrective force provided by the fins, which is usually the main one in the overall normal force.

The stability margin and damping ratio can be expressed as a function of the $(S; k)$ parameters only if the center of gravity and longitudinal moment of inertia of the rocket are assigned. In the following figures the original values of CG and MoI. The procedure to keep their variation into account is detailed in the next section. Note that the jet damping term has been neglected.

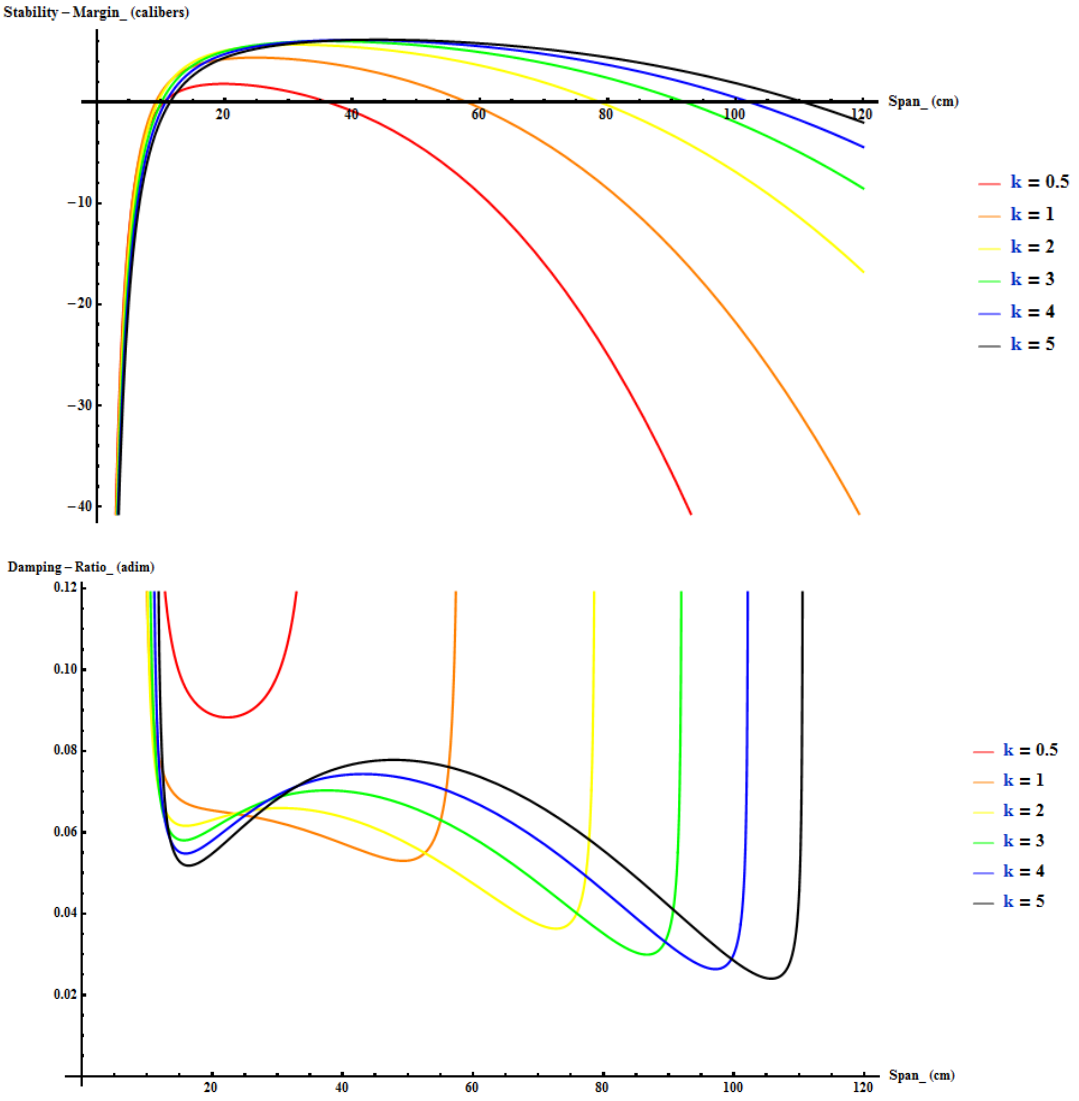

Figure 45: Fin stability margin and damping ratio as a function of the fin span and non-dimensional area.

The stability margin depends mainly on the intensity of the normal force and its point of application. Therefore its behavior is quite similar to that exhibited by the fins Cp. However it should be noted that

it is also highly dependent on the CG. Even a slight increase of the gravity center position wrt the nose of the rocket can reduce sensitively the stability margin. Since the previous graph is referred to the original CG position, the real curves for $(S;k)$ greater than the original should be shifted downwards. The damping ratio is defined only inside a span interval proportional to the fins area. The k parameter determines also if the damping ratio is going to exhibit a peak or not. From fig. 44 it can be seen how the growth of the fins normal coefficient continues only up to a span value which is proportional to k. If the latter is big enough, the greater increase in C_2 wrt C_1 results in a higher damping ratio. As soon as the C_{na} of the fins is flattened, the corrective coefficient returns to overcome the damping one hence decreasing the damping ratio. Note however that the actual range of values covered by the damping ratio remains always small for any combinations of $(S;k)$. This is due to the very high longitudinal moment of inertia of the current rocket. Enlarging the span or the fin area further lower the damping because of the increased MoI.

Assuming fins realized in CFRP with an uniform density of $1600\,\mathrm{kg/m^3}$, the variations of the mass properties related to a given fin change are shown below. The subscript "0" refers to the original design values. Note that the fins is approximated as a point mass for the calculation of the longitudinal MoI.

$$\begin{aligned} m_{tot}X_G &= \left[4m_{fin}X_{G-fin} + (m_{tot_0}X_{G_0} - 4m_{fin_0}X_{G-fin_0})\right] \\ I_L &= (X_G - X_{G-fin})^2\, 4m_{fin} + \left[I_{L_0} - (X_{G_0} - X_{G-fin_0})^2\, 4m_{fin_0}\right] \\ I_R &= 4I_{R-fin} + (I_{R_0} - 4I_{R-fin_0}) \end{aligned} \tag{48}$$

where I_{R-fin} is the moment of inertia wrt the x_b-axis and it is calculated according to [2].

The previous data regarding the moments of inertia has been compared with that given by an ANSYS model of the rocket, which is shown in the figure below. The inner subsystems have been modeled as concentrated mass points placed at the current estimated location according to [6]. The previous analytical equation matches the true variations of the radial MoI while it overestimates those related to the longitudinal one. This is due to the approximation of the fins as a point mass, which makes the resulting approach conservative.

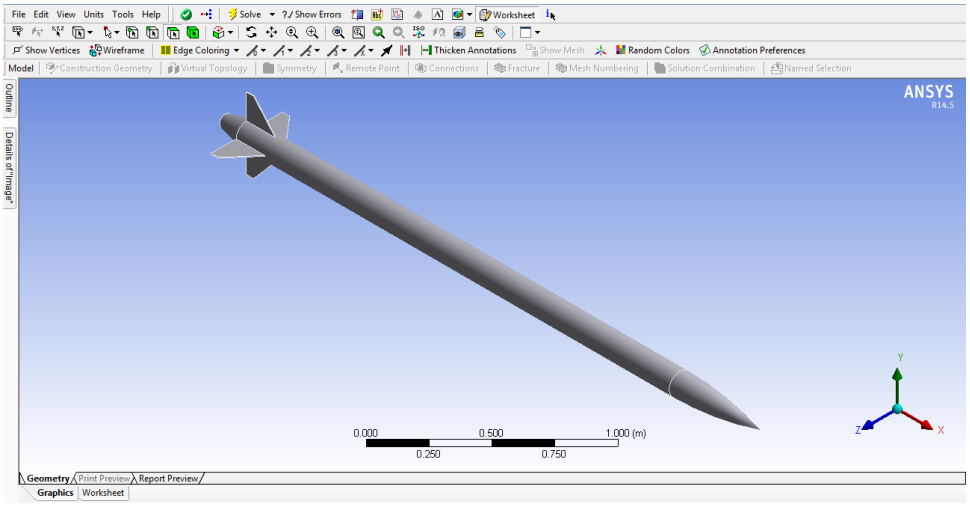

Figure 46: ANSYS model of the SMART rocket.

5.2 Iterative Procedure and Updated Design Validation

In the previous section all the relevant parameters have been written as a function of the fin's dimensions. Now the aerodynamic response of a generic design different from the original one can be calculated for a given external perturbation. The thrust misalignments are the most critical for the current rocket and so only them are going to be considered. Anyway the approach can be extended to any type of disturbance. Note however that the fluttering analysis is not left out because it is the only one able to constraint the thickness of the fins. In other words if the fin planform area is defined by the aerodynamic stability in the presence of thrust misalignments, the thickness derives from the non-fluttering condition. Note that the maximum AoA considered are obtained from the numerical approach described in section 4.2. The results are in any case conservative wrt those coming from the ASTOS software.

Any arbitrary combination of (S, k) resulting in the maximum 4 calibers stability margin can be used as a starting point. Overcoming this value would results in a model too much sensitive in weathercocking. The iterative procedure followed for the SMART rocket is reported below:

1. Assume a value for the k parameter.
2. Evaluate the span required to obtain a 4 calibers stability margin at launch from fig. 45.
3. Assume an average thickness $\hat{t}$ for the fins.
4. Calculate the root and tip chords from fig.(42).
5. Verify the assumed $\hat{t}$ with the new geometry from fig.(28). If the non-fluttering condition is invalid restart from point 2 with a greater value of $\hat{t}$.
6. Calculate the new mass properties of the updated rocket according to eq. 48.
7. Iterate from point 1 in order to consider the possible CG shift.
8. Evaluate the launch velocity from the scaled thrust profile of fig. 33. Eq. 46 can also be used since it just slightly overestimates v_L.
9. Calculate the aerodynamic coefficients according to eq.s 12-13-15.
10. Evaluate $\alpha_{1.5}$ (α_{max}) from eq. 29.
11. Find the thrust misalignment angle β_F resulting in $\alpha_{1.5}$ (α_{max}) from eq. 45 with 2.75 (2) calibers stability margin.
12. Verify β_F with the maximum allowable β_{F-max}. If $\beta_F > \beta_{F-max}$ restart from point 1 with a greater value of k.

Since no specification is provided either by DLR, NAR or Esrange about the maximum amount of thrust error, the last step of the previous procedure cannot be verified. Therefore a different way to close the design procedure is required. The $\alpha_{1.5}$, α_{max} and respective β_F resulting for some combinations of (S, k) are shown below. The variation in terms of mass and drag coefficient wrt the original SMART rocket are also reported.

k [−]	S [mm]	$\alpha_{1.5}$ [°]	α_{max} [°]	$[\beta_F]_{1.5}$ [°]	$[\beta_F]_{max}$ [°]	Δm_{tot} [kg]	ΔC_{d_0} [−]
1	140	9	26	0.15	0.35	0	0
1.5	155	17	40	0.4	0.7	0.2	0.003
2.5	160	20	47	0.5	0.9	0.8	0.01
3.5	180	23	55	0.6	1.2	1.4	0.12
4.5	200	28	65	0.8	1.6	2.1	0.16

Table 13: Design characteristics obtained from the previous procedure.

It can be seen how the bigger fins increase both the admissible AoA and the maximum misalignment angles of the thrust vector. The greatest improvement happens between the original configuration and the second design considered, which can sustain almost the double as before in terms of $\alpha_{1.5}$, α_{max} and related β_F . The following configurations present a gradually bettering response which is however paid in terms of greater mass and drag coefficient. Both are detrimental for the maximum altitude and velocity attainable by the rocket. As it will be shown later the most serious is the mass increase because it makes the rocket even more sensitive to the turn due to gravity. Moreover note that the drag coefficient jumps of about one order of magnitude between the second and third design. This happens because the average chord of the greater fin allows the flow to pass from the initially laminar to the turbulent fashion. The critical Reynolds number at which transition has assumed to occur is about $5 \cdot 10^5$ according to [2]. Therefore a possible choice is the third aerodynamics in table 13 because it ensures a sufficiently high β_F without increasing too much the mass and drag of the model.

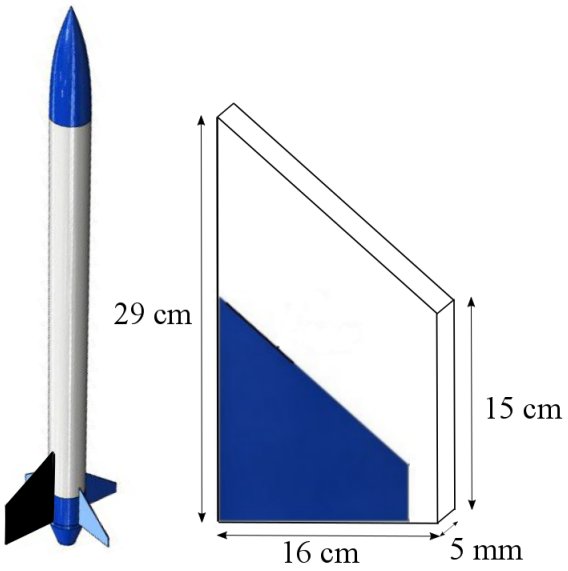

Figure 47: Sketch of the updated fin's design wrt the original one.

The figure above sketches the difference between the original design of the rocket aerodynamics and the one obtained from the previous section. The geometrical dimensions of the new fins are reported too. The table below summarizes the main characteristics of the updated version of the SMART rocket.

X_G $[m]$	m_{tot} $[kg]$	I_L $[kg \cdot m^2]$	I_R $[kg \cdot m^2]$	v_L $[\frac{m}{s}]$	C_{na} $[-]$	SM_L $[calibers]$	ξ_L $[-]$	$(\omega_n)_L$ $[\frac{rad}{s}]$	$\alpha_{1.5}$ $[^\circ]$	α_{max} $[^\circ]$	C_{d_0} $[-]$
1.95	25.8	13.4	0.06	13	16.1	4	0.07	0.75	20	47	0.4

Table 14: Main characteristics of the updated design.

This design has been validated against all the previous types of perturbations with the same procedure adopted in the previous chapter. As expected the numerical approach provides conservative results in terms of maximum AoA wrt the values obtained from ASTOS. The plot below shows the AoA profile for a 0.5° thrust misalignment. The simulation followed the same rules described in section 4.3 as much regards the shift of the Cp. The 75% curve corresponds to the solution with the mean stability margin.

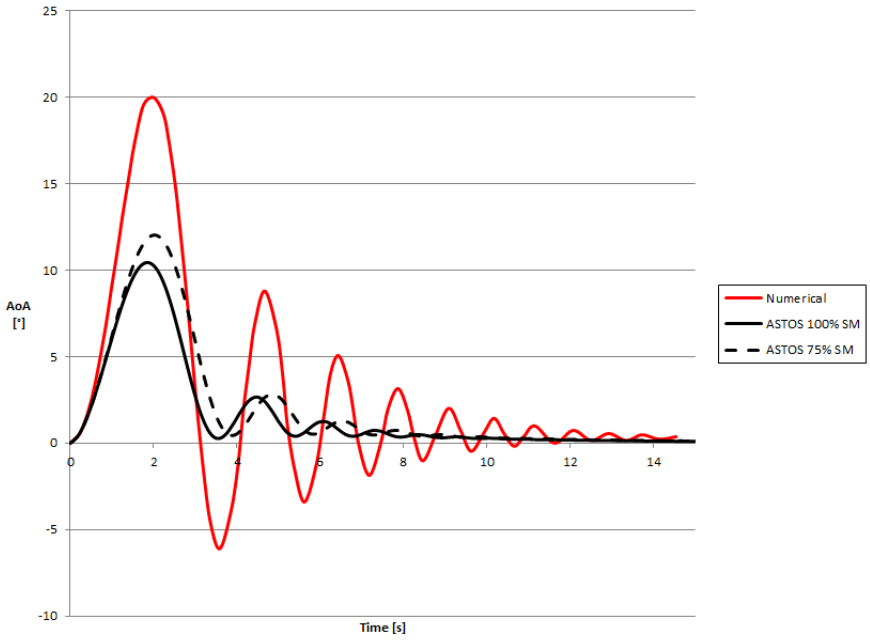

Figure 48: Numerical approach vs ASTOS solutions for a 0.5° thrust misalignment of the updated design.

The true margin in terms of misalignment angles for the maximum AoA given in table 14 has been again obtained from several ASTOS simulations with increasing β_F values. The results are shown below together with those related to the combustion instabilities and misaligned fins, both in terms of

AoA and induced roll rates. These are all calculated with the same procedure of the previous section. The flutter safe condition has been already considered inside the design procedure described before and so does not need to be further verified.

β_F [°]	e_F $[mm]$	$\alpha_{1st-peak}$ [°]	SM $[calibers]$
1.5	29	47	$SM = 0$
0.8	15	19	$SM = 1.5$

Table 15: Max thrust misalignment angles and offsets of the updated design.

ϵ [–]	H $[N \cdot m \cdot s]$	α_{1st} [°]	SM $[calibers]$
41	13	47	$SM = 0$
17	5	19	$SM = 1.5$

β_f [°]	$\alpha_{1st-peak}$ [°]
1	1.9
2	3.6

Table 16: Max combustion instabilities and fin misalignments of the updated design.

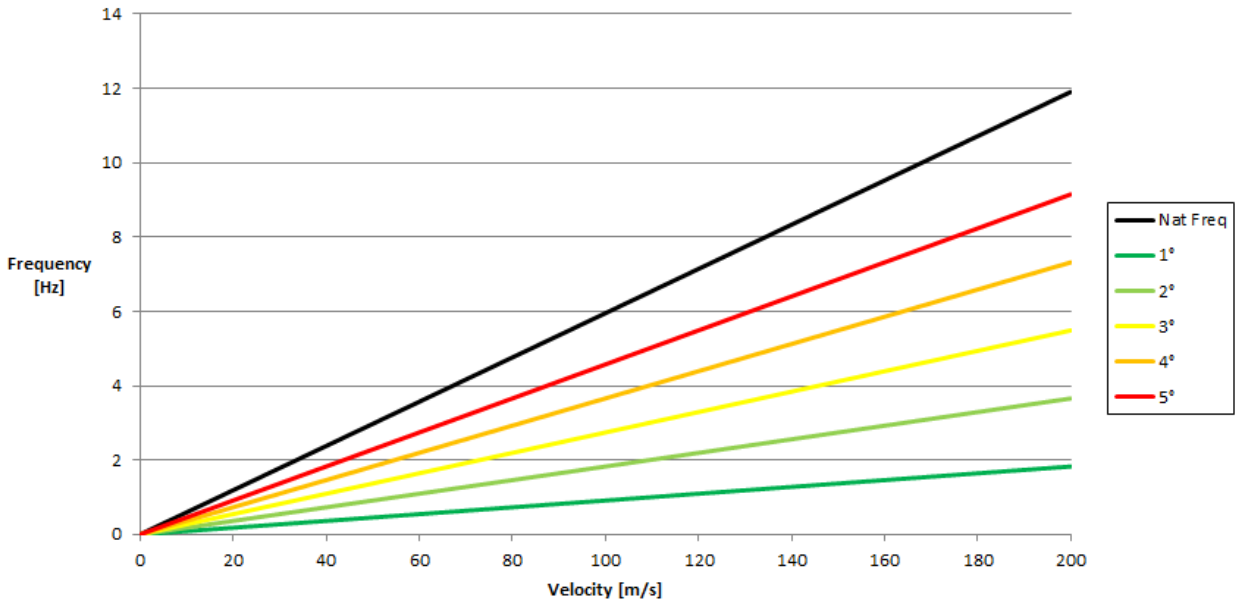

Figure 49: Induced roll rates and natural frequencies for the updated design.

As expected the rocket has benefited from the bigger fins for the combustion instabilities too. The maximum AoA in the presence of a couple of misaligned fins has been slightly worsened because of the

lower damping ratio. However the difference is negligible wrt the original aerodynamics. Note how the sustainable roll rates wrt the the pitch natural frequencies has been enhanced by the greater radial MoI. In fact even if the natural frequency has slightly decrease because of the greater longitudinal MoI, the increase in radial rotational inertia due to the larger span reduces the roll motion induced on the vehicle. This allows theoretically sustainable misalignment angles up to 5°, which is a very conservative margin wrt the maximum 2° imposed by the previous requirements. The AoA reached in the presence of wind could have been worsened but since the mass has been just slightly increased, the launch velocity is almost unchanged wrt the original design. Therefore the wind response can be assumed equal to the previous one described by table 9 and it is not repeated here. This updated design is going to be validated together with the original one from the trajectory point of view in the next chapter.

The SMART rocket is not probably going to remain equal to the configuration considered at the moment this analysis has been conducted. In particular as the project proceeds, the various subsystems of the vehicle get closer to their final shapes which may be more or less different from the one estimated at the beginning. This results in a different distribution of the masses inside the final configuration which on the other hand implies variations in the position of the center of gravity and moments of inertia. Therefore the evaluated stability margin and damping ratio may also vary consequently together with the stability response of the rocket wrt the different perturbations. The plots below show the change in stability margin and damping ratio of the improved SMART design with enlarged fins for a variation of the rocket mass properties. In particular the abscissa refers to the distance of the overall center of gravity of the vehicle from the nose cone tip.

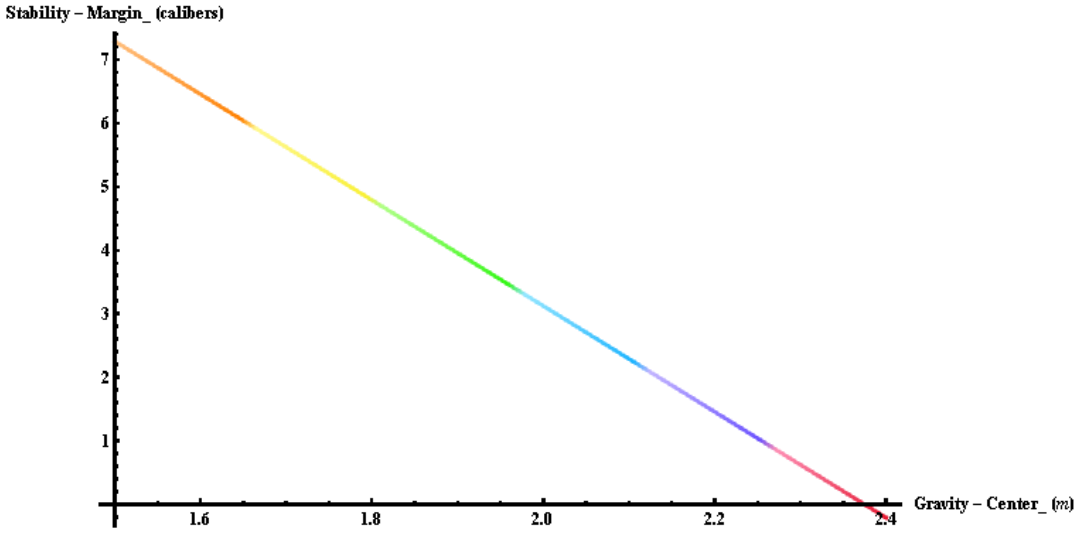

Figure 50: Variation of the stability margin wrt the center of gravity for the updated design.

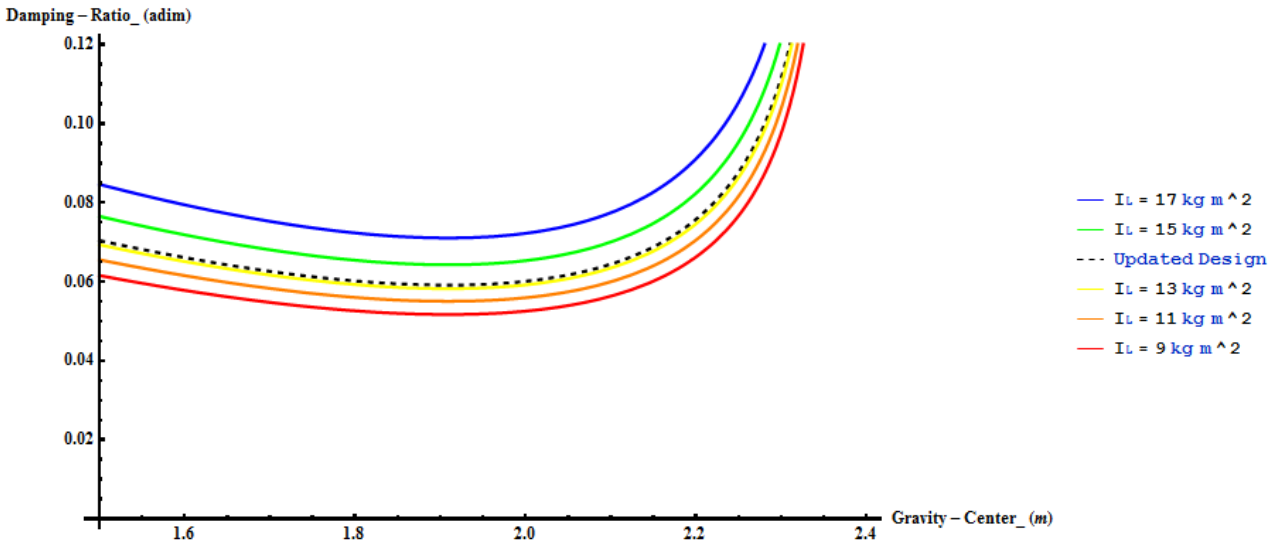

Figure 51: Variation of the damping ratio wrt the center of gravity and longitudinal moment of inertia for the updated design.

The stability margin of the rocket exhibits a perfectly linear dependance according to eq. 15. If the rocket CG moves toward the nose of the vehicle, the improved stability margin benefits the rocket stability against the thrust errors and induced roll rates in the presence of fins misalignment. In this second situation the maximum AoA reached will not increase too much since the damping ratio does not vary notably. The weathercocking in the wind is worsened by a greater stability margin but as it will be shown in the subsequent section, it can be effectively controlled by proper choice of the launch angle. On the other hand no good can come from moving the center of gravity further toward the aft of the vehicle. The reduction in stability margin decreases the maximum AoA sustainable by the rocket and so the engine and airframe errors are correspondingly lowered. In this case bigger fins should be provided in order to recover the previous stability margins.

6 Trajectory Simulation

This chapter deals with the analysis of the trajectory followed by the rocket under different launch and flight conditions. Since the ASTOS software has been intensively used for evaluating the results presented here, the first section introduces the program and its main characteristics. The general data adopted in the various simulations are presented too. Subsequently the motion of the rocket when launched both vertically and non-vertically is studied assuming that no perturbations is acting throughout the flight. The numerical results obtained have been compared to those provided by any known analytical methods whenever possible. In the last part of this chapter the perturbed trajectory due to the presence of constant horizontal winds and thrust misalignment is analyzed. The whole chapter is dedicated to the SMART rocket and the related sequence of flight events, which are detailed in the introduction of this paper. The requirements relevant from the trajectory point of view are the assurance of the rocket safe recovery, the minimum apogee of 3 km and the achievement of the speed of sound.

6.1 The ASTOS Software

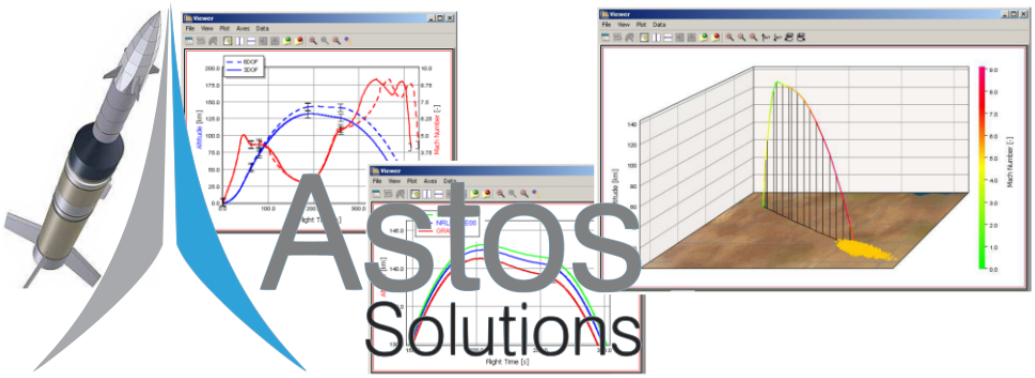

Figure 52: ASTOS Screenshot.

The ASTOS (Aero- Space Trajectory Optimization Software) software is aimed to the mission and system analysis and optimization. It combines a highly flexible scenario definition based on a graphical user interface and an extensive object oriented model library [24, 25]. ASTOS is suited to model and analyze atmospheric, orbital and interplanetary missions. However in a typical sounding rocket mission the possibility to modify some parameters is very limited. Therefore only the simulation capabilities of the software has been used. The procedure followed by the software during a simulation is made of several steps: initially the states are integrated according to the selected mode (multiple-, single-shooting or connected-phases) in every phase of the simulation, then the constraints are evaluated and verified. Finally the auxiliary functions are computed and the data are written to the output files. The multiple- and single-shooting are more suitable for an optimization analysis because they are able to detect the discrepancies in the states respectively inside or between each different phase of the model. The connected-phases mode takes the initial value of phase one for the state and then integrates over the full mission, using the phase connect conditions at each phase boundary as new

starters. The differences between the various mode is depicted below. At the actual status only the Runge-Kutta-45 integration method is present. This is an iterative method with variable step size for the approximation of solutions of ordinary differential equations.

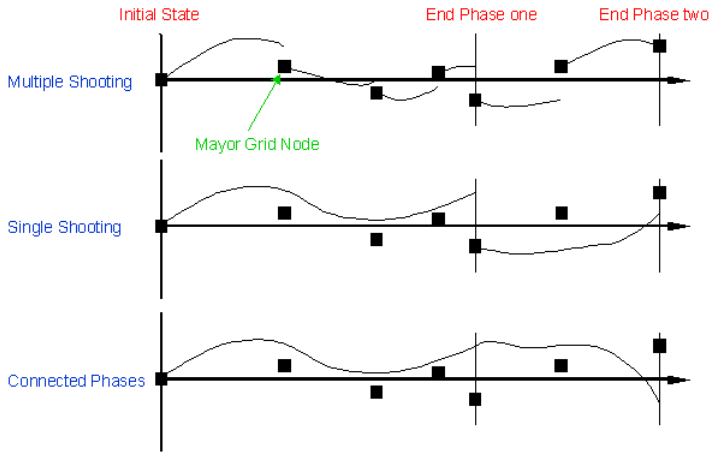

Figure 53: Possible ASTOS integration modes.

The main windows of ASTOS is a graphical user interface that makes the use of the program much easier than a traditional, command line based solution would. All the inputs in terms of aerodynamic coefficients, propulsion and attitude data are provided to the software inside the Model Browser, then initialized and simulated for each phase according to the selected type of equation of motion (EoM). The latter uniquely defines the position and velocity vector wrt an inertial reference frame as a function of six state variables. The type of EoM depends on the phase that needs to be simulated. For the SMART rocket the model adopted to describe the flight sequence is reported below.

1. Initial state. Rather than being a real phase of the model, this is used to define the initial state of the vehicle. In the case of a non-vertical launch the direction of the velocity vector is defined here.

2. Ignition. The moment at which the rocket has turned on the engine but the thrust has not yet overcome the initial weight. Therefore the vehicle is not moving with an increasing acceleration. If the rigid-body motion of the rocket is considered during the simulation, the launch orientation of its body axis reference system is defined here.

3. Launch. The vehicle moves guided by the launch tower. If a perturbation such as wind or thrust misalignment has been inserted in the simulation, it does not affect the rocket during this phase.

4. Powered flight. The rocket flies in the atmosphere under the action of thrust, weight and aerodynamic forces. The presence of possible disturbances can be modeled too.

5. Coasting flight. After the burnout the vehicle proceeds inertially toward the apogee of its trajectory. If the ballistic motion of the rocket needs to be simulated, this phase lasts until the ground impact.

6. Drogue chute descend. The first recovery device is deployed after the culmination has been reached. This allows to better control the descent of the rocket. The phase-is-over command allows to impose the end of the coasting flight and the beginning of the drogue descent without manually iterating the time interval of each phase.

7. Main chute descend. The main parachute will further reduce the descend rate of the rocket until landing. It is supposed to be ejected at an altitude of 500 m. Again this can be imposed in the model by another phase-is-over constraint. The landing of the vehicle too is defined by a similar constraint on the final altitude.

Once that the phases are defined it is necessary to provide the software the required attitude control, propulsive and aerodynamic data. The SMART rocket is not supposed to be actively controlled during any portion of its flight. Therefore the attitude of the vehicle will act as a 6dof uncontrolled body and it has been effectively simulated by means of the *aerodynamic angles uncontrolled* attitude model. The propulsive data consist of the constant thrust and mass flow rate that the engine is supposed to provide at the design operational point. The distance between the gravity center and the nozzle exit area is also provided in order to consider the jet damping effect too. The aerodynamic models provided by ASTOS can be divided in two main groups:

- 3dof models, which consider the vehicle as a point mass coincident with its gravity center.
- 6dof models, which describes the rigid-body motion of the $\{x_b; y_b; z_b\}$ reference system too.

The first category was used for the preliminary analysis of the rocket vertical flight with no perturbing terms. The second instead has been intensively adopted for the description of the rocket trajectory when launched at an angle and in presence of possible disturbances. Therefore the only aerodynamic coefficient provided to the 3dof model is the drag coefficient C_D. The latter can be defined in the Model Browser as a function of the Reynolds number according to eq. 9. Note that in this way the induced drag when flying at an AoA is neglected. ASTOS can account for the latter with the *Lift_ Tan_ Alpha* record, which compute the induced drag coefficient $C_{D_{AoA}}$ as the velocity projection of the overall normal force of the rocket. Otherwise [2] provides an empirical equation which describes the induced drag due to the body and fins only. The same technique is used for the drag data in the 6dof analysis. In this case however it is also necessary to provide the coefficients of the other aerodynamic forces and moments which act on the rocket during the flight. The general aerodynamic moment according to ASTOS is given by:

$$\left[\overrightarrow{M}\right]_{aero} = \frac{1}{2}\rho A_{ref} L_{tot} \overrightarrow{C_M} + \overrightarrow{F_a} \Delta \overrightarrow{x} \tag{49}$$

where $\overrightarrow{C_M}$ is the overall aerodynamic moment coefficient and $\Delta \overrightarrow{x}$ the position vector between the CG and the Cp of the vehicle.

As stated before ASTOS does not allows to define the components of the $\Delta \overline{x}$ vector as a function of the AoA. This means that the shift of the Cp must be considered manually every time the rocket is exposed to a relevant deflection. The procedure to overcome this problem has been already described in section 4.3. For the current symmetrical rocket design the previous vector reduces to the Δx_b distance measured along the body frame. The only aerodynamic force to be considered is the normal force developed as the vehicle flies at a non-zero AoA. ASTOS allows to define it as a function of the

AoA derivative, which is assumed to coincide with the Barrowman C_{na} coefficient. The body term contribute is neglected because of its direct dependance on the AoA which would require the choice of a different aerodynamic model. The results obtained in this way are conservative because the corrective moment has been in any case underestimated (see fig. 23). The only aerodynamic moment still left out is the damping one given by eq. 13. This can be defined in the $\overrightarrow{C_M}$ coefficient as a function of the first AoA derivative according to:

$$C_{damp} = \frac{2}{L_{tot}^2} \Sigma C_{na_i} \left(X_{Cp} - X_G\right)^2 \tag{50}$$

where the $\frac{2}{L_{tot}^2}$ is just a normalization factor used by ASTOS to adimensionalize the $\overrightarrow{C_M}$ coefficient.

Now that all the data required have been provided to the software, it is possible to simulate the flight in a lot of different conditions. Vertical and non-vertical launch, presence of thrust misalignments and windy conditions have been all considered to validate the trajectory of the SMART rocket. The differences between the original design and the one with slightly bigger fins have been analyzed too. The respective data can be found in table 5-14. From now on the second will be referred to as the *updated* SMART version of the rocket. As an example the problem summary for the 6dof analysis in the presence of wind is shown in appendix 8.3.

The Rocksim and Openrocket software have also been considered in the study of the rocket trajectory. The first is a commercial program which model rocketeers have been employed for fifteen years [4]. It has been only partially used because of the limitations of the trial version. The Openrocket is an open source software developed by S. Niskanen in his master-thesis work [3]. Altough valid it does not suit to the STERN project because it does not allow the customization of the engine thrust-profile. However it is one of the only freely available programs able to take into account of the Cp shift, as it is shown in the figure below.

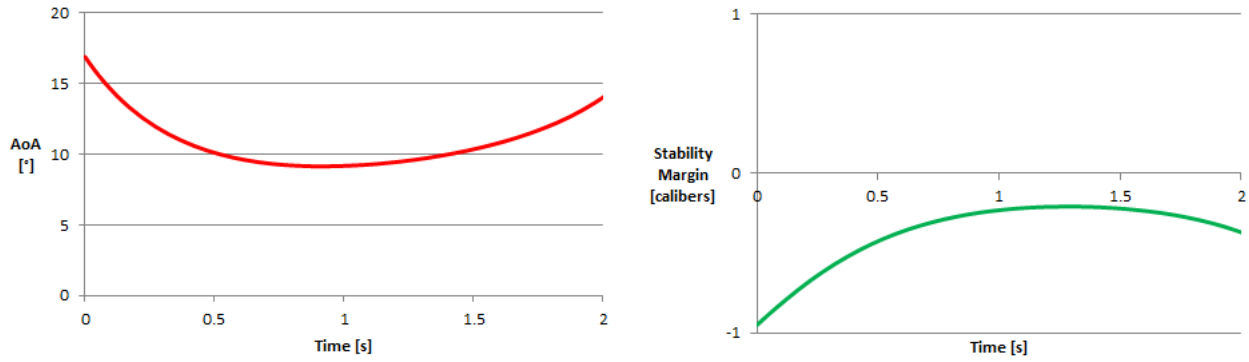

Figure 54: Cp shift capability of the Openrocket software.

6.2 Vertical Launch

As the rocket is assumed to be launched vertically and to encounter no perturbations, the AoA of the vehicle will remain equal to zero throughout the flight. Therefore the aerodynamic force vector reduces to the drag force only. The flightpath is so reduced to a 1-dimensional motion under the action of thrust, weight and drag. The eq. 1 simplifies into:

$$m\frac{dv}{dt} = F - mg - kv^2 \tag{51}$$

where $k = \frac{1}{2}\rho A_{ref} C_D$ is the *drag constant*.

The drag coefficient C_D depends on the shape of the aerodynamic surfaces and on the Reynolds number encountered by the rocket during the flight. As stated in section 2.2 a constant average C_{D_0} can be defined without compromising the accuracy of the results. The value obtained previously has been overestimated to 0.4 in order to keep into account for the factors neglected in the analytical calculation. The mean values of the rocket mass, gravity acceleration and density are considered too. The first one is given by the mean between the initial and burnout mass while the others can be iterated when a possible final altitude is assumed. The engine is supposed to produce an average thrust of 500N at the design conditions. With these simplifications eq. 51 can be written as:

$$\frac{dv}{dt} = c_1 - c_2 v^2 \tag{52}$$

where $c_1 = \frac{F}{m} - g$;$c_2 = \frac{1}{2}\frac{\rho A_{ref}}{m} C_{D_0}$

Two methods permit to solve the previous equation applied to the powered part of the trajectory, one derived by L. G. Fehskens and D. J. Malewicki and the other by G. J. Caporaso [2]. These have been extended to the other portion of the flight, i.e. the coasting flight until culmination and the subsequent descent.

The Fehskens-Malewicki solution (F-M from now on) is obtained by direct integration of eq. 52 through separation of variables. The Caporaso method (Cap) adopts the following simplification:

$$\int_0^{Bo} v^2 dt = \int_0^{Bo} \frac{dz}{dt} v dt = [zv]_0^{Bo} - \int_0^{Bo} z a dt = z_{Bo} v_{Bo} - \int_0^{Bo} z a dt \cong z_{Bo} v_{Bo} \tag{53}$$

This is justified by the fact that the vertical acceleration typically grows at a much higher rate than the displacement does. The Caporaso solution is of particular interest in the case of non-constant thrust because it allows its direct integration over the time. After the burnout, the constant c_1 reduces to $(-g)$ and eq. 52 can still be integrated with a slightly different procedure.

At the culmination c_1 reverses its sign because now the velocity is directed toward the ground, i .e. the gravity accelerates the rocket. If a second chute is supposed to deploy, eq. 52 is simply spit in two parts and integrated separately with different initial conditions and c_2 coefficients. The latter depend on the descend velocity which the parachute is supposed to provide and can be obtained from the following relation.

$$c_2 v_{eq}^2 = \frac{1}{2}\rho A_{chute} C_{D-chute} v_{eq}^2 = m_{Bo} g \tag{54}$$

The SMART rocket's descent is controlled by means of two parachutes, the drogue and the main one. The first is deployed at apogee and it is designed for a descend rate of about 20-25 m/s while the second deploys at 500 m and provides a 5-6-m/s descend velocity. The time solutions of displacement, velocity and acceleration are reported in appendix 8.2. These have been applied to the original and updated version of the SMART rocket and the results in terms of apogee and burnout velocity are reported below.

	Original SMART rocket		Updated SMART rocket	
	Caporaso	F-M	Caporaso	F-M
Max altitude $[km]$	4.1	4.3	3.9	4.2
Max velocity $[\mathrm{m/s}]$	205	215	200	210

Table 17: Analytical results for the original and updated design of SMART rocket launched vertically.

The differences between the two are negligible because of the minimal mass and drag increase. This is also confirmed by the simulations which have been conducted with ASTOS. In particular the original design has been studied only with a 3dof model while the updated in both 3dof and 6dof fashions. However as it shown in fig. 55, there is no difference between the last two because of the no-perturbation assumption.

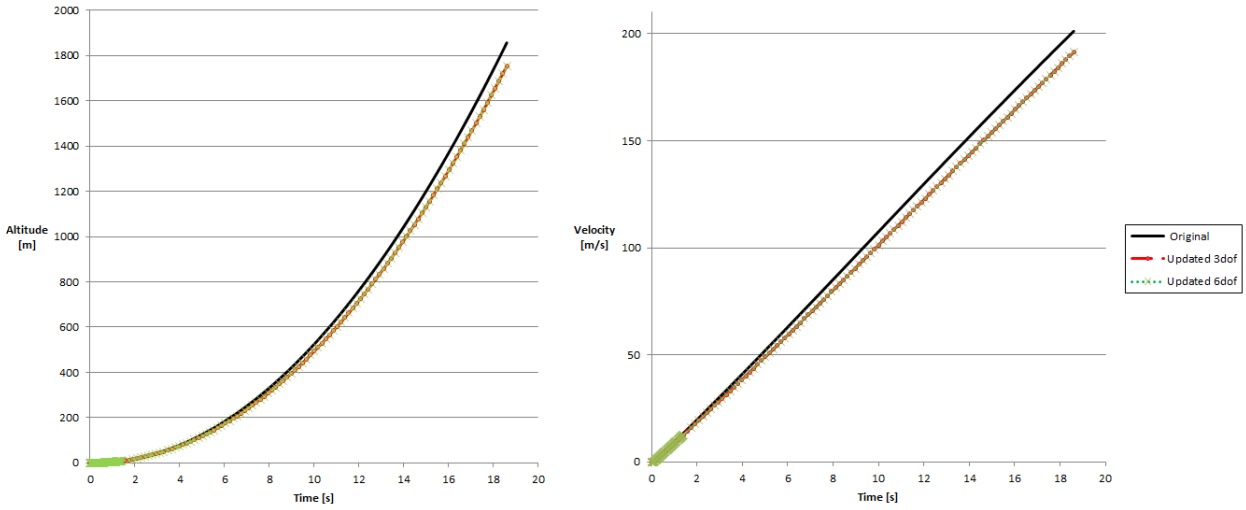

Figure 55: ASTOS results for the original and updated design of SMART rocket launched vertically.

The complete time profiles of displacement, velocity and acceleration for the original SMART design are reported below. Note that also the number of the phase is reported too.

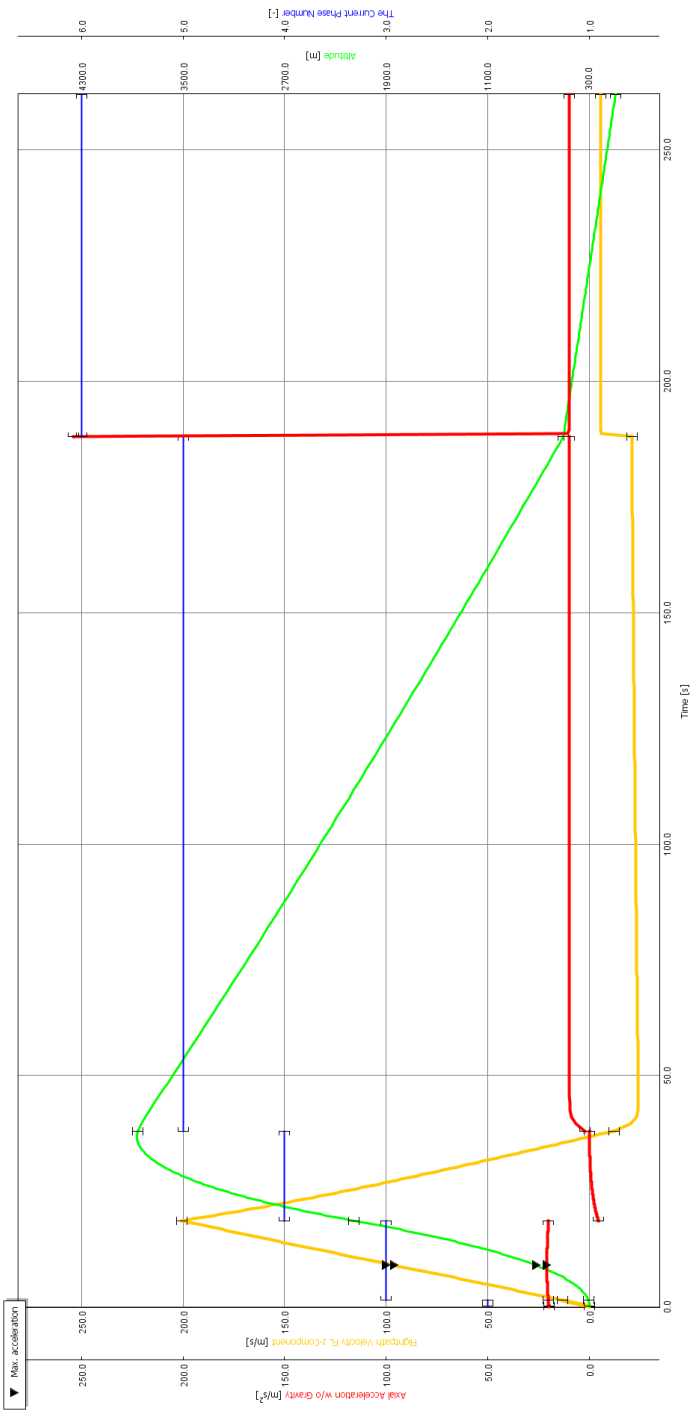

Figure 56: ASTOS 3 dof results for the original design of SMART rocket launched vertically.

During the descent the peak of acceleration at about 500m corresponds to the moment at which the drogue is released and the main chute deploys. Actually it is due to the impulsive shift in drag coefficient seen by the program as the integration proceeds from phase 5 to phase 6. The model can be refined by considering a time changing reference area for the aerodynamic coefficients. This would simulate better the gradual opening of the deployment device. The same peak is not present at the moment the drogue deploys just because at culmination the velocities are much closer to zero. The data obtained from the ASTOS simulation of the updated design have been compared with those of the analytical approach. The various solutions are plotted below. Note again how the results only slightly differ from those of the original design shown before.

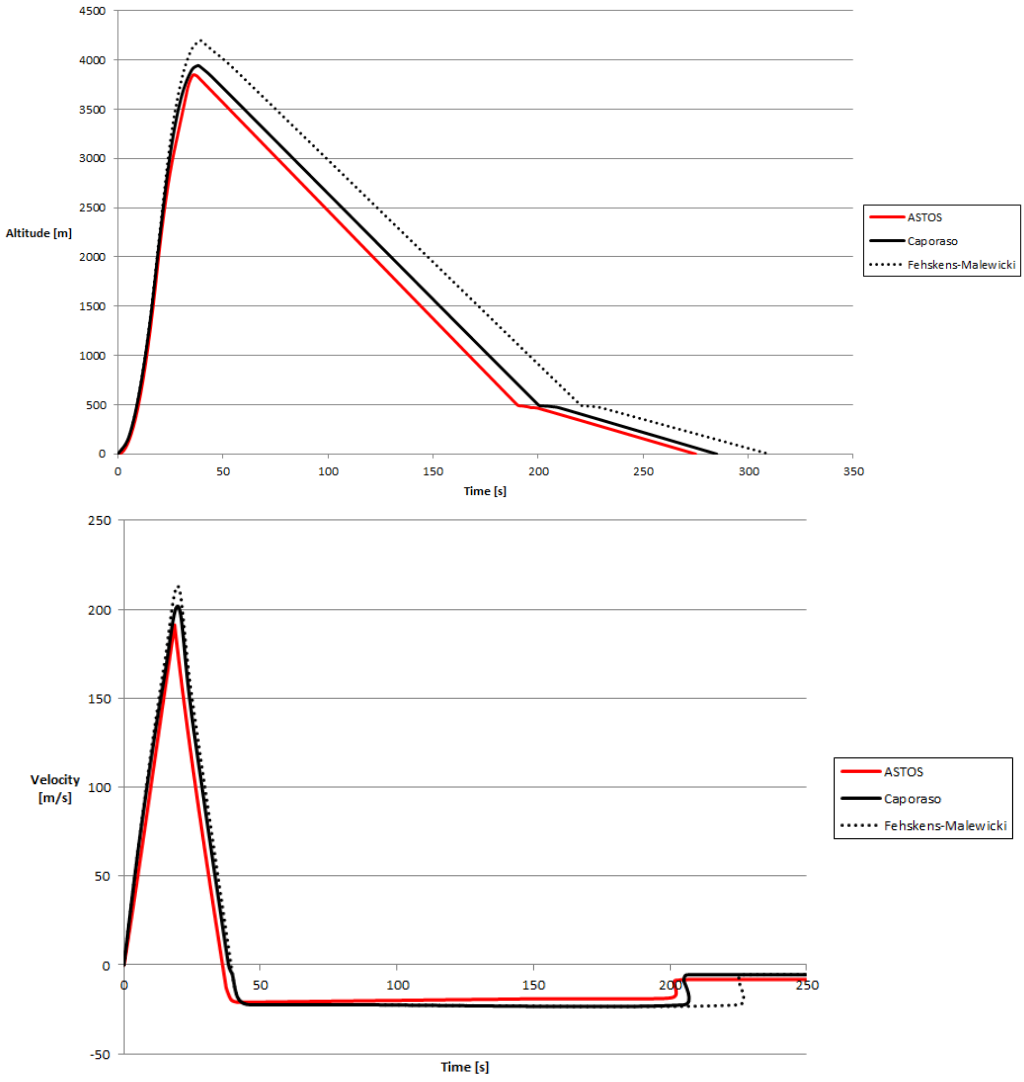

Figure 57: Analytical and ASTOS results for the updated design of SMART rocket launched vertically.

As you can see the analytical approach slightly overestimates both the maximum altitude and velocity reached by the rocket. This is due to the approximation of considering a constant C_{D_0}throughout the calculations. However all the solutions confirm that the rocket is not able to reach the speed of sound. Although the altitude requirement is fully satisfied, the excessive weight and low thrust prevent the velocity to overcome mach of about 0.6. The thrust and the structural mass of the rocket have been varied in order to evaluate the improvement that would be needed to achieve the sonic condition. The first is considered because there may be the possibility to increase the pressure in the propellant tanks hence providing higher mass flow rate to the engine. On the other hand the final value of the structural mass is not yet fixed at the actual state of the project. The results are shown in the following table.

	Thrust [N]				Structural Mass [kg]			
	500	600	650	700	20	18	15	13
Mach [−]	0.6	0.75	0.9	1	0.6	0.7	0.85	0.95
Max velocity [m/s]	200	240	295	320	200	230	280	310

Table 18: Mass and thrust values required to achieve the speed of sound.

The previous data comes from the ASTOS simulations. The analytical solution reaches the requirement with lower variations of thrust and structural mass. Because of the effort required the sonic-speed requirement is not likely to be achieved and it has been therefore neglected in the subsequent analysis. The main problem is due to the choice of a liquid propelled engine which is typically characterized by higher structural mass wrt a solid propelled rocket.

6.3 Non-Vertical Launch

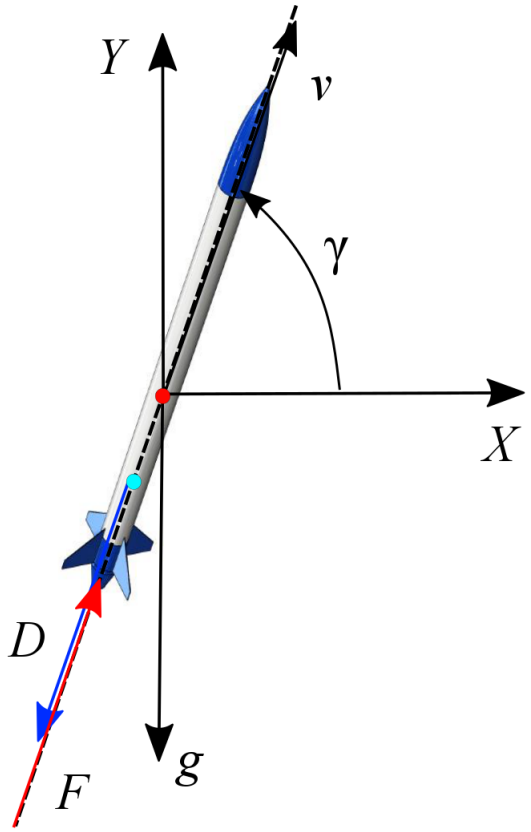

Figure 58: Non-vertical motion of the unpertubed rocket.

Usually launches are never exactly vertical in order to avoid the risk of landing in the proximity of the launch site. General maximum allowed angle in Esrange is 89° but for the STERN project it is just 80° because of the experimental nature of the project itself. If the rocket is launched at an angle, the resulting trajectory will be a 2-dimensional one in the plane of the initial launch velocity vector. Therefore eq. 1 can be written as a function of the X-Y components defined in fig. 58 in the following form:

$$\frac{dv_X}{dt} = \frac{F - D}{m} \cos\gamma$$

$$\frac{dv_Y}{dt} = \frac{F - D}{m} \sin\gamma - g$$

However it is convenient to use the speed v and the flightpath angle γ, still defined in fig. 58, as dependent variables instead than v_X and v_Y. Previous eq.s become:

$$\frac{dv}{dt} = \frac{F - D}{m} - g \sin \gamma \tag{55}$$

$$\frac{d\gamma}{dt} = -\frac{g}{v} \cos \gamma \tag{56}$$

As soon as the rocket is launched non-vertically, the velocity vector will start to rotate because of the gravitational component acting on the perpendicular direction wrt the longitudinal body-axis (see eq. 56). This effect is commonly called *gravity-turn* and it is also employed during the ascent of modern launchers to start rotating the vehicle without any propellant consumption. However this g-turn is only detrimental for the purpose of the SMART rocket. The amount of rotation imposed on the vehicle depends mainly on the specific thrust and initial launch condition. Rockets with a low thrust-to-weight ratio experience severe g-turns as the gravity is comparable to the thrust acceleration. Moreover launching at a great angle wrt the vertical and at low speeds further worsen the overall situation.

Despite there are no closed-form solutions describing the whole trajectory for a non-vertical launch, [26] presents an analytical method which is valid up to the burnout point. It is based on the assumption of a constant effective specific thrust equal to:

$$\beta_{eff} = \frac{F_{eff}}{mg} = \frac{F - D}{mg}$$

The results given by the analytical approach are shown below for different effective specific thrusts, launch speeds and launch angles. The ranges of variation have been chosen in the vicinity of the original SMART rocket values.

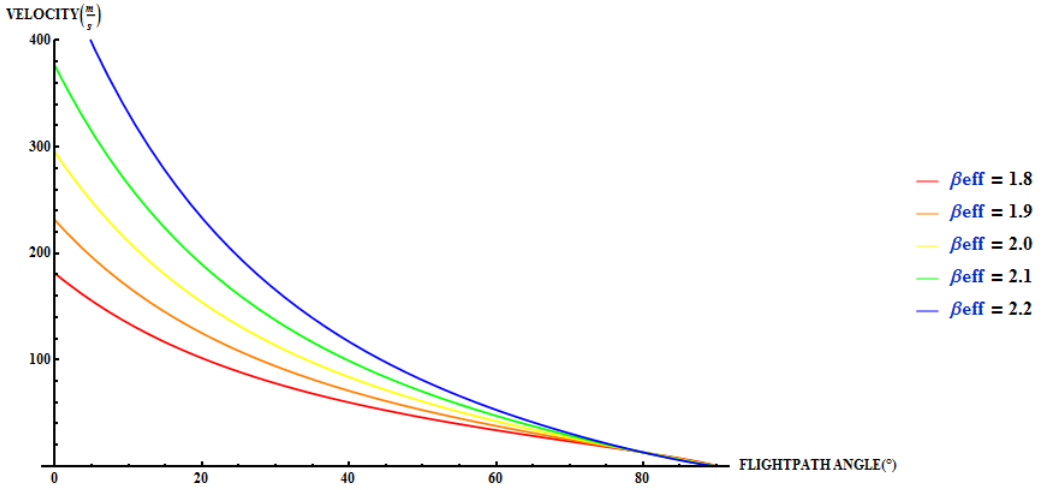

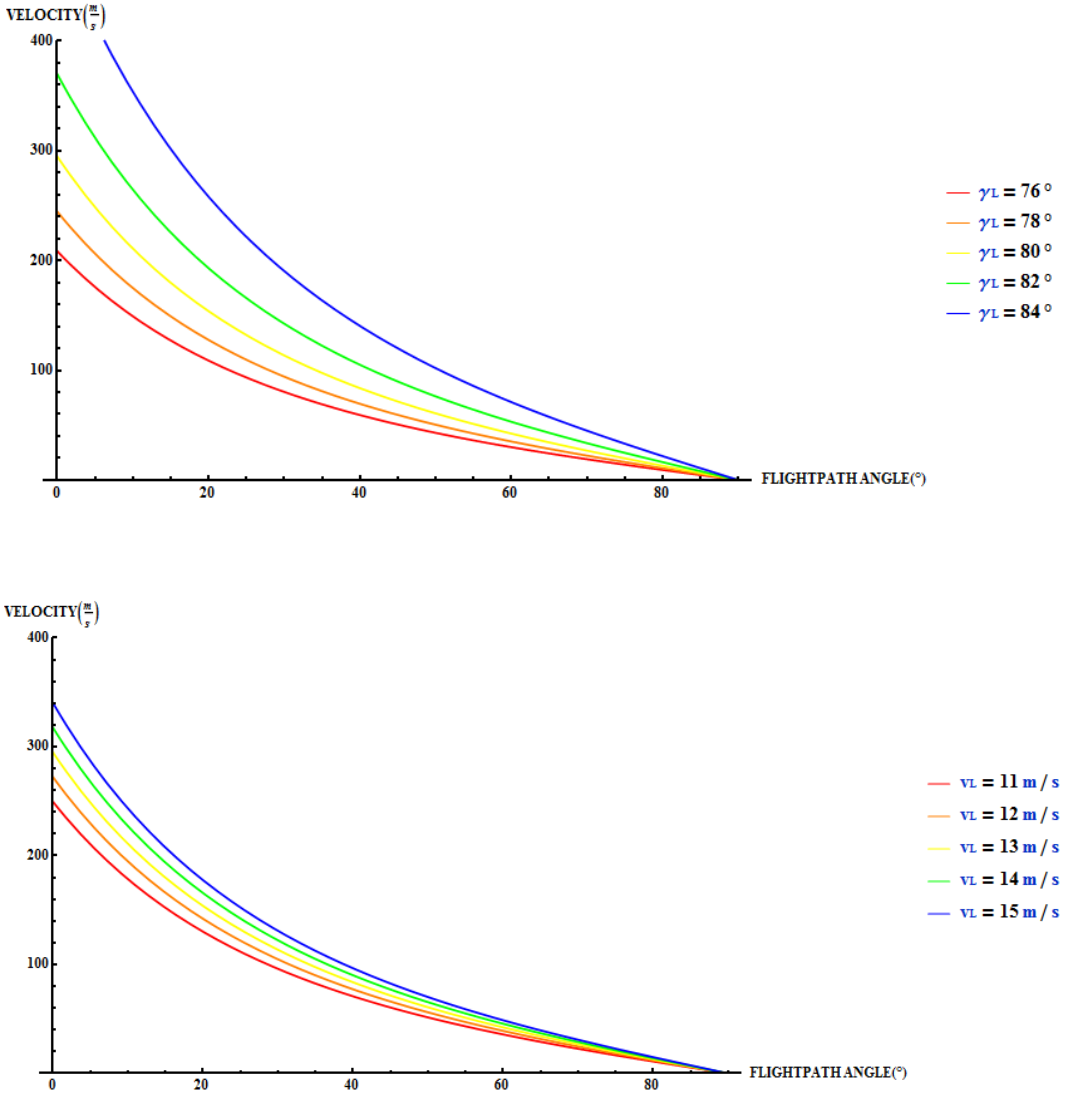

Figure 59: Gravity turn sensitivity charts for the flightpath angle with different launch conditions.

From the previous it can be seen that the g-turn is more sensitive to a change of β_{eff} or γ_L rather than v_L. The analytical results for the the updated design are compared below with those obtained from ASTOS, both with 3dof and 6dof models. Those related with the original design of the SMART rocket are not showed because they are only slightly different from the other. Note that only the vehicle ballistic motion has been considered, i.e. the motion without the opening of the parachutes.

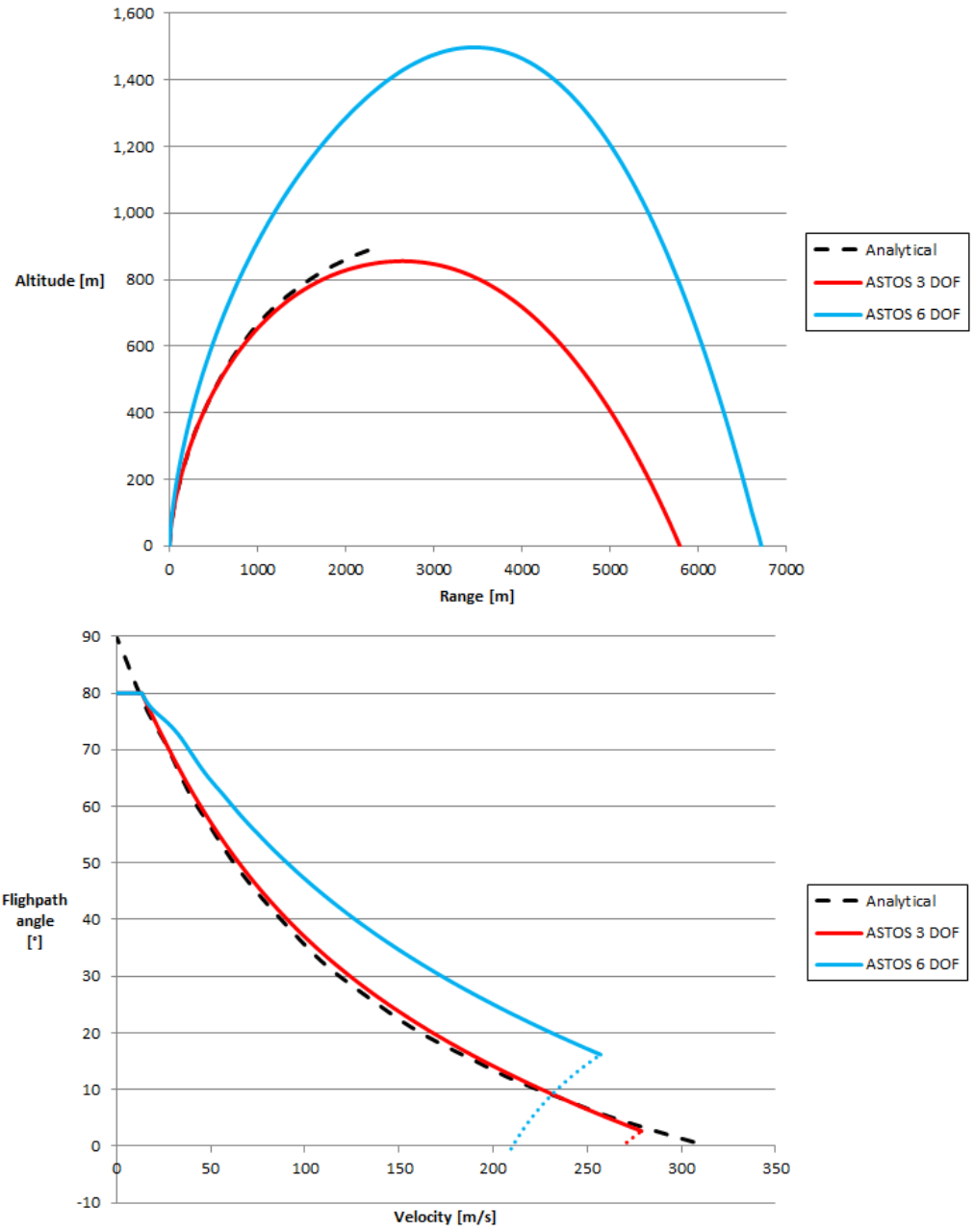

Figure 60: Analytical and ASTOS results for the updated design of the SMART rocket launched non-vertically.

From the previous it can be seen how the altitude requirement is far from being fulfilled. For the SMART rocket the β_{eff} is about constantly equal to 2 throughout the flight. This together with the

80° launch angle and the low launch speeds makes the initial turn so severe that the apogee is about half wrt the one obtained for a vertical launch. Moreover the rocket reaches the culmination point with horizontal velocities above 200$^{m}/_{s}$! This makes extremely hazardous the recovery of the vehicle. At such high speeds the ejection of the upper part of the rocket may be prevented by the high dynamic pressure acting on the nose cone. Moreover even if the latter is successfully ejected, the deployment of the chutes is highly uncertain. It is more likely that the chords of the chute will tangle together or around the vehicle hence becoming completely ineffective in slowing down the rocket descent. These high culmination velocities are due to the fact that only the drag is contributing in dissipating the horizontal kinetic energy after burnout. Therefore its decreasing rate is much lower than the one of the vertical component, which feels also the losses due to gravity.

Note that the analytical method almost coincides with the 3dof ASTOS analysis. The 6dof instead exhibits a notable shift. This is due to high rotational inertia of the rocket that slows down the gravity turn in the initial part of the flight. As soon as the rocket has left the launch tower, its velocity starts to rotate downwards under the effect of the gravity according to eq. 56. This turn is very effective for the SMART rocket because of the very low launch speed. However the high longitudinal moment of inertia makes the body vertical axis hard to be deviated from the original intended direction. Moreover the natural pitch (or yaw) frequency of oscillation is minimum at launch because of its velocity dependance. The overall effect is that the rigid-body motion develops on slower time-scale wrt the one of the velocity turn. This is demonstrated by the time-profile of the vehicle AoA shown in the figure below.

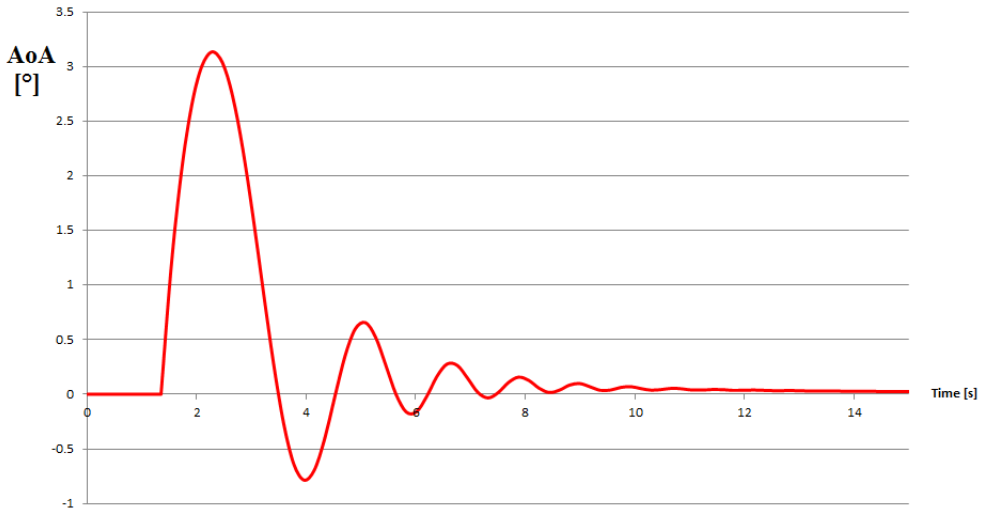

Figure 61: Time profile of the AoA for the updated design of SMART rocket launched non-vertically.

Until the rocket is moving on the rails the AoA remains constantly equal to zero. As the vehicle clears the rails, the gravity rotates the velocity vector toward the ground while the rocket vertical axis remains fixed in the original direction. The resulting non-zero AoA is then smoothed down by the corrective aerodynamic moment of the rocket. Even if the maximum angles reached are about equal to 3° only, the overall effect is quite relevant since it almost doubles the maximum trajectory achieved by the rocket wrt the other approaches. The 3dof and the analytical analysis in fact are not able to separate the rigid-body dynamics from the point mass motion of the vehicle. Therefore as soon as

the velocity vector is rotated the thrust immediately follows this turn. In reality the thrust vector is pointing toward the intended flight direction for a longer time due to the rotational inertia of the rocket. To further demostrate this statement, several simulations with gradually reducing MoI were run in ASTOS. In the next figure the MoI is scaled as a percentage of the initial value presented in the 6dof model.

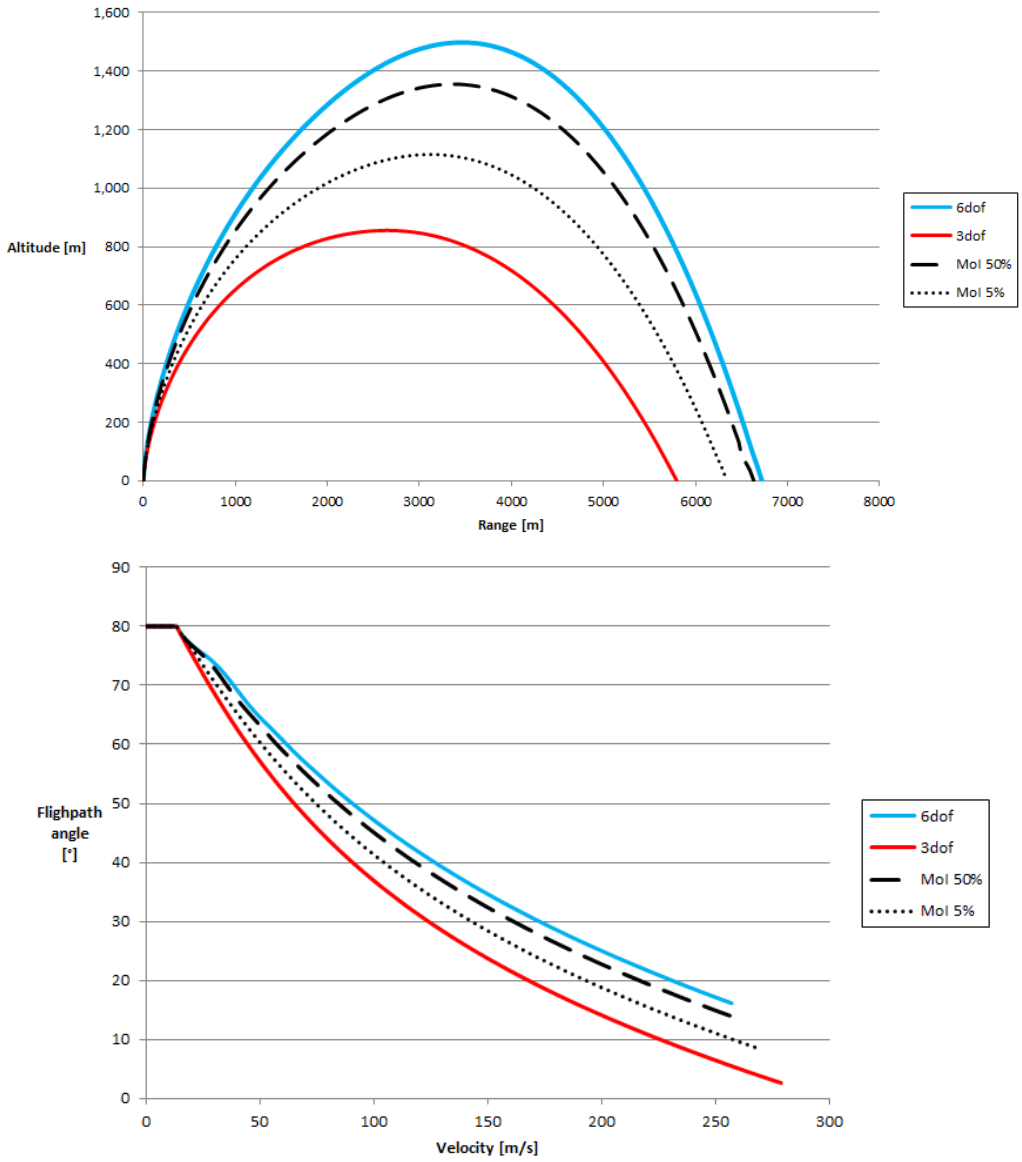

Figure 62: 6dof results for scaled longitudinal moments of inertia.

As expected the curves tend to the 3dof result with lower values of the moment of inertia. This is reasonable because the natural frequency of oscillation increases as the MoI decreases hence fastening the rigid-body dynamics of the vehicle.

However even with this benefits from the high MoI, the rocket can neither reach the minimum altitude nor achieve sufficiently low culmination velocity able to ensure a safe recovery. The simplest way to overcome these problems is to increase the launch angle. Assuming 89° as the maximum elevation for the launch tower, the flight of the updated rocket has been simulated with different launch angles in order to verify which one is the minimum satisfying the previous requirements. The results are reported below. The continuous line in the velocity plots corresponds to the powered flight until burnout while the dashed one to the coasting until culmination.

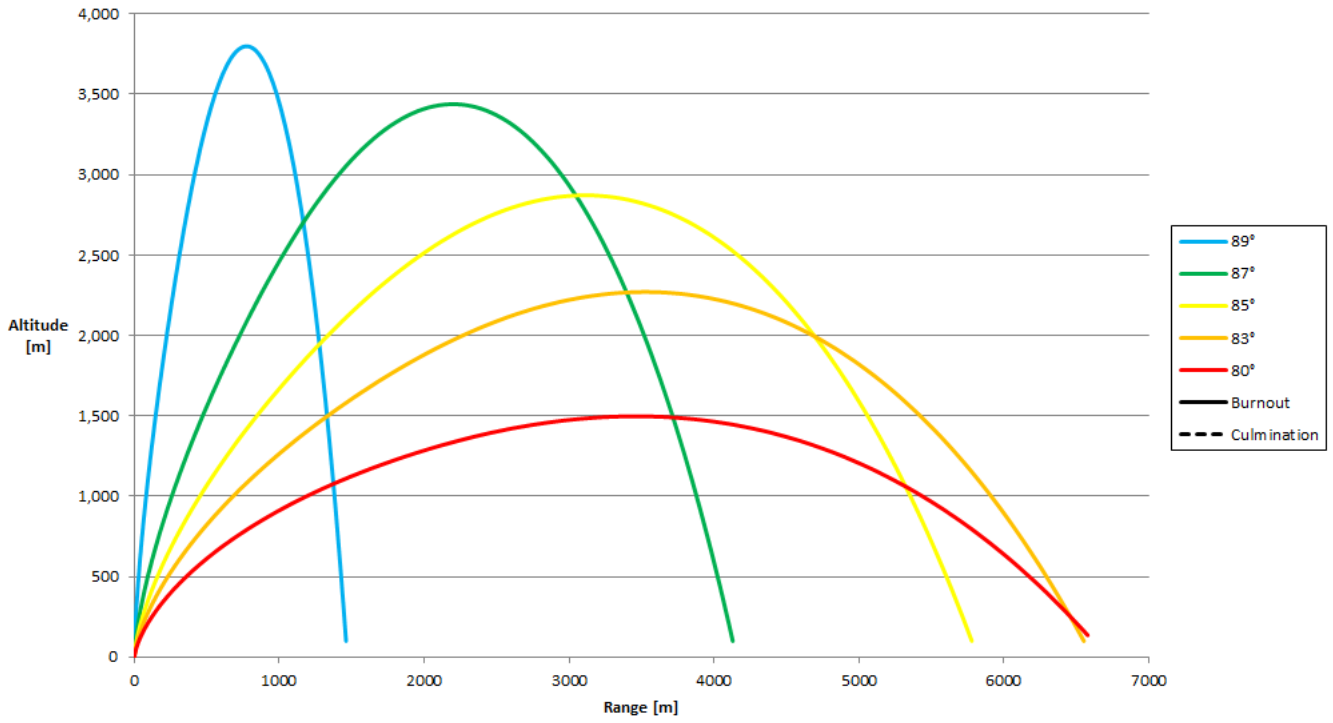

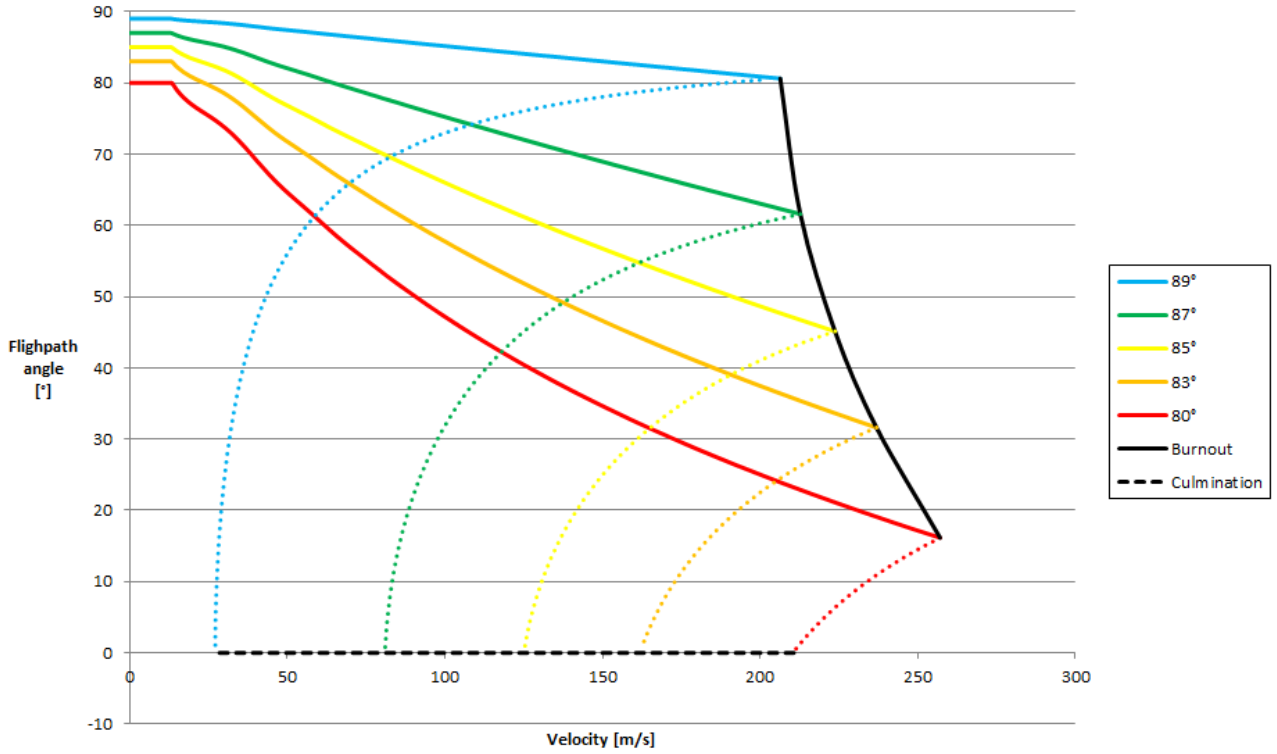

Figure 63: Flight profiles of the updated SMART rocket launched at various angles.

From above the minimum angle needed to reach the 3km apogee is about equal to 86°. The related culmination speeds are still too high to ensure the safe recovery of the vehicle with common parachutes. Further analysis is needed once that the requirements of the deployment devices are known. However the previous study is useless if the possibility to choose the launch angle is not allowed by the provider of the launch site. Therefore again a parametric study involving the structural mass and the thrust of the final rocket has been realized. Different situations involving variableβ_{eff} have been considered. In particular the thrust and mass have been varied respectively between 500-700N and 15-20kg. In the figures below there are plotted the curves for thrusts of 500 (black lines), 600 (red) and 700N (blue), maximum (dashed) or minimum (continuous) mass. Note that in the legend the overall mass is indicated rather than the structural mass. The intermediate combinations can be extrapolated depending on the relative values of thrust and mass considered. For example the trajectory of a rocket with 600N thrust and 18kg structural mass will lie somewhere between the continuous red and dashed red curves in the corresponding launch angle plot. The one for a 650N-20kg design instead will be comprised in the middle of the continuous red and blue curves. Note that only the time evolution near the culmination point has been included in the velocity graphs not to overload the plots. The burnout conditions are included inside the dash-dotted-continuous rectangle.

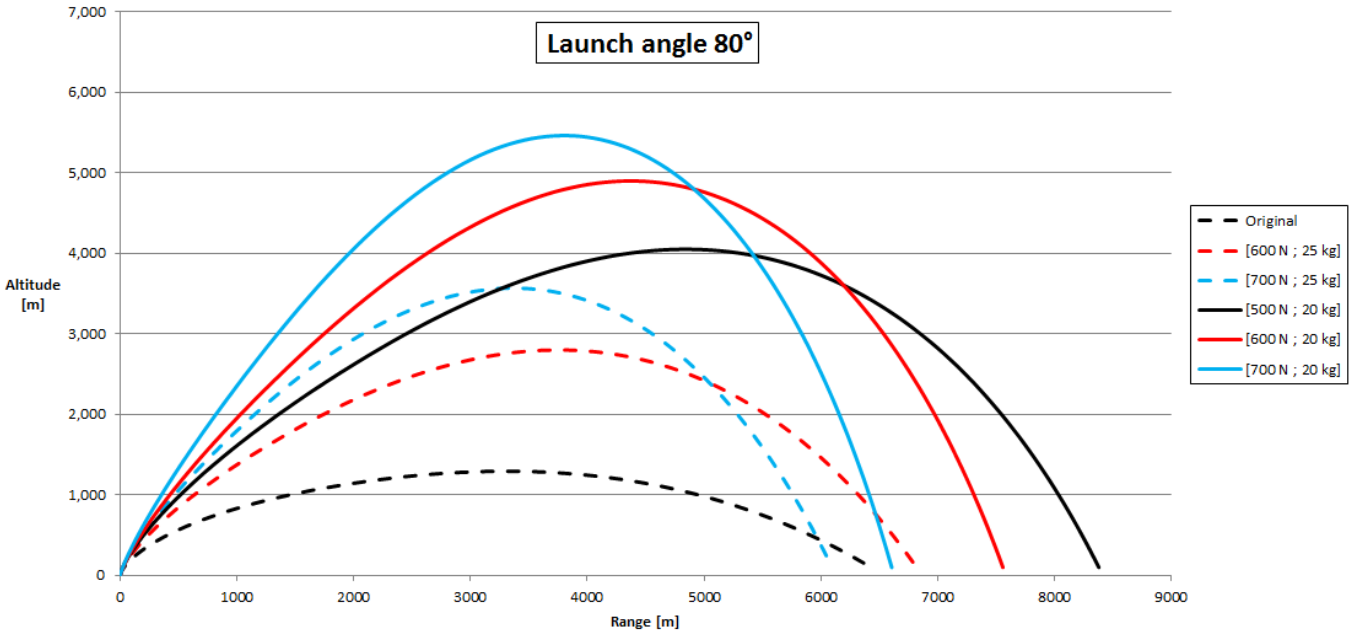
Launch angle 80°
Altitude [m]
Range [m]
Original
[600 N ; 25 kg]
[700 N ; 25 kg]
[500 N ; 20 kg]
[600 N ; 20 kg]
[700 N ; 20 kg]

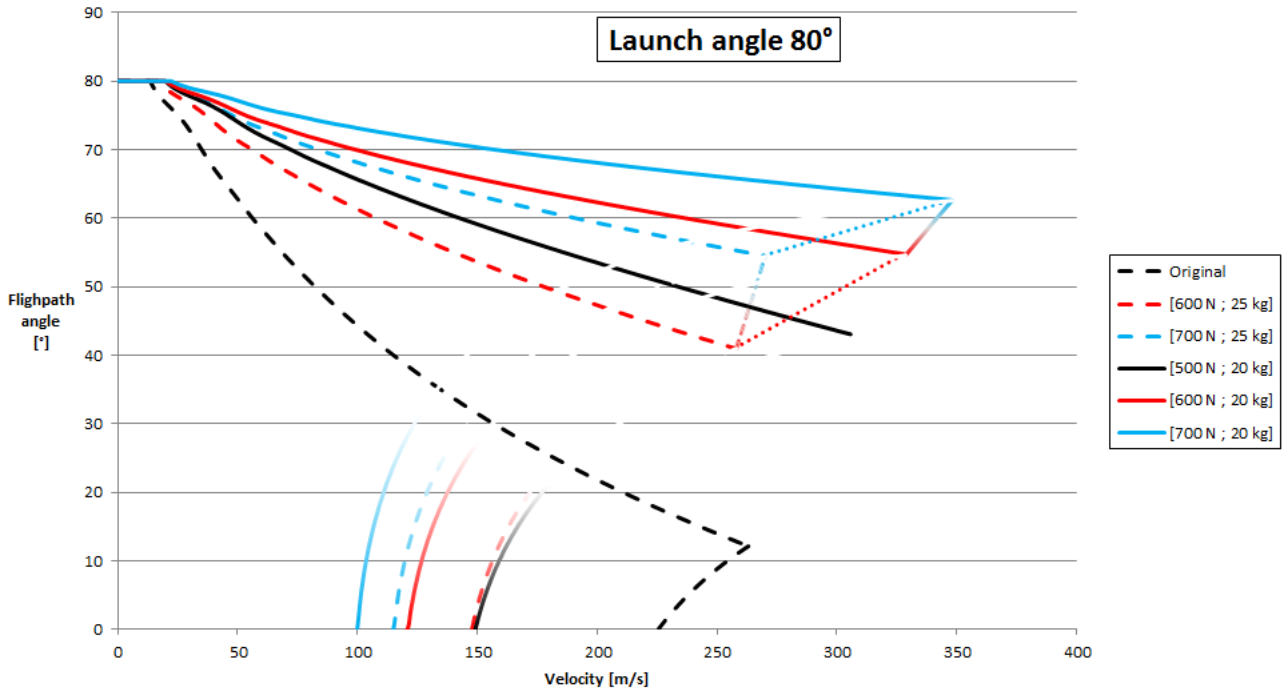
Launch angle 80°
Flighpath angle [°]
Velocity [m/s]
Original
[600 N ; 25 kg]
[700 N ; 25 kg]
[500 N ; 20 kg]
[600 N ; 20 kg]
[700 N ; 20 kg]

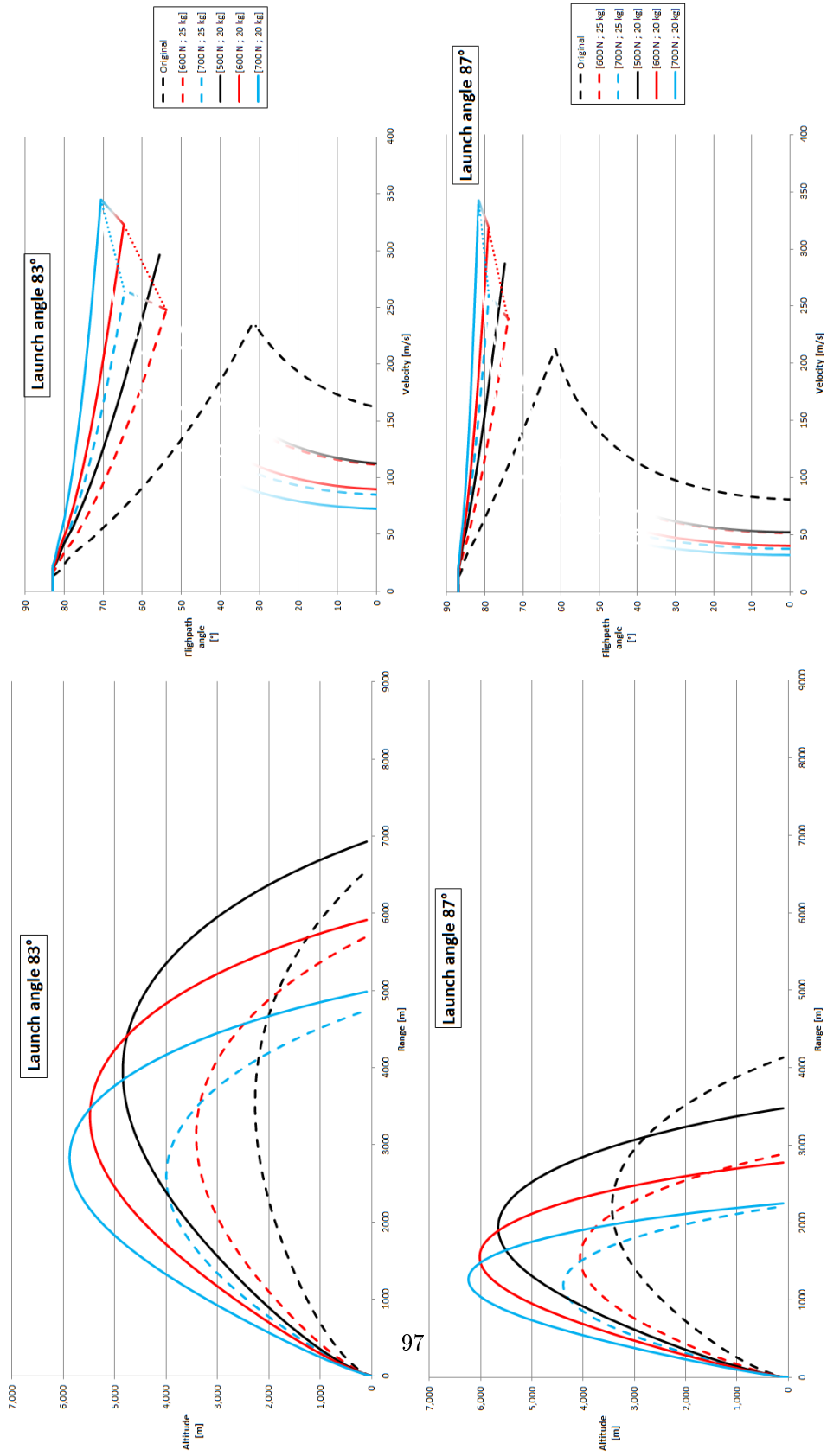

Figure 64: Sensitiviy charts for the updated SMART rocket at various launch angles and specific thrusts.

From the 80° graph it can be seen that the minimum altitude is reached either by increasing the thrust up to 600N or by reducing the structural mass of about 3kg. Increasing the launch angle lowers the extra thrust or the weight reduction required. However although increasing the thrust and/or decreasing the weight reduces the bending of the rocket trajectory, it also increases the maximum velocities achievable during the flight. Therefore the only way to reduce the culmination speeds is to launch the rocket closer to the vertical. The culmination velocities for various launch angles are summarized below. The 80°-launch conditions are not reported because they all end up in culmination velocities higher than 100m/s.

Launch angle [°]	Thrust [N]	Initial mass [kg]	Culmination velocity [m/s]
83	500	25	160
		20	110
	600	25	110
		20	90
	700	25	85
		20	80
87	500	25	80
		20	55
	600	25	55
		20	40
	700	25	65
		20	30

Table 19: Culmination velocity for various launch conditions and specific thrusts.

6.4 Perturbed Trajectory

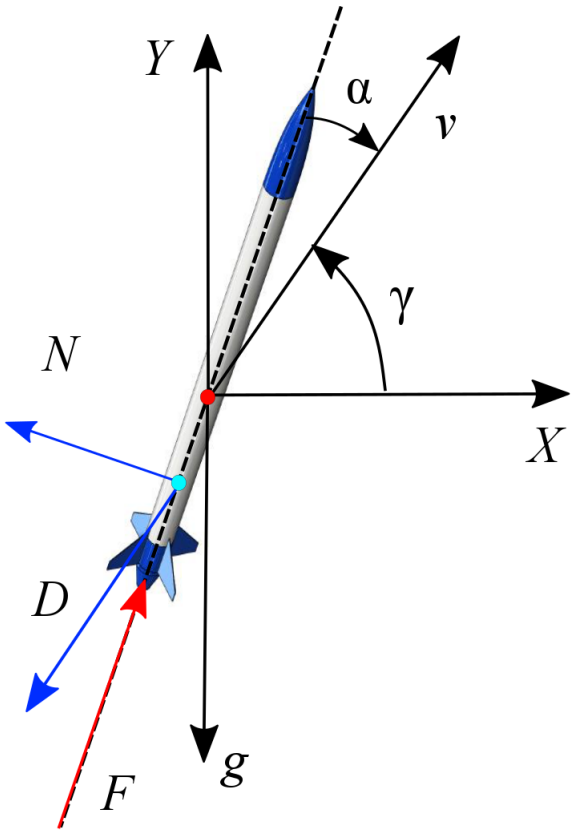

Figure 65: Generic configuration of perturbed rocket.

Until now the trajectory has been studied without considering the effects of any perturbation. Actually during the atmospheric flight all the disturbances described from section 3.1 to 3.3 may act on the rocket resulting in a more or less severe deviation from the intended path. The flight configuration of a generic perturbed rocket is depicted in the figure above. The dynamics of the vehicle CG described by eq.s 1 becomes:

$$\frac{dv}{dt} = \frac{F\cos\alpha - D}{m} - g\sin\gamma - \frac{N}{m}\frac{\alpha}{\|\alpha\|}\sin\alpha + \frac{P_v}{m} \tag{57}$$

$$\frac{d\gamma}{dt} = \frac{F}{mv}\sin\alpha - \frac{g}{v}\cos\gamma + \frac{N}{mv}\frac{\alpha}{\|\alpha\|}\cos\alpha + \frac{P_n}{mv} \tag{58}$$

where P_v and P_n are the components of the generic perturbing term respectively along the parallel and normal direction wrt the velocity vector and α is considered positive upwards (see figure above).

Note that the previous set of equation is valid only for disturbances acting on the same plane of the trajectory. The most general case should include the presence of out-of-plane disturbances. In this case the rocket will follow a 3-dimensional trajectory. The previous equations are always coupled with the time evolution of the vehicle's AoA. Only when the rigid-body dynamics is sufficiently fast wrt the velocity variations, i.e. at sufficiently high speeds, it is possible to study the two problems separately. Therefore no analytical solutions exist for the general case of coupled dynamics. The complete trajectory profile in perturbed flight conditions is obtained from ASTOS by numerical integration. Only the presence of wind and thrust misalignments have been analyzed and the results are reported in the following sections.

Although ASTOS permits to simulate the presence of a fin angle, this is applied to all the fins, i.e. as a canting angle rather than a fin misalignment. It would be theoretically possible to consider such a condition if all the related perturbing moments had been known. In this way a proper definition of the $\overrightarrow{C_M}$ coefficient in eq. 49 could allow to simulate their effects on the rocket trajectory. As much regards the case of two opposite misaligned fins in the same direction (see fig. 27) the overall effects will be similar to those given by a thrust misalignment. Both in fact present the same time-reducing AoA response. However the deviation from the intended trajectory will be much smaller because of the much lower AoA caused by the fin misalignment. The sinusoidal disturbances due to flutter have not been considered because they only lead to a greater trajectory dispersion. If no resonance occurs, the perturbed velocity vector will still be oscillating about the intended path. This effect should however be kept into account when dealing with the dispersion analysis of the trajectory. Finally if the combustion instabilities can be described as impulsive disturbances, their effect on the point mass motion of the rocket is to induce an instantaneous change of the velocity vector. If the vehicle has been launched vertically, the addition of a lateral component results in a rotation of the velocity vector which on the other hand triggers off the detrimental gravity turn dynamics. For a rocket launched at an angle the change in trajectory depends on the direction of the thrust instability wrt the present orientation of the vehicle. Since these disturbances are intrinsic random, their effect should be again included in a dedicated dispersion analysis. They could be simulated in ASTOS by defining an additional phase of very small time duration where the thrust is firing at an angle. This phase should happen casually during the burning interval of the engine.

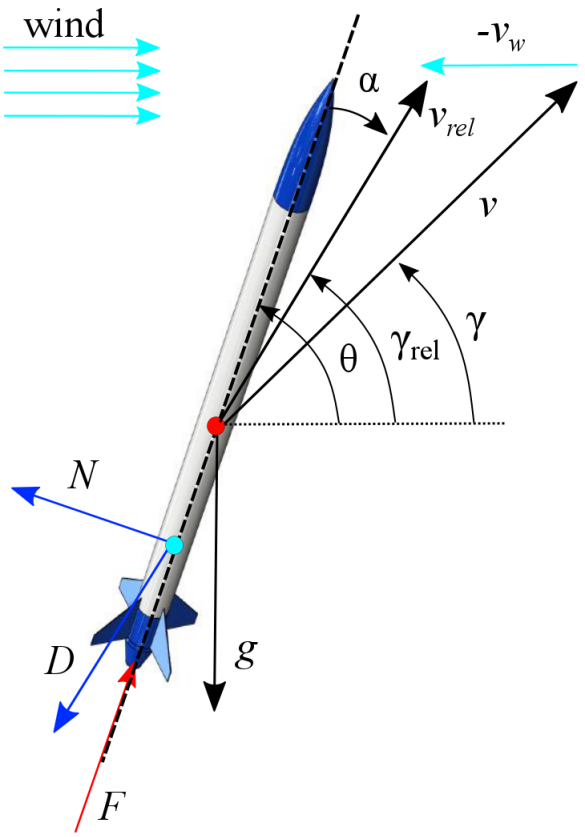

Figure 66: Wind superimposition.

Wind Typically every vehicle flying through the atmosphere is always going to face the presence of the wind. The wind may be present only beyond a certain altitude or act since the ground level. It is usually characterized by a turbulent airflow with a mean velocity component along a generic direction. In the subsequent analysis only the very simplified case of horizontal constant-velocity wind is considered. Further analysis should consider the presence of turbulence and possible random motion of the airflow. For now consider just the case of wind blowing in the same plane of the rocket trajectory. Under the previous assumption the wind can be seen from the rocket point of view as an additional velocity component of the airstream. Therefore an observer solidal to the rocket will see the air moving at a velocity equal and opposite to the vehicle's speed plus the component given by the wind, as it is shown in the figure above. The related eq.s 1 then become:

$$\frac{dv}{dt} = \frac{F}{m}\cos(\theta-\gamma) - \frac{D}{m}\cos(\gamma_{rel}-\gamma) - g\sin\gamma - \frac{N}{m}\frac{\alpha}{\|\alpha\|}\sin(\theta-\gamma) \tag{59}$$

$$\frac{d\gamma}{dt} = \frac{F}{mv}\sin(\theta-\gamma) - \frac{D}{mv}\sin(\gamma_{rel}-\gamma) - \frac{g}{v}\cos\gamma + \frac{N}{mv}\frac{\alpha}{\|\alpha\|}\cos(\theta-\gamma) \tag{60}$$

As stated before in section 3.3, the net result on the trajectory is that the rocket weathercock in the wind direction. This happens because the normal force tends to stabilize the body vertical axis about the relative-velocity direction, which is given by the vector difference between the rocket and the wind speed. The severity of the weathercocking depends mainly on the relative importance of the wind intensity wrt the vehicle velocity at the moment the wind shows up. The ASTOS software allows to simulate the presence of wind acting beyond a given altitude. A dedicated test-case has been created in order to compare the results obtained from ASTOS and Rocksim. A 4 m/s wind has been considered to act since either 0, 500 or 1500 m, which correspond to a wind showing up respectively at launch, before and after the burnout of the engine. The ASTOS results are reported below while the Rocksim's plot are given in fig. 68. Note that these results are not applicable to any SMART design.

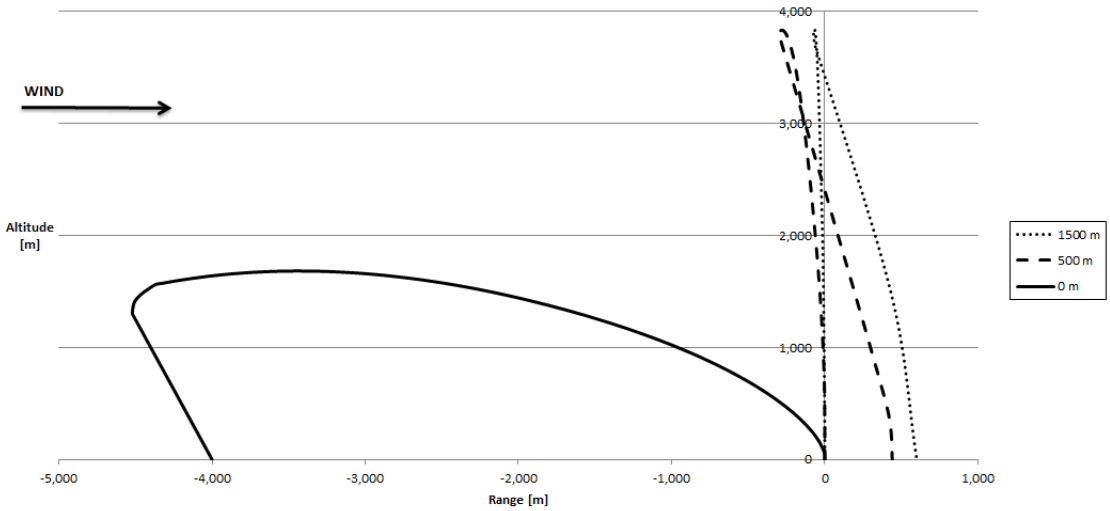

Figure 67: ASTOS results for wind blowing at different altitude.

Note that in the 0 m wind-case, the deflection is much more severe than in all the other cases. This happens because since the launch velocity is proportional to the wind speed, the superposition results in a substantial rotation of the initial launch velocity vector. The vehicle vertical axis is deviated consequently and a notable lateral component of thrust is developed. On the other side if the wind is present from an altitude high enough for the rocket to reach higher speeds, at the moment the wind superimposes the resultant vector remains almost unchanged in direction hence resulting in only slightly deviations from the original intended path. This is why the 500 and 1500 m curves are similar to each other. Hence a vehicle facing the wind during the early portion of the flight is going to be subjected to a very intense weathercocking if the initial velocity is not sufficiently high. This is also the reason why NAR suggested a minimum launch speed equal to about four times the wind speed (see section 4.1).

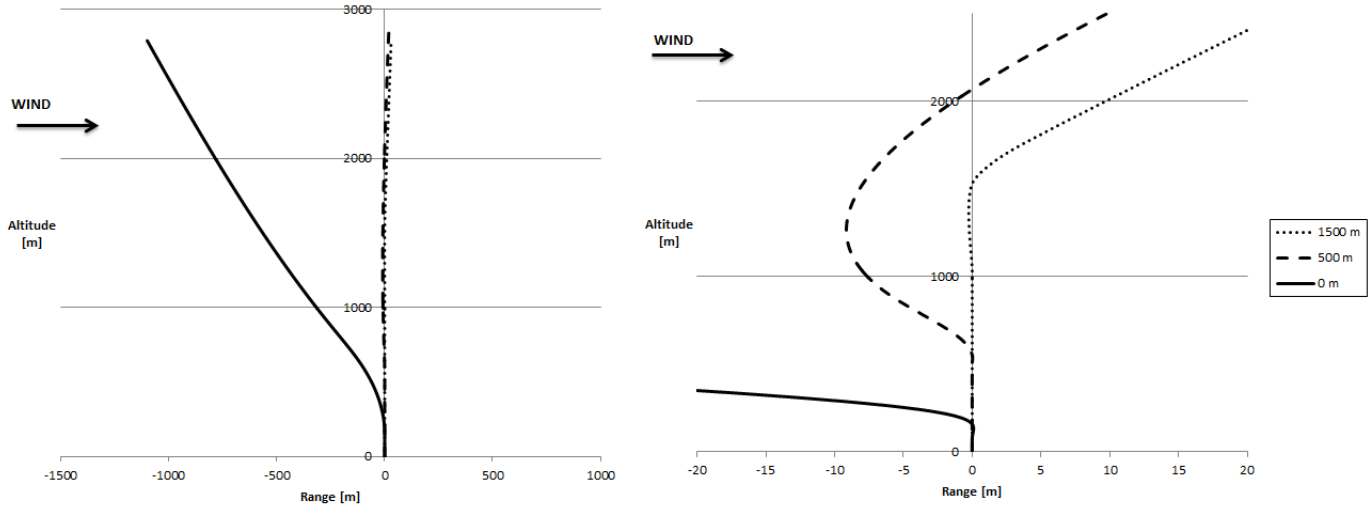

Figure 68: Rocksim results for wind blowing at different altitude.

Note how the Rocksim software gives a different interpretation of the wind effect wrt the ASTOS one. As a vehicle is flying inside a wind layer, it does not see only a change in the incoming flow velocity but it feels also the presence of an additional force acting along the wind direction. This force is responsible for the downwind motion of the rocket in the cases of wind acting from 500 and 1500 m. The Rocksim software has been used only in the early part of this study because of the limitations imposed on the trial version. Deeper studies with the full program are required if the ASTOS results need to be further validated.

The previous study shows how the presence of wind becomes a problem when it blows since the ground level with an intensity comparable with the launch speed. The induced weathercocking not only greatly reduces the maximum altitude but lead also to high residual velocity at the culmination point. The best way to solve these problems is obviously to postpone the launch and wait for better weather condition. However this may not be always possible. The launch site usually imposes a time window within which the launch has to be done. The duration of this interval depends on the number of launches expected every day. For the STERN project where many rockets needs to be launched together, the schedule may be not flexible enough. Another solution consists in exploiting the weathercocking in order to obtain a better trajectory, closer to the vertical one. This can be done by proper choice of the launch angle. Assume that the figure 66 refers to the superimposition at the moment of launch. The vector difference of the two speeds tends to rotate the relative velocity vector toward the vertical if the rocket is launched downwind. Theoretically it would also be possible for a given launch angle to put the rocket's vertical axis perfectly aligned with the vertical direction. The rocket axis will still oscillate during the initial rotational response, but these oscillations will happen about the desired vertical direction hence producing a pure vertical thrust acceleration. This optimum launch angle depends on both the wind and the launch speeds. Assuming that the rigid-body dynamics is much faster than the velocity variations, the optimum launch angle is given by:

$$\gamma_{L-opt} = 180^\circ - \left[\arccos\left(\frac{v_w}{v_L}\right)\right]_{degree} \tag{61}$$

where $\gamma_L \geq 90^\circ$ implies a downwind launch (see section 3.3).

In order to validate the previous statement the same test-case of the wind-layer analysis has been simulated with 1 m/s ground-level wind at different launch angles. This model is characterized by a launch speed of about 13 m/s, which corresponds to an optimum launch angle of about 94-95°. The results in terms of ballistic trajectories obtained from ASTOS are plotted below.

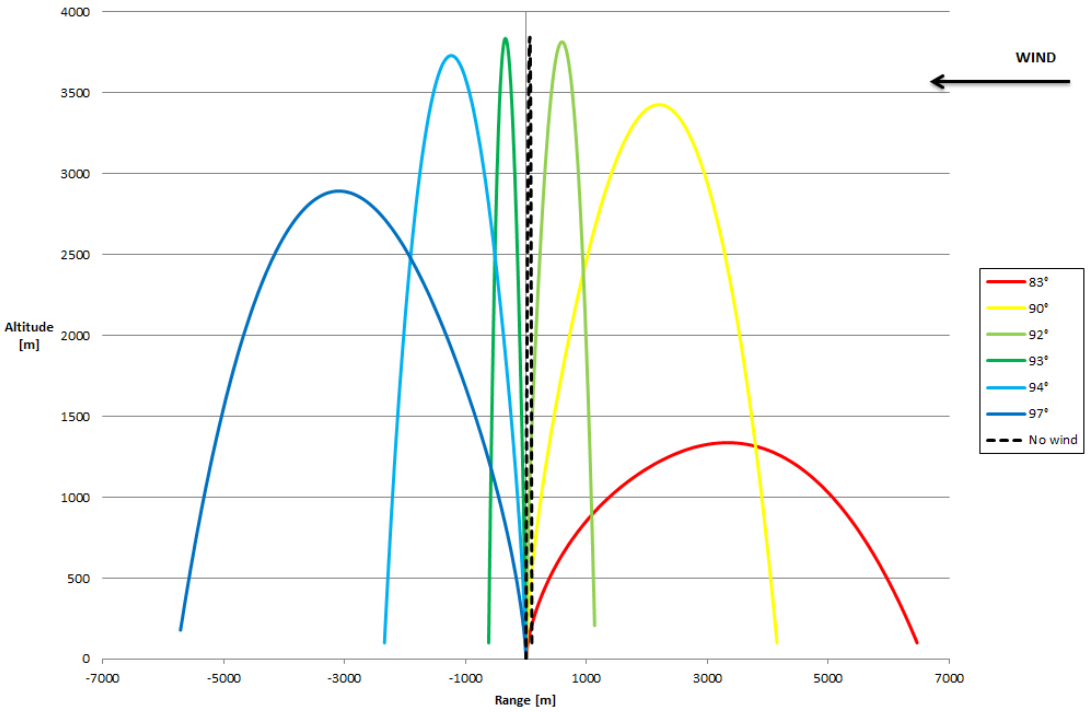

Figure 69: Trajectories with ground-level wind at different launch angles.

The maximum altitude is obtained by launching downwind at about 93° launch angle. Moreover this maximum is very close to the one reachable in the ideal situation of vertical launch without any wind effect. Note also the differences between launching downwind and upwind: the red curve corresponds to a 7° shift from the vertical in the upwind direction while the blue one in the downwind direction. The apogee reached in the first case is about half of the second one. This is due to the fact that as the vehicle is launched against the incoming wind, the superimposition further rotates the relative velocity vector toward the ground. This is confirmed by the following fig. 70 of the rocket attitude. The flightpath and pitch angles correspond respectively to γ and θ defined in fig. 58. Note that the notation used in section 3.3 for the γ_L is not compatible with the ASTOS software. Therefore the initial values in the attitude plot differ from those indicated in the legend.

The pitch of the downwind case (dashed curve) exhibits a growth after the vehicle has left the launch pad. This is because the wind superimposition has rotated the relative velocity vector and consequently the vehicle axis upwards. The gravity turn acting on the rocket will eventually overcome this effect resulting in a downward deflection as for the upwind-launched case (dotted curve). However the vertical

component of thrust acceleration has benefited from the small initial growth, as it is shown in fig.71.

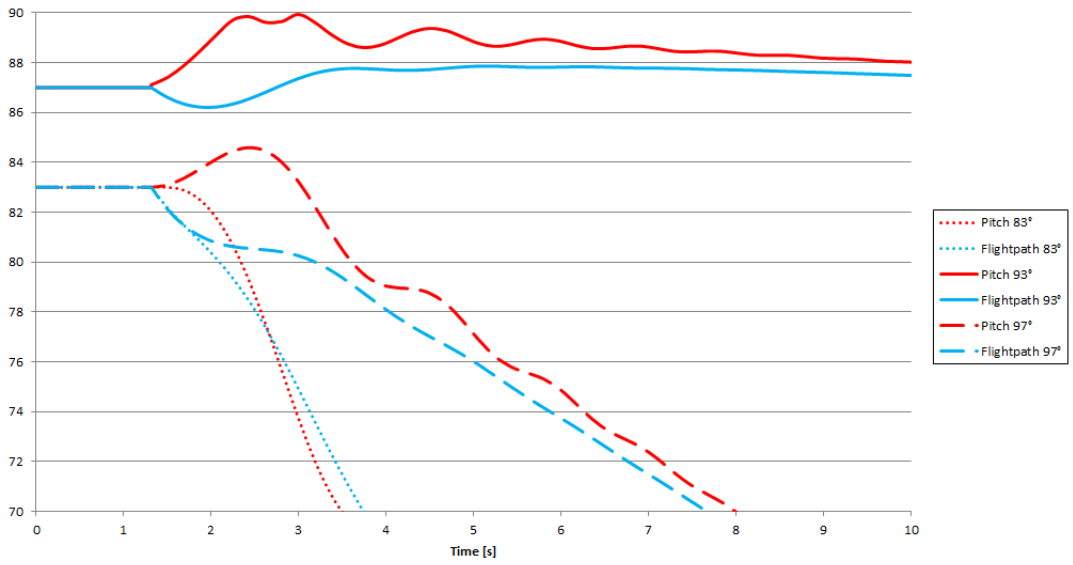

Figure 70: Time profile of the flightpath angle and pitch angle.

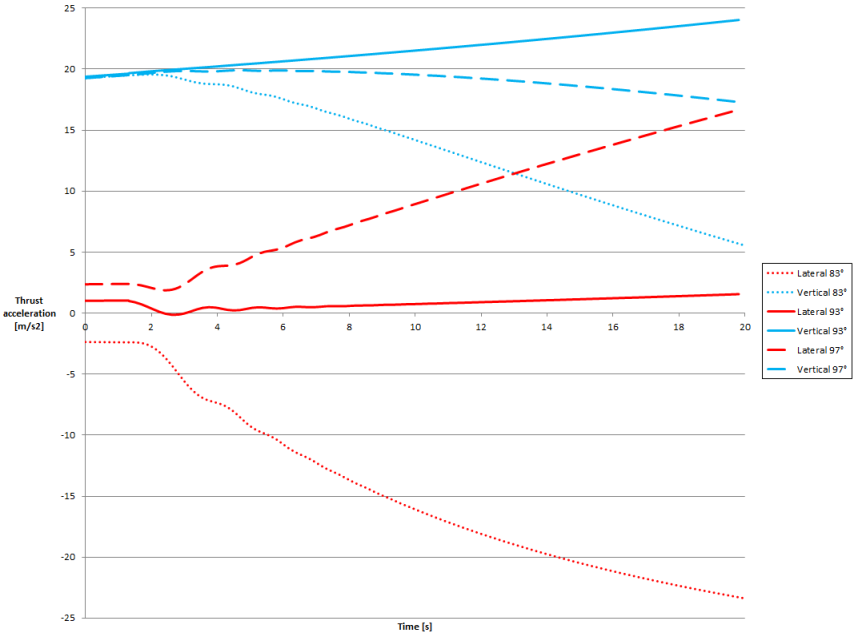

Figure 71: Acceleration components due to thrust.

Note how the reduction of the vertical component for the 83° case happens much before wrt the 97° one. On the other side the continuous curve representing the optimum launch angle profile is much more effective in balancing the g-turn effects. The vertical axis of the vehicle is in fact oscillating close to the vertical resulting in an almost zero lateral component of thrust. However it can be seen from the next enlargement of fig. 70 that the rotation due to gravity is not negligible even in the early portion of this flight configuration.

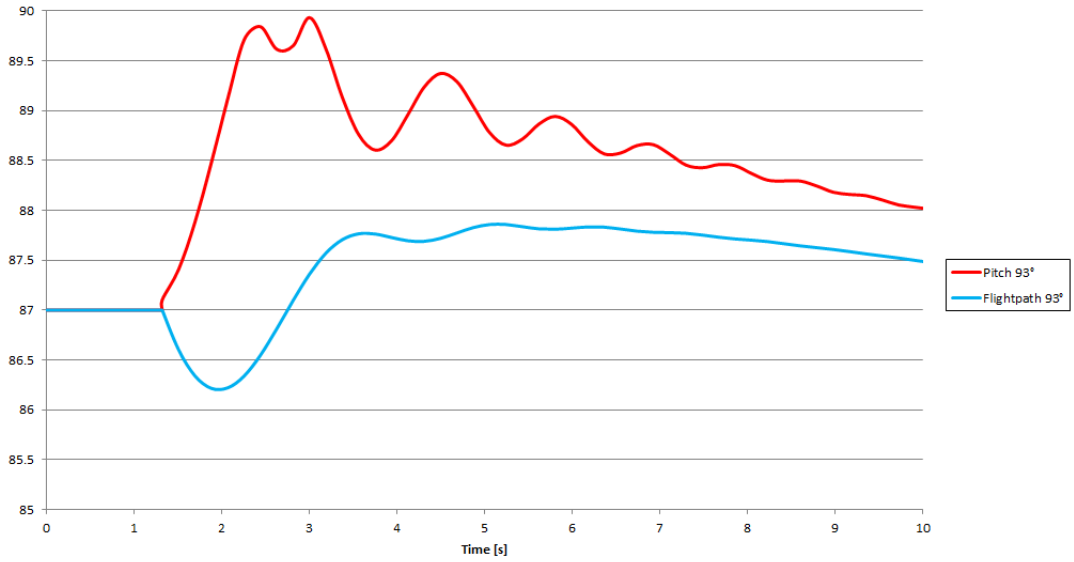

Figure 72: Attitude of the optimum launch angle configuration.

Only after that the vehicle axis has got sufficiently closer to the 90°, the greater vertical component of thrust is able to overcome the g-turn effects. This is also the reason why the optimum launch angle given by ASTOS slightly differs from that predicted by eq. 61. The latter fits better to rockets characterized by higher specific thrust where the initial velocity rotation due to gravity is less severe. For a low thrust-to-weight rocket like the SMART one, the optimum angle will be lower than that of eq. 61, i.e. the rocket needs to be launched closer to the vertical.

The previous analysis however is useless if the launch direction cannot be freely chosen for a given wind strength. Usually the provider of the launch site imposes a maximum launch angle in order to ensure that the vehicle will not go out of the designated landing area. Therefore the SMART updated design has been analyzed for various wind profiles with a fixed value of the launch angle. The 86° launch wrt the ground has been considered because it is the minimum one satisfying the required 3 km apogee with a no-wind model (see fig. 63). Although Esrange does not allow such high angles inside the STERN program, the wind values provided by fig. 36 have been adopted. Different wind directions have been analyzed in order to simulate both the upwind and downwind launch conditions. The results are plotted below.

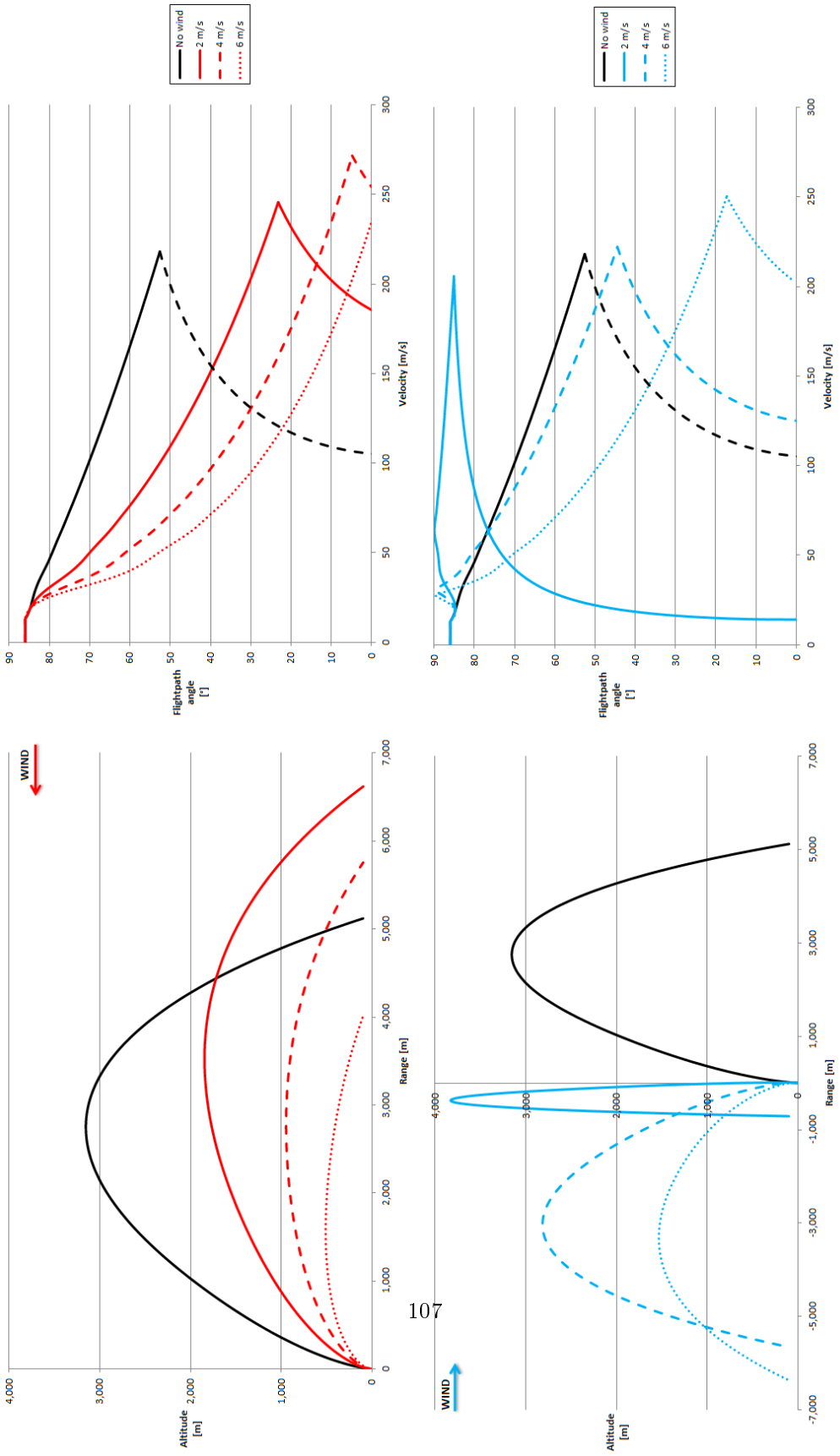

Figure 73: Downwind and upwind launch results for the updated SMART rocket.

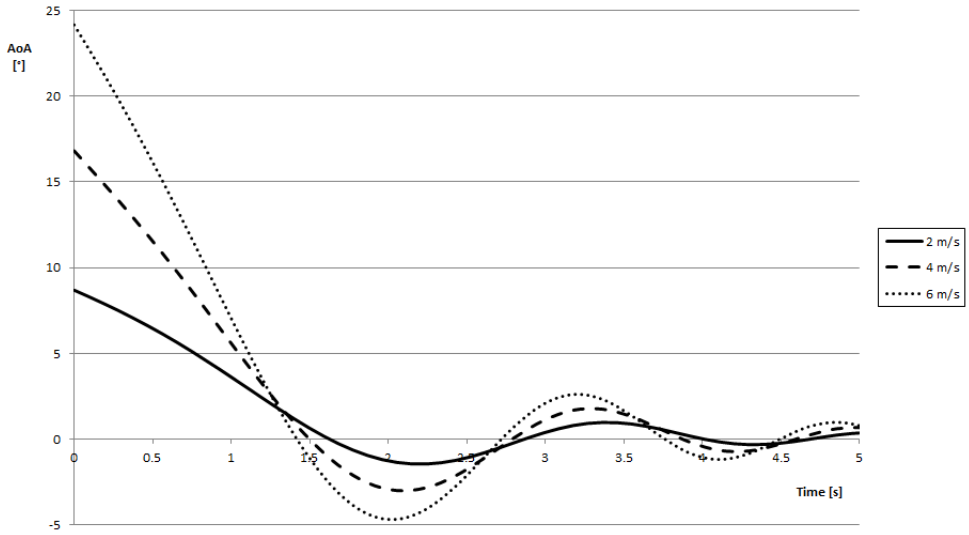

Figure 74: Initial AoA for the updated SMART rocket.

Launching upwind always results in a lowering of the apogee and worsening of the velocity profile. For the 6 m/s wind the weathercocking is so severe that actually the rocket reaches the culmination point before the burnout of the engine. Only if the rocket is launched downwind, the altitude requirement is still fulfilled. Also in this way the wind should not overcome the speed limit of about 4 m/s. In general if the launch angle is lowered, greater wind intensity are acceptable but the launch still needs to be directed downwind. Note that in this case the initial AoA seen by the rocket increases too. It is necessary therefore to ensure that the required stability margin is not invalidated. For the current analysis the 2, 4 and 6 m/s wind result respectively in about 8, 17 and 24° initial AoA as shown in the figure below. The differences between the upwind and downwind case are negligible for the 13 m/s launch speed (see fig. 32).

The 4 m/s wind lowers the stability margin at the minimum limit of 1.5 calibers suggested by Moraba. Therefore the rocket should not be launched with stronger winds if the previous requirement need to be verified.

Note that the apogee of the 2 m/s downwind profile is quite close to that of a vertically-launched rocket. In fact if there is an optimum launch angle for a given wind strength, for a fixed launch angle there will be an optimum wind speed. This can be obtained by evaluating v_w in eq. 61 as a function of γ_L. Again this value slightly differs from the numerical one because of the g-turn effect. However flight profiles resulting in a rotation of the trajectory beyond the vertical are usually not acceptable. The provider of the launch site always imposes a nominal landing site where the vehicle has to impact. If the launch is going to take place in Esrange the typical nominal impact point for sounding rockets is located 75 km north of the launch pads (see fig. 75). For each of the STERN rockets however this point will be much closer, depending on the respective apogee.

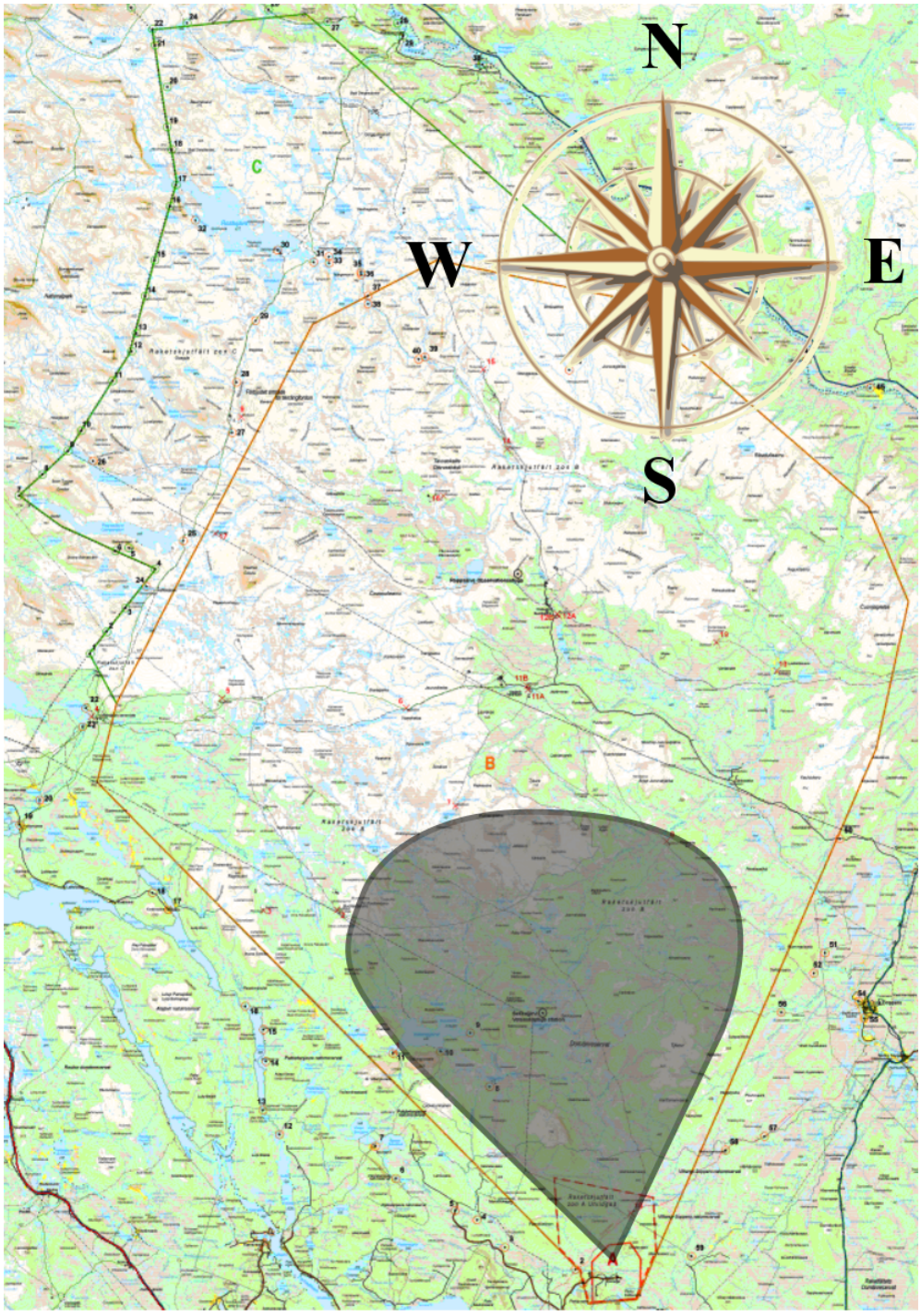

Figure 75: Esrange launch and impact zones.

The Esrange site has an overall impact area of about 5600 km^2 but in any case the rocket is allowed to land behind the launch pads. Therefore none of the downwind trajectories shown in fig. 73 is acceptable even if they results in the maximum altitude. It is true that actually as the vehicle reaches the apogee, the parachute is deployed and the ensemble will be carried downwind far from the culmination point (see fig. 67). However a possible failure in the chutes may result in a catastrophic landing on the Esrange's operational buildings. Hence the wind speed acceptable for the updated SMART design launched downwind at 86° under the requirements on altitude and landing site is about equal to 1 m/s only. This very low margin would seems to compromise the feasibility of the whole mission. Anyway until now only launches in the wind plane have been considered. The presence of perpendicular wind wrt the launch vector deflects the relative flow velocity out of the original flightpath plane. The vertical axis of the rocket is forced to follow this deflection because of the normal force as for the previous cases in-plane wind. Therefore the resulting trajectory is developing somewhere in between the original and the wind plane, depending on the relative importance of wind strength and launch speed. If the wind velocity is negligible wrt the rocket one, the trajectory will remain closer to the original plane. On the other hand if the wind intensity is much more elevated, the deflection will be much more severe. Fig. 76 shows the flight profile of the updated SMART rocket launched at 86° under the effect of various crosswinds.

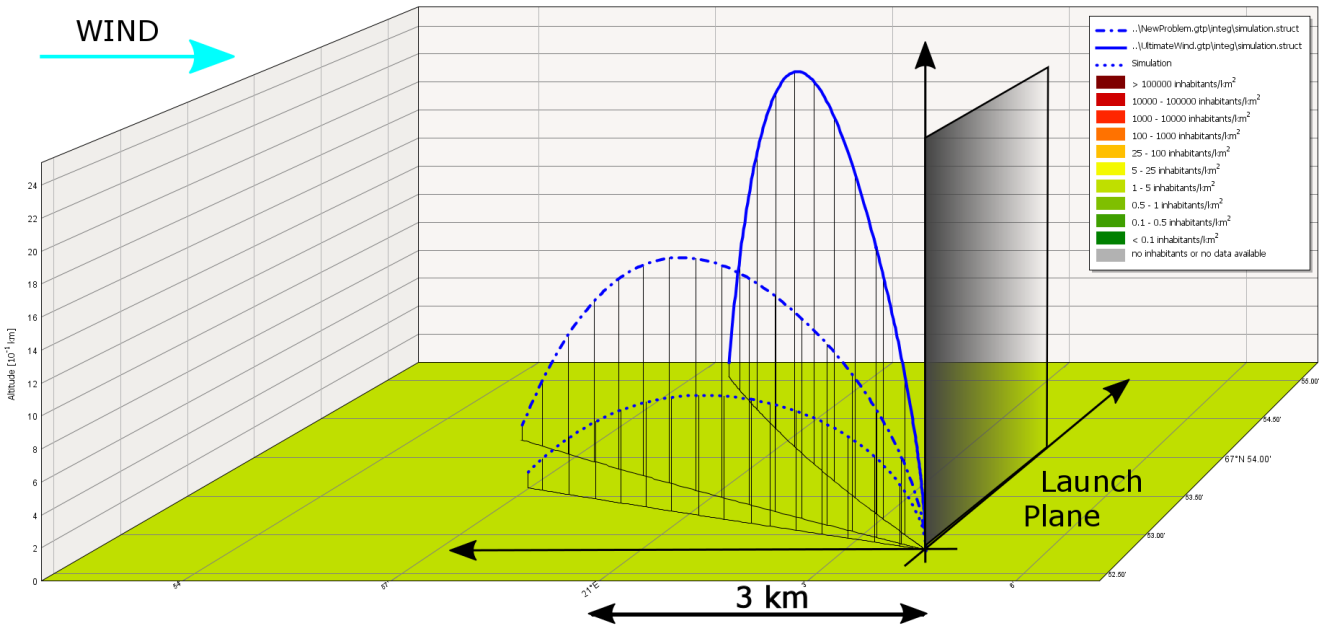

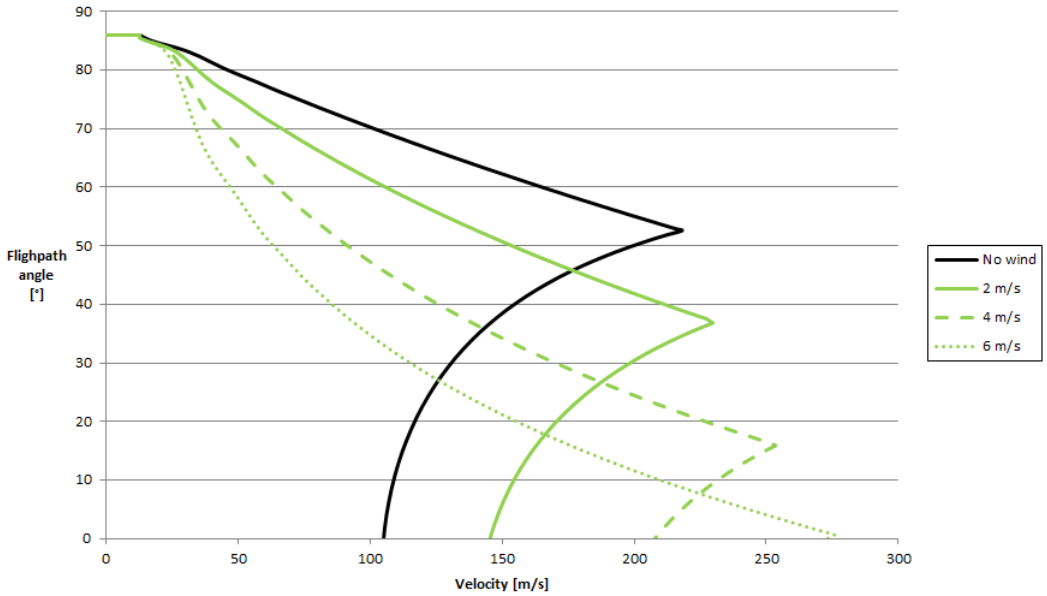

Figure 76: Crosswind launch results for the updated SMART rocket.

Note that both apogees and culmination velocities are worsened by the presence of crosswinds but not as much as in the upwind case. Therefore if the wind intensity is excessive for a pure downwind launch, the orientation of the launch tower wrt a given ground reference point should be changed in order to convert part of the downwind speed into a crosswind component. For example consider the updated SMART rocket launched from Esrange at an angle of 86° wrt the ground. If the rocket is launched toward north with a 2 m/s southern wind, it can be seen from fig. 73 there is the risk of possible crash on the launch site. By rotating the launcher toward east (or west) the ballistic impact point is detached from the Esrange periphery thanks to the crosswind deflection. The trajectory in fact will develop on a plane inclined slightly further toward east (west) wrt the original launch direction. The maximum altitude is lowered but since the 2 m/s downwind profile was quite above the required 3 km apogee, the crosswind losses are still acceptable if the launcher has been not rotated too much. With the same procedure it is also possible to extend the range of sustainable wind strength up to 3 m/s downwind. In this case the launcher should remain closer to the north direction because of the lower margin wrt the required minimum apogee. The launch should not take place with stronger winds otherwise the rocket will not reach the required altitude even in the downwind fashion.

Note that all the previous simulations have been conducted assuming that the Cp would remain fixed in the original position. Since the weathercocking is proportional to the stability margin of the rocket, the worsening effect of the wind on the maximum altitude and culmination velocities will be less severe than that given by the previous results, which are therefore conservative. For more accurate results the analysis should be done with the mean stability margin, which is given by the average between the original and the minimum value. The latter is obtained from eq. 29 once that the maximum AoA for a given wind speed and launch configuration is known either from fig. 32 or by a preliminary simulation with the original stability margin.

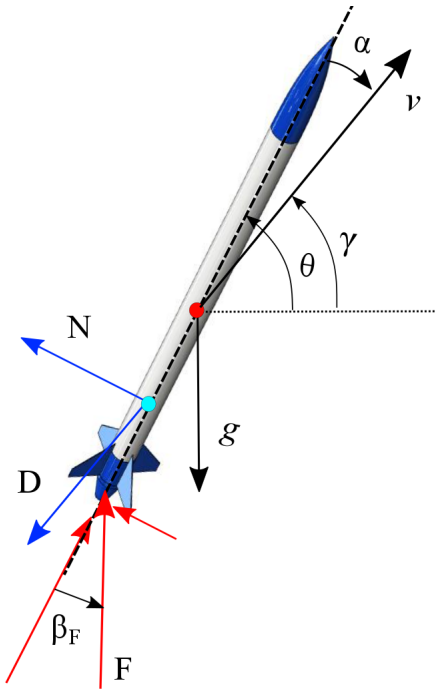

Figure 77: Rocket flying with a thrust misalignment.

Thrust Vector Misalignment and Engine Offset The thrust vector misalignments and offsets are the most critical types of disturbance that may be present on the rocket. They impose a severe deflection of the trajectory since the rocket clears the launch rod and remain active throughout the burning phase of the engine. Moreover their severity depends on the manufacturing accuracy, which is not easily quantified. Therefore they are always present at launch, at least in a minimal amount.

The figure above shows the rocket under the effect of a thrust misalignment only but its effect on the trajectory is equivalent to that of an offset. The misalignment will rotate the rocket vertical axis in the opposite direction wrt the β_F angle and the offset in the opposite side wrt the longitudinal axis of the rocket. Since ASTOS is able to simulate the presence of a thrust vectoring angle for an actively attitude-controlled vehicle, from now on only the misalignment is considered. The general eq.s 57-58 for a positive β_F as indicated in fig. 77 becomes:

$$\frac{dv}{dt} = \frac{F\cos\beta_F - D}{m}\cos\alpha - g\sin\gamma - \frac{N}{m}\frac{\alpha}{\|\alpha\|}\sin\alpha - \frac{F}{m}\sin\beta_F\sin\alpha \tag{62}$$

$$\frac{d\gamma}{dt} = \frac{F\cos\beta_F - D}{mv}\sin\alpha - \frac{g}{v}\cos\gamma + \frac{N}{mv}\frac{\alpha}{\|\alpha\|}\cos\alpha + \frac{F}{m}\sin\beta_F\cos\alpha \tag{63}$$

As stated before the perturbed trajectory will be bent laterally in the opposite direction wrt the misaligned angle. The amount of deflection for a given β_F depends on the dynamics of the AoA and so on the aerodynamic stability of the rocket. Larger fins and greater stability margins result in lower

maximum AoA and faster restoration of the vehicle. The detachment from the original trajectory is therefore reduced. The velocity growth is also important because it is directly related to the generated corrective force. The ASTOS software has been used to simulate the presence of a 0.5° misalignment angle for both the updated and original design of the SMART rocket. This value corresponds to the one required to reduce the stability margin to the minimum 1.5 calibers according to the procedure of section 4.1. The following curves are obtained considering the mean stability margins for each design, 75% and 50% respectively for the updated and the original one. Only the case of vertical launch has been analyzed.

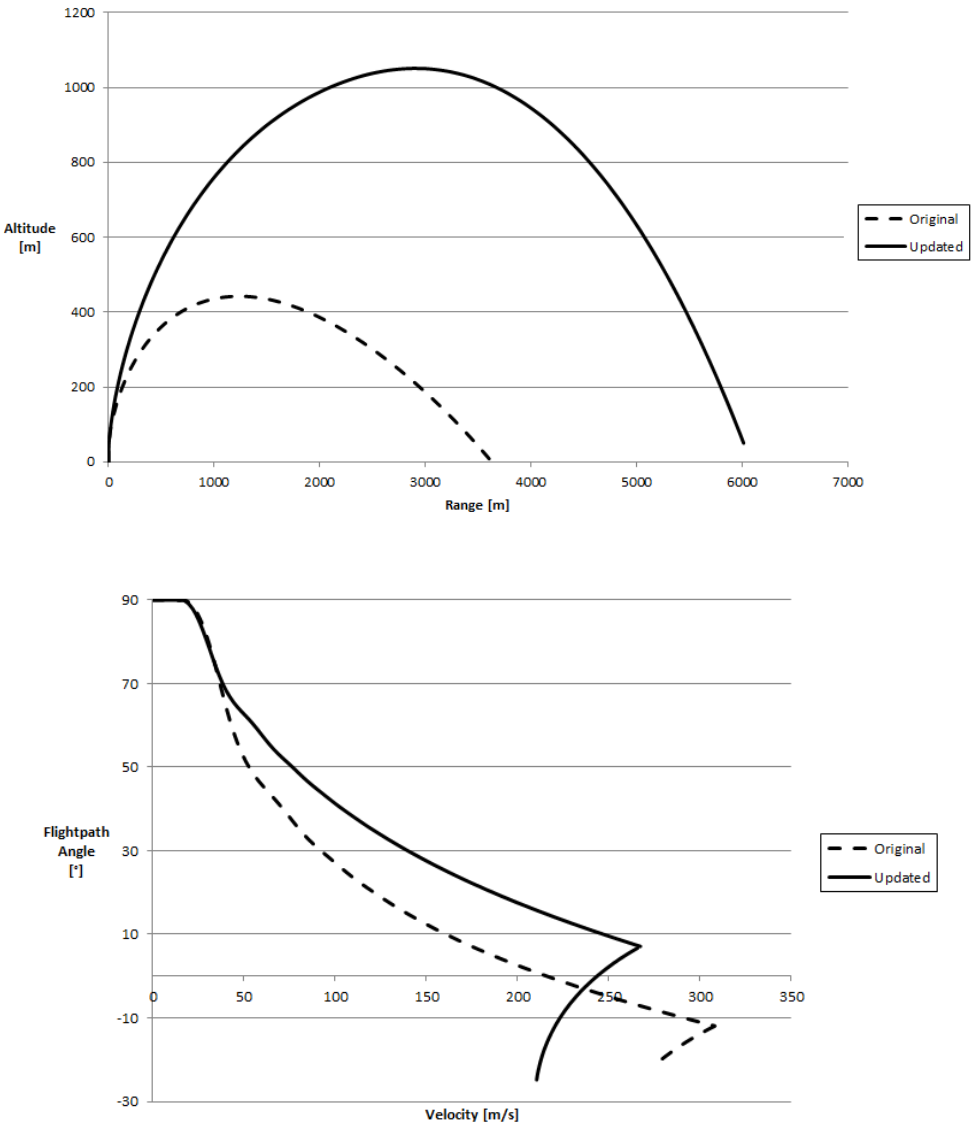

Figure 78: Flight profile with a 0.5° thrust misalignment for the original and updated SMART rocket.

The difference between the two rocket configurations is evident. The original design is much more sensitive to the disturbance because of the poor aerodynamic stability. Its deflection in the initial portion of the flight is so severe that actually the culmination point is reached before the burnout of the engine. Although the updated design does not present the same issue, the resulting apogee is still not acceptable. Several simulations have been done in order to evaluate the maximum β_F angle which guarantees the fulfillment of the altitude requirement. This results to be equal to about 0.2°. Together with the updated and the original design, a third possible SMART configuration has been considered in the analysis too. This correspond to a rocket with very large fins, which will be referred to as the *overstable* design. It is depicted below together with its main characteristics. The Δm_{tot} and ΔC_{d_0} values are expressed wrt the original design.

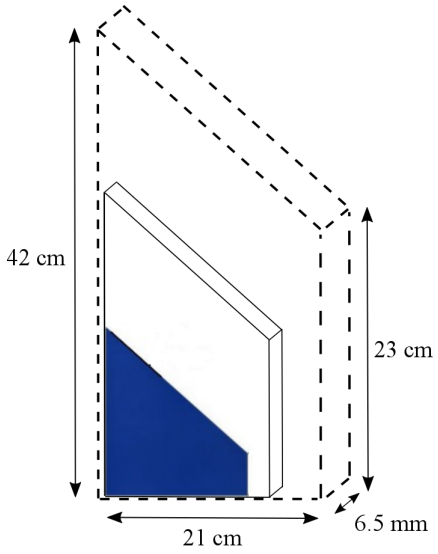

Figure 79: Overstable, updated and original fin design.

k [−]	S [mm]	$\alpha_{1.5}$ [°]	α_{max} [°]	$[\beta_F]_{1.5}$ [°]	$[\beta_F]_{max}$ [°]	Δm_{tot} [kg]	ΔC_{d_0} [−]
5	215	30	70	1.0	1.8	2.6	0.18

Table 20: Main characteristics of the overstable configuration.

The overstable design has been obtained with the same procedure of section 5.2. Therefore although characterized by a very high normal force coefficient, its stability margin is still equal to 4 calibers at 0° AoA in order not to increase too much the weathercocking in the wind. It is expected that this third design is going to be more effective than the others in facing the thrust disturbance. The figures show the results of the various configurations launched vertically with a β_F equal to 0.2° and mean stability margins. Note that the drag increase of the overstable profile has been neglected. The related performance are therefore overestimated.

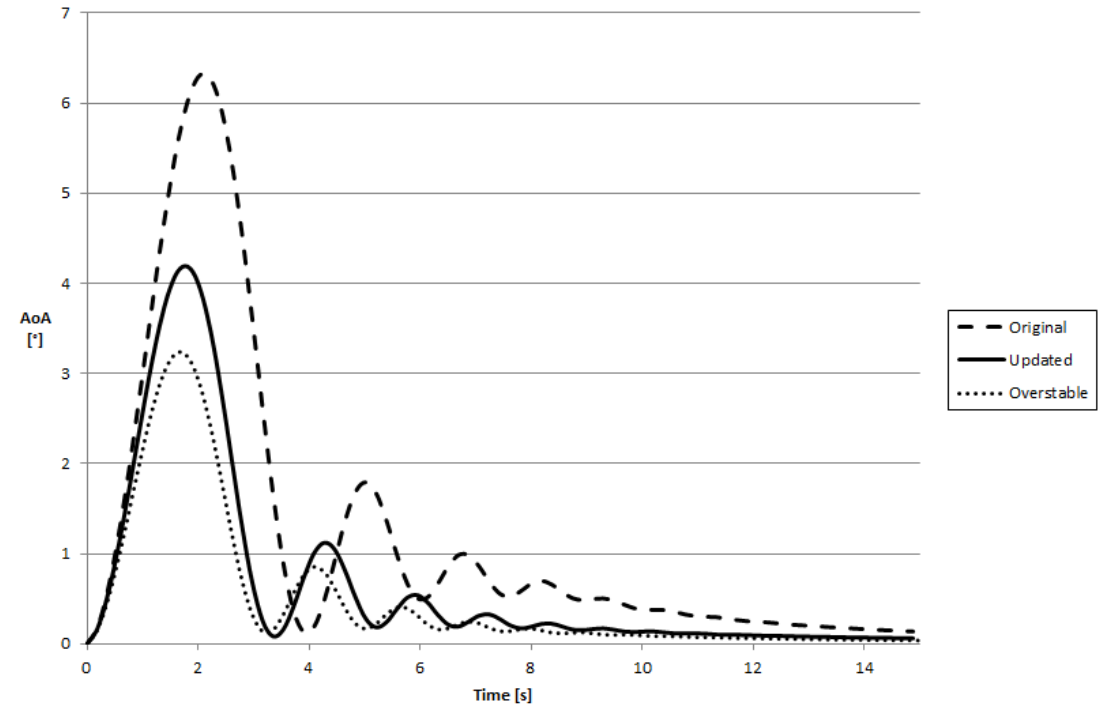
AoA [°]
Time [s]
Original
Updated
Overstable

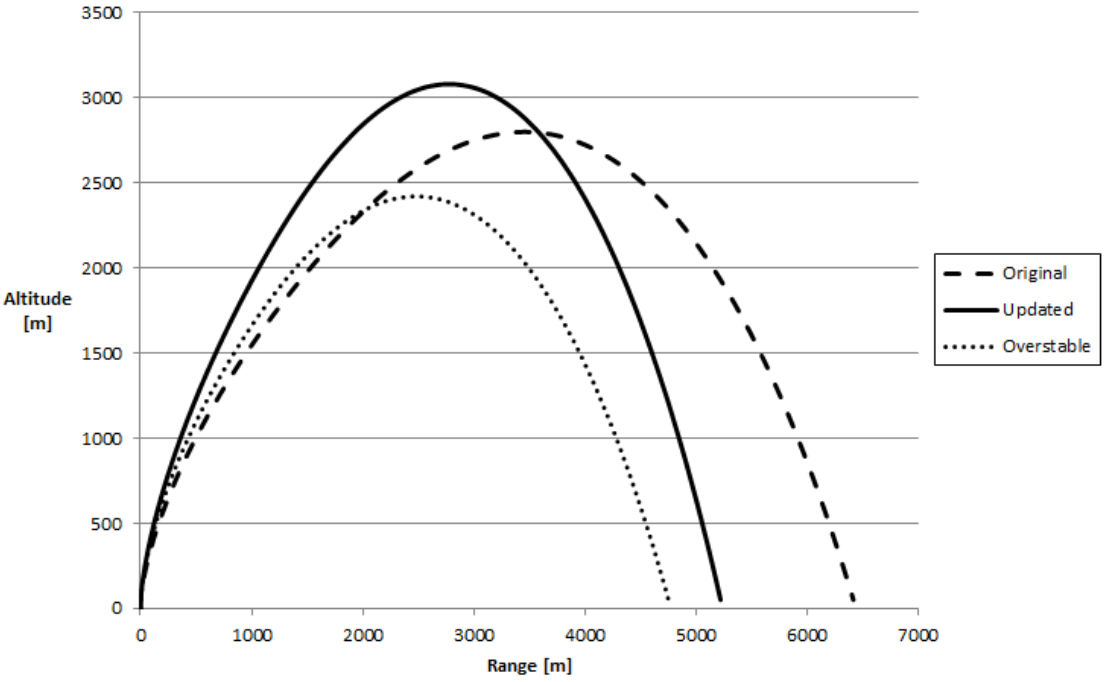
Altitude [m]
Range [m]
Original
Updated
Overstable

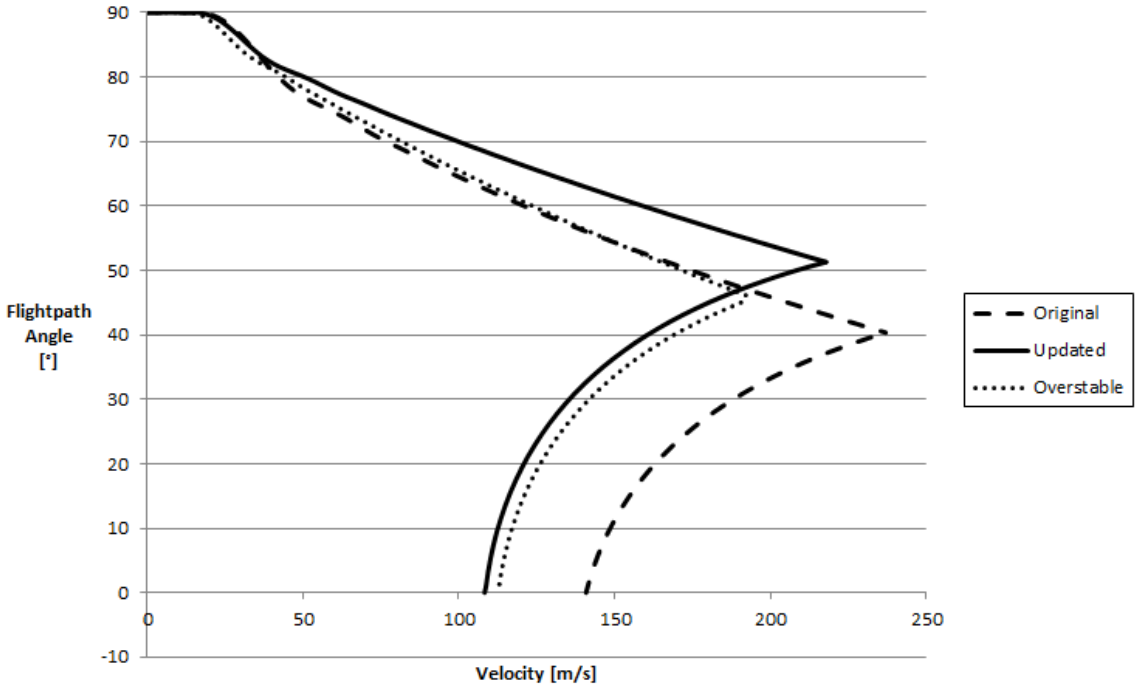

Figure 80: AoA and flight profile with a 0.2° thrust misalignment for the original, updated and overstable SMART rocket.

Although the AoA of the overstable configuration reaches smaller values wrt the other designs, the related apogee is not even greater than that of the original SMART rocket. This is due to the notable mass increase of the vehicle which on the other side has worsened the turn due to gravity. Therefore even if the lower deviation of the rocket axis from the intended trajectory reduces the lateral thrust losses, the sensitivity to the g-turn has increased because of the extra mass and related low launch velocity. The situation would be further aggravated if the increment of drag coefficient would have been considered. Therefore even increasing the fin's size the apogee is not improving consequently. There is some kind of optimum fin which guarantees the maximum altitude for a given thrust misalignment. Unfortunately in order to reach the required altitude it is possible to accept only a very narrow range of about 0.2°. The main responsible is again the very low specific thrust of the SMART rocket.

Finally note from fig. 81 that as expected the weathercocking of the overstable design is the highest because of the greater fin's area. This result has been obtained for a vertical launch with a 2 m/s constant horizontal wind. The stability margin is again assumed constantly equal to the 0° AoA value.

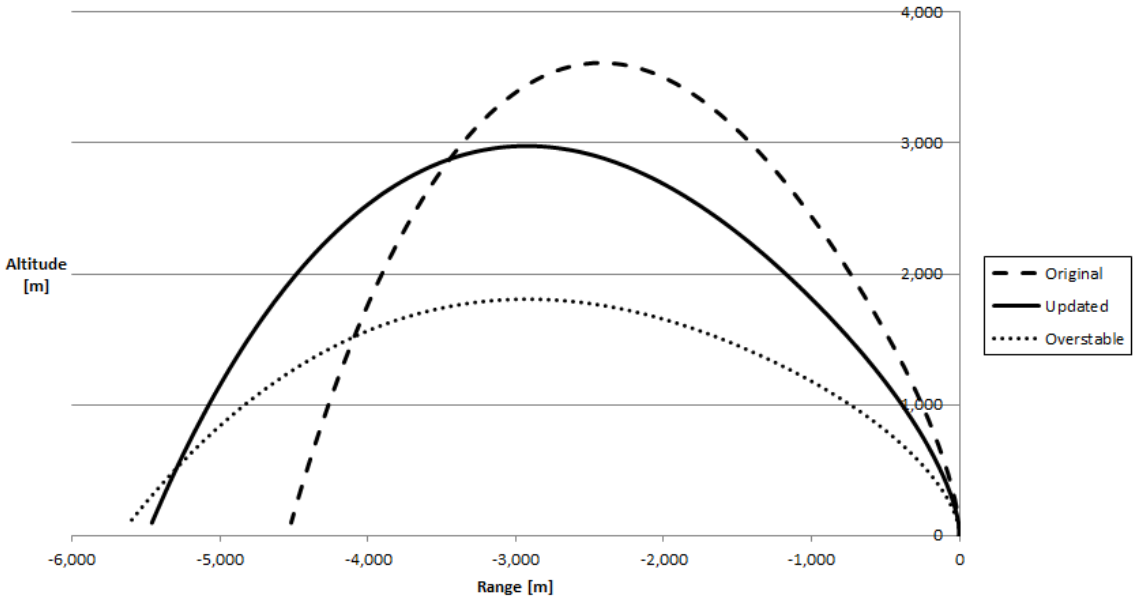

Figure 81: Weathercocking profile for the original, updated and overstable SMART rocket.

The assumption of vertical launch has been made throughout this analysis only to better clarify the effects of the thrust misalignments. Actually the rocket is going to be launched at an angle so that the position of the misalignment wrt the inertial orientation of the rocket is very important. The various possibilities should be studied with a series of dedicated simulations. In general the trajectory deflection may develop in the same plane or in a perpendicular plane wrt the launch vector. Clearly the first is more dangerous because it may happen that the rocket is further deflected downward by an upward misalignment. In this case the acceptable margin is even lower than before. The opposite situation of rocket bent upward would be beneficial from the trajectory point of view. However do not forget that the thrust misalignment is by its nature an imperfection, hence its exact position and intensity is not certain at all. It could be theoretically possible to design the rocket with a deliberate thrust vector angle in order to correct the problems due to the g-turn. In this case the load paths of the rocket structure should be accurately analyzed in order to avoid possible points of stress concentration. Moreover precise manufacture for the combustion chamber and thrust scaffold should be provided together with rigid launch tolerance. A possible mechanism constraining the rocket to the launcher until the engine transient has passed over would be desirable too.

7 Conclusions

Although the satisfaction in achieving the challenging goal of designing a liquid propelled rocket in its entirety greatly overcomes the time and effort spent in pursuing it, this category of rockets is very sensitive to a wide spectrum of problems which need to be fully understood and solved in order to guarantee the success of the mission in terms of both safe recovery and required apogee. Liquid propelled rockets typically demand higher structural mass with respect to the solid propelled brothers because of the intrinsic complexities of the engine and related subsystems. It is so not hard to fall inside the dilemma of underpowered rockets, which actually means that the realized vehicle is flying with a not high enough thrust or an excessive initial mass. This implies on one side a notably sensitivity of the rocket to the gravity-turn phenomena while on the other a poorly effective aerodynamic stability in the initial portion of the flight. The current design of the SMART rocket is affected by both of these problems. In particular the rocket is so heavy that it is actually unfeasible the achievement of the projected speed of sound. In fact it would require either the reduction of the rocket structural mass to about half of the actual value or the increase of the operating thrust to about 700 N (see table 18). Moreover if the rocket is going to be launched from Esrange, the effect of the gravity together with the very low launch angles imposed results not only in a much lower apogee wrt that obtainable from an ideal vertical trajectory, but also in culmination velocities way to high for the common types of recovery devices. Special parachutes would be needed in order to ensure the correct deployment at such velocities and so the safe recovery of the vehicle. These chutes are typically more complex and heavier and their use should be avoided if other solutions to the problem can be found. The most simple one would be to increase the launch angles. A common recovery device for model rockets deploys safely at about 20 m/s which implies for the SMART a launch not below the 89° wrt the ground! The minimum 3 km apogee is instead reached for about 86° but the resulting culmination speeds are still excessive. Since there is no assurance that such high angles can be achieved, another possible solution is to increase the specific thrust of the rocket in order to lower the severity of the g-turn. This can be done either by increasing the engine thrust or by reducing the structural mass of the vehicle. From fig. 64 it can be seen that if the launch angles is kept equal to 80°, the altitude requirement is fulfilled for a rocket with either a thrust increased of about 150 N or a 3 kg lighter overall structure. The achievement of sufficiently low culmination speeds is however never attained. This is due to the higher flight velocities reached by the vehicle thanks to the enhanced specific thrust. For the same reason even if the launch angles are increased the situation is not substantially bettering. Only at 87° the culmination speeds are able to drop below the 50 m/s (see again fig. 64).

Note that the aerodynamic stability would also benefit from the increased specific thrust. In fact the resulting higher launch speeds would improve the effectiveness of the vehicle wrt any of the previous modeled perturbations. The weathercocking due to a wind of given strength would become less severe and the margins in terms of airframe and engine errors would also be enhanced. In general the procedure described in chapter 4 together with the analytical perturbing models of chapter 3 allow for the immediate evaluation of the limit values of the various perturbations for any common rocket. In particular the SMART design has been proved to be highly sensitive to the presence of thrust misalignment in terms of both the peaks of angles of attack and the trajectory deflection. However if the first can be reduced by the use of bigger fins, as it has been demonstrated in section 5.2, there is actually no possible solution to the deviation imposed to the trajectory. Although bigger fins reduce the peak of the AoA and make the vehicle restore itself faster, the increase in overall mass worsens the severity of the g-turn. There is so some kind of optimum fin's dimension that maximize the altitude in the presence of a misalignment angle. This is about equal to 0.2° for the updated SMART configuration

(see table 14) launched vertically in order to satisfy the apogee requirement. If the rocket is launched at an angle, this value will be even inferior, depending on the direction of the misalignment relative to the vehicle attitude. The design procedure described in section 5.2 has been used to look for a new configuration in an attempt to increase the margin of the rocket wrt thrust misalignment. The previous procedure is of general use and can be extended to any model rocket particularly sensitive to its specific type of disturbance. The resultant updated design has demonstrated to be more effective than the original in the flight margins wrt the various perturbations (see data from fig. 48 until 49) without any notable lose in the altitude and velocity performance.

The only relevant penalty is found in the weathercocking encountered by the rocket when flying in windy conditions (see fig. 81). However as it is shown in section 6.4, the issues related to the presence of winds can be effectively reduced by means of a proper calibration of the launch angle. Actually the trajectory could also benefit from the presence of a theoretically horizontal wind blowing at the suitable mean speed. There is in fact an optimum angle for a given wind speed (so as there is an optimum wind speed for a given launch angle) that maximizes the apogee and minimizes the culmination velocities. This optimum can be calculated from eq. 61 which is strictly valid for high-powered rockets. In the case of the SMART rocket the optimum wind strength for an imposed launch angle should be slightly increased wrt the calculated one. Besides the previous equation is valid only if the rocket is launched downwind, i.e. with the wind blowing from behind the intended launch direction. The upwind launch should in fact be avoided whenever is possible because it worsens greatly the trajectory profile (see fig. 69). In the case of a downwind launch it exists a maximum value of the wind speed beyond which the vehicle is not allowed to flight. This is because the excessive downwind strength would reverse the direction of motion wrt the vertical. In the unlucky case of a chute deployment malfunction this would end up in a catastrophic crash too close to the launch pads. Anyway this problem can be solved by simply changing the azimuth of the launch tower, i.e. rotating it out of the wind plane. In this way part of the overall wind speed is converted from downwind into a crosswind component which results in a further rotation wrt the launcher of the rocket trajectory (see fig. 76). The ballistic landing point is so more detached in the incoming wind direction thanks to the weathercocking of the vehicle. The ideal trajectory with the correct opening of the recovery devices will end up somewhere in the cross-downwind direction due to the drift of the chutes but anyway far from the launcher periphery. The maximum altitude is also reduced but not as much as in an upwind case of equal intensity. Moreover the rotation of the launcher orientation can be adjusted in order to balance the altitude losses due to the crosswind with the benefits from the downwind.

Summarizing the SMART rocket should be provided with slightly bigger fins with respect to the actual one if higher margins of thrust misalignment are desirable. This enlargement should not result in a too excessive increase of the overall vehicle mass. The proposed optimum fin's design of section 5.2 should be validated once that the final mass distribution of the rocket is known. The flight margins for the other types of disturbances will be positively affected by this improved aerodynamics. They can be calculated according to the procedure of chapter 4. If the proposed fins are eventually chosen, the variation in stability margin and damping ratio can be directly obtained from fig.s 50-51 as a function of the final position of the center of gravity and longitudinal moment of inertia. In any case however the highest possible precision in the manufacture and mounting of the engine should be pursued because of the very low amount of imperfection affordable.

If the launch angles cannot be increased the thrust or the structural mass of the rocket should be respectively increased or decreased in order to ensure the required apogee. In any case the recovery device will have to be properly chosen on the basis of the resulting culmination speeds. These can be directly obtained from fig.s 64 once that the final rocket thrust and mass are established. Note that an

increase of the specific thrust increases consequently the margins wrt the thrust misalignment. In fact even if the thrust perturbing moment rises, the AoA will lower because of the inverse proportionality with the increased velocity (see eq. 33). Therefore the previous 0.2° maximum value can be further enlarged.

Once that the definitive specific thrust of the rocket is known, the corresponding trajectory can be evaluated in the ideal case of no wind. The margins of the latter wrt the imposed requirements of 3 km apogee and sufficiently low culmination speed determines the acceptable conditions in terms of mean horizontal wind speed and direction. If this ideal trajectory is just enough sufficient to achieve the previous requirements, the launch should never be directed against the incoming wind direction. Only downwind launches are allowed and in particular the wind speed has to range between zero and a maximum value which depends on the launch conditions. Beyond this maximum there is the risk of possible crash on the launch pad's outskirts. For example a SMART rocket launched at 80° and corrected with either 650 N of thrust or about 17 kg structural mass would result in a launch speed of about 18 m/s. This on the other hand implies an optimum downwind speed of about 3 m/s according to eq. 61. Since this equation underestimates the true value for underpowered rockets, the maximum downwind limit can be conservatively assumed equal to 3 m/s. This limit can be further increased if the launcher is rotated crosswind. The amount of rotation granted depends on the dimensions of the landing area, both in the crosswind and downwind direction. If the provided area is wide, the launcher can be rotated of a large amount and the maximum wind speed is correspondingly enhanced. Vice versa if the landing site is narrow, the rotation allowable will be smaller and the actual wind limit will remain closer to the previous value.

If the launch is going to take place at the Esrange Space Center, since the provided landing area is located north than the launch pads, the rocket is most likely going to be launched toward north. During the pre-launch tests proper measuring systems, such as balloons with GPS are used to analyze the actual wind profile. After that the mean wind direction and speed are known, the feasibility of the launch can be evaluated according to the following guideline.

Northwards launchs can take place if:

1. with north wind:
    - the apogee and culmination velocity required are not invalidated by the upwind effects;
2. with east or west wind:
    - the apogee and culmination velocity required are not invalidated by the crosswind effects;
    - the landing point does not exit from the provided area due to crosswind weathercoking;
3. with south wind:
    - the landing point does not exit from the provided area due to downwind weathercoking;
4. with north-east or north-west wind:
    - the apogee and culmination velocity required are not invalidated by the upwind and crosswind effects;
    - the landing point does not exit from the provided area due to crosswind weathercoking;

5. with south-east or south-west wind:

    - the apogee and culmination velocity required are not invalidated by the crosswind effects;
    - the landing point does not exit from the provided area due to crosswind and downwind weathercoking.

Note that the combined losses due to crosswind and upwind case (4) are typically lower than those related to the upwind one only (1). In the case of down-crosswind (5) it is also theoretically possible to have no net variations in apogee and culmination speed. The maximum wind speed can be so evaluated for each of the previous case once that the ideal no-wind trajectory is known. Since according to [19] the winds in Esrange are typically out of the south, south-west, it should always be possible to direct the launch as in the case (5). If the provided landing area is enough elevated the crosswind weathercocking does not represent an issue.

The natural prosecution of this thesis is the improvement of the various methods and models adopted so far. As the definitive SMART configuration is approached, the various characteristics of the rocket become closer to the final ones. Therefore the procedure used to calculate the flight margins of chapter 4 needs to be redone with the updated values of the vehicle mass properties as soon as they will be available. The same holds for the models defined inside the ASTOS software, that also have to be improved by the inclusion of the effective time profile of the engine thrust, the related variations in center of gravity and moments of inertia and a more accurate calculation of the aerodynamic properties of the rocket. More specifically the drag coefficient should be better analyzed with the help of computational fluid dynamics (CFD), which calculates the exact air flow in a discrete mesh around the vehicle. In this way it can be taken into account for the drag components that have been previously empirically assumed, like the parasitic drag due to launch lugs. The normal force coefficient and related moment's coefficients defined by eq.s 12-13 are reasonably accurate up to at least Mach 0.4, after which they start increasing because of the effects of the air compressibility. The results obtained before in terms of flight stability are therefore slightly conservative.

As much regards the considered perturbations their modeling requires further advancements to improve the likelihood with the real case. The perturbing moments generated by a generic configuration of airframe errors need to be better studied in order to provide to ASTOS the input required to simulate their effects on the rocket trajectory. This analysis can be later refined by the addition of the uncertainty of the fin angles inside a dedicated statistical analysis. The latter can be defined also for other kinds of disturbances such as the combustion instabilities and the possible fin flutter. More information about the simulation for the previous can be found at the beginning of section 6.4. The empirical flutter analysis of section 3.2 has to be integrated with numerical results obtained through the use of dedicated software. From this point of view the ANSYS model depicted in fig. 46 represents a good starting point for a complete aeroelastic analysis of the whole rocket, in particular of the cylindrical body. The deflections caused by the airflow on the latter can be relevant because of the very high slenderness of the vehicle. On the other side this implies a notable importance of the aeroelastic dynamics on the stability and trajectory of the rocket. The wind model has to be further enhanced to keep into account for the possible presence of the free turbulence inside the flow and the average vertical components of the wind velocity vector. The first may produces resonant coupling of the oscillations of the rocket vertical axis if the natural pitch frequency ranges inside the frequency spectrum of the turbulent wind. The vertical motion of the airstream instead alters the velocity of the vehicle wrt the flow and so the developed aerodynamic forces. In particular if the wind is averagely directed upward, the relative velocity is reduced so that respectively the actual drag felt

is lowered and the normal force produced is increased. A set of dedicated simulations has to be done to analyze the effects of the engine errors on the trajectory when the rocket is launched non-vertically. A great deal of attention has to be placed on the impact of the position of the thrust misalignment, engine offset or combustion instability relative to the inertial orientation of the rocket. Subsequent statistical analysis should focus not only on the inner defects of the vehicle but also on the possible uncertainties that may characterize the environment. Proper choice of suitable atmospheric models inside the ASTOS Model Browser allows to consider the complete seasonal and monthly variability of the winds and thermodynamic variables. A complete dispersion analysis of the rocket impact point should encompass all the previous remarks in order to predict the sensitivity of the trajectory to the various involved parameters.

Finally it must be emphasized that this thesis represents only the starting point of a series of studies that will proceed in parallel with the advancement of the project, needed at any crucial decision regarding the final design. Moreover even after that the definitive rocket will have been placed on the launch tower, the launch provider will require the calculation of the optimum launcher orientation for the environmental conditions that will be present. The recovery team also will be directed toward the impact point by the information given by the same analysis. Therefore it is clear how the topics exposed in this paper are going to follow the SMART rocket throughout its life, from the moment the engine is ignited until it eventually alights on the ground again.

Acknowledgments

I would like to express my gratitude to Dipl. Ing. Christian Bach for his patience and support especially in the very final part of my work. Without his presence the draft of this thesis would have been much more laborious. Special thanks are due to Prof. Luca d'Agostino and Dipl. Ing. Jan Sieder, for their contribute in creating the opportunity to join the SRP project and its challenges, and to Dipl. Ing. Giuseppe Fiore, for having shared this (and others) challenges together.

I am also deeply grateful to my parents, my brother, my entire family and all my friends not only for the support provided me in the realization of this paper but in general for having always encouraged me onwards in my life. Above all I want to thank my father, Alfredo Vallini and mother, Melania Spampinato, without which I would simply never be able to get this far.

References

[1] Barrowman, J., Barrowman, J., The theoretical prediction of the center of pressure, National Association of Rocketry Annual Meet 8, 1966. Available at http://www.apogeerockets.com/Education/downloads/barrowman_report.pdf, retrieved 20.10.2014.

[2] Mandell, G., Caporaso, G., Bengen, W., Topics in Advanced Model Rocketry, MIT Press, 1973.

[3] Niskanen, S., The OpenRocket web-site, http://openrocket. sourceforge.net/, retrieved 20.10.2014.

[4] Van Milligan, T., RockSim Model Rocket Design and Simulation Software, http://www.apogeerockets.com/RockSim.asp, retrieved 14.5.2009.

[5] Brandt, M., Diplomarbeit ILR-RSN DA 13-05 Untersuchung zur Flugstabilität einer studentischen Höhenforschungsrakete mit CFD-Analysen, Technische Universitat Dresden, 2013.

[6] Bach, C., Sieder, J., Przybilski, O., Brandt, M., SPD STERN Project Documentation, Technische Universitat Dresden, 2014.

[7] Stine, H., Stine, B., Handbook of Model Rocketry, 7th edition, Wiley, 2004.

[8] Strumia, A., Lezioni di Meccanica Razionale, ED. Equazioni cardinali della dinamica, Available at http://www.albertostrumia.it/libri/didattica/Meccanica/18_capitolo18.pdf, retrieved 25.10.2014.

[9] Barrowman, J., The practical calculation of the aerodynamic characteristics of slender finned vehicles, M.Sc. thesis, The Catholic University of America, 1968.

[10] Newlands, R., A Dynamic Stability Analysis Rocket Simulator, AspireSpace, 2011, Available at http://www.ricknewlands.webspace.virginmedia.com/downloads/technical-papers/A%20dynamic%20stability%20rocket%20simulator.pdf

[11] Rogers, C. E., Cooper, D., Rogers Aeroscience RASAero Aerodynamic Analysis and Flight Simulation Program, Users Manual, Rogers Aeroscience, Available at http://rasaero.com/dloads/RASAero%20Users%20Manual.pdf.

[12] Galejs, R., Wind instability|What Barrowman left out, http://projetosulfos.if.sc.usp.br/artigos/sentinel39-galejs.pdf, retrieved 14.5.2009.

[13] Ersdal, R., An Experimental Study of Hydrodynamic Forces on Cylinders and Cables in Near Axial Flow, Norwegian University of Science and Technology, 2004.

[14] Andrew, B., Wardlaw, Jr., PREDICTION OF NORMAL FORCE, PITCHING MOMENT, AND YAWING FORCE ON BODIES OF REVOLUTION AT ANGLES OF ATTACK UP TO 50 DEGREES USING A CONCENTRATED VORTEX FLOW·FIELD MODEL, NOLTR, 1973.

[15] Jorgensen, L. H., A METHOD FOR ESTIMATING STATIC AERODYNAMIC CHARACTERISTICS FOR SLENDER BODIES OF CIRCULAR AND I NONCIRCULAR CROSS SECTION ALONE AND WITH LIFTING SURFACES AT ANGLES OF ATTACK FROM O° TO 90", NASA TN 0-7228, 1973.

[16] d'Agostino, L., Rocket Propulsion, Liquid Propellant Rockets, Dipartimento di Ingegneria Aerospaziale, Università di Pisa, 2010/2011.

[17] Martin, D. J., Summary of Flutter Experiences as a Guide to the Preliminary Design of Lifting Surfaces on Missiles / NACA National Advisory Committee for Aeronautics. 1958.

[18] Performance Composite Ltd, http://www.performance-composites.com/carbonfibre/mechanicalproperties_2.asp, retrieved 20.03.2015.

[19] Viertotak, M., Poromaa, L., Järnmark, J., Gardefjord, J., Esrange Safety Manual, Swedish Space Corporation, Version 7.

[20] NAR, Launching Safely in the 21st Century, Final Report of the Special Committee on Range Operation and Procedure to the National Association of Rocketry, 2005.

[21] NAR, Division - F39 Space Tech - Rocketry, Available at http://www.nar.org.

[22] WOLFRAM, http://www.wolfram.com/mathematica/?source=nav.

[23] Liu, Y., Zuoand, L., Wang, J., Effects of flexibility on aerodynamic performance of delta wings with different sweep angles, Springer, 2010. Available at http://adsabs.harvard.edu/abs/2010SCPMA..53..915L

[24] ASTOS Solutions, ASTOS Model Library, Version 7.

[25] ASTOS Solutions, User Manual, Version 7.

[26] Cornelisse, J.W., Schoyer, H.F.R., Wakker, K.F., Rocket Propulsion and Spaceflight Dynamics, Pitman, 1979.

8 Appendix

8.1 Parametric Equations

The analytical expressions of the various quantities plotted in section 5.1 are reported below as a function of the fin span S and the non-dimensional fin area k. The stability margin and damping ratio can be obtained by direct substitution of the following in eq. 15 and 22 respectively.

$$c_r = \frac{kA_{fin_0}}{S} + \frac{S}{2}\tan\zeta$$

$$c_t = \frac{kA_{fin_0}}{S} - \frac{S}{2}\tan\zeta$$

$$(C_D)_{fin} = 2\left[\frac{4kA_{fin_0} + D_{ref}\left(2\frac{kA_{fin_0}}{S} + \left(S + \frac{D_{ref}}{2}\right)\tan\zeta\right)}{A_{ref}}\right]\left(1 + 2t\frac{S}{kA_{fin_0}}\right)\left(1.328\sqrt{\frac{\rho}{\mu v}\frac{S}{kA_{fin_0}}}\right)$$

$$C_{na-fin} = \frac{4n\left(\frac{S}{D_{ref}}\right)^2}{1+\sqrt{1+\left(\frac{2l}{c_r+c_t}\right)^2}}\left(1+\frac{D_{ref}}{2S+D_{ref}}\right) = \frac{4n\left(\frac{S}{D_{ref}}\right)^2}{1+\sqrt{1+\left(\frac{S^2}{kA_{fin_0}\cos(\Gamma_c)}\right)^2}}\left(1+\frac{D_{ref}}{2S+D_{ref}}\right)$$

$$C_{p-fin} = L_{tot} - L_{boat} - c_r + \frac{c_r - c_t}{3}\left(\frac{c_r + 2c_t}{c_r + c_t}\right) + \frac{1}{6}\left(c_r + c_t - \frac{c_r c_t}{c_r + c_t}\right) = L_{tot} - L_{boat} - \frac{1}{16}\left(\tan^2\zeta\right)\frac{S^3}{kA_{fin_0}} - \frac{3}{4}\frac{kA_{fin_0}}{S}$$

where n is the number of fins, l the mid-chord length, $\Gamma_c = \arctan\left(\frac{1}{2}\tan\zeta\right)$ is the mid chord sweepback angle.

8.2 Vertical Flight Equations

The general equations of motion for the vertical flight are reported below together with the related solutions. The Caporaso and the Fehskens approaches are shown too. For the descent phase, the use of two chutes has been considered but the procedure can be virtually extended to any number of recovery devices. Positive altitude, velocity and acceleration are considered upwards both for the ascent and descent phase.

Phase	Burning Flight	
Equation	$\frac{dv}{dt} = c_1 - c_2 v^2$	
Constants	$c_1 = \frac{F}{m} - g \; ; \; c_2 = \frac{1}{2}\frac{\rho A_{ref}}{m} C_{D_0}$	
Solution	CAPORASO- BENGEL	FEHSKENS - MALEWICKI
Displacement	$\frac{1}{c_2}\left(\sqrt{1 + c_1 c_2 t^2} - 1\right)$	$\frac{1}{c_2}\ln\left[\cosh\left(t\sqrt{c_1 c_2}\right)\right]$
Velocity	$\frac{c_1 t}{\sqrt{1+c_1 c_2 t^2}}$	$\sqrt{\frac{c_1}{c_2}}\tanh\left(t\sqrt{c_1 c_2}\right)$
Acceleration	$\frac{c_1}{(1+c_1 c_2 t^2)^{\frac{3}{2}}}$	$\frac{c_1}{\cosh^2(t\sqrt{c_1 c_2})}$

Phase	Coasting Flight
Equation	$\frac{dv}{dt} = -c_1 - c_2 v^2$
Constants	$c_1 = g \; ; \; c_2 = \frac{1}{2}\frac{\rho A_{ref}}{m_{Bo}} C_{D_0}$
Displacement	$z_{Bo} + \frac{1}{2c_2}\ln\frac{1+\frac{c_2}{c_1}v_{bo}^2}{1+\tan^2\left[\arctan\left(v_{Bo}\sqrt{\frac{c_2}{c_1}}\right) - (t-t_{Bo})\sqrt{c_1 c_2}\right]}$
Velocity	$\sqrt{\frac{c_1}{c_2}}\tan\left[\arctan\left(v_{Bo}\sqrt{\frac{c_2}{c_1}}\right).(t-t_{Bo})\sqrt{c_1 c_2}\right]$
Acceleration	$-\frac{c_2}{\cos^2\left[\arctan\left(v_{Bo}\sqrt{\frac{c_2}{c_1}}\right).(t-t_{Bo})\sqrt{c_1 c_2}\right]}$

Table 21: Equations of motion for the ascent phase of the vertical flight.

Phase	Drogue Chute Descend
Equation	$\frac{dv}{dt} = -c_1 + c_2 v^2$
Constants	$c_1 = g \; ; \; c_2 = \frac{g}{v^2_{eq-drogue}}$
Displacement	$z_{Culm} - \frac{1}{c_2} \ln \left[\cosh \left((t - t_{culm}) \sqrt{c_1 c_2} \right) \right]$
Velocity	$-\sqrt{\frac{c_1}{c_2}} \tanh \left((t - t_{culm}) \sqrt{c_1 c_2} \right)$
Acceleration	$-\frac{c_1}{\cosh^2((t - t_{Culm})\sqrt{c_1 c_2})}$

Phase	Main Chute Descend
Equation	$\frac{dv}{dt} = -c_1 + c_2 v^2$
Constants	$c_1 = g \; ; \; c_2 = \frac{g}{v^2_{eq-main}}$
Displacement	$z_{500m} + \frac{1}{2c_2} \ln \left[\frac{1 - \left(\frac{V - \exp[2(t - t_{500m})\sqrt{c_1 c_2}]}{V + \exp[2(t - t_{500m})\sqrt{c_1 c_2}]} \right)^2}{1 - \frac{c_2}{c_1} v^2_{500m}} \right]$
Velocity	$\frac{V - \exp[2(t - t_{500m})\sqrt{c_1 c_2}]}{V + \exp[2(t - t_{500m})\sqrt{c_1 c_2}]}$
Acceleration	$-4V \frac{\exp[2(t - t_{500m})\sqrt{c_1 c_2}]}{(V + \exp[2(t - t_{500m})\sqrt{c_1 c_2}])^2}$

Table 22: Equations of motion for the descent phase of the vertical flight.

8.3 ASTOS Simulation

Problem Summary

Cost Function

Type	Name	Value	Scaled	Scaling	Proportion
Terminal	None	0.000	-	-	-
Final	-	-	-	-	100%

Initial Position

Altitude	Longitude	Latitude	Flight-Path Velocity	Flight-Path Azimuth	Flight-Path Angle
0.000 km	21.07° E	67.88° N	0.1 m/s	0.00°	86.00°

Model Description

P	Phase Time & Duration	Vehicle Components[1]	Initial Total Mass	Propulsion Consumption	Jettisoned Mass	Active Propulsion	Total Initial Thrust	Aerodynamic Configuration
1	0.00 s - 1.32 s D_{fix} = 1.318 s	1 x Payload 1 x **Body_Nose_Tail**	0.0258 Mg	0.0003 Mg	0.0000 Mg	1 x Main_Engine	0.500 kN	Aero_Ascent_SixDOF
2	1.32 s - 20.00 s D_{fix} = 18.682 s	1 x Payload 1 x **Body_Nose_Tail**	0.0254 Mg	0.0047 Mg	0.0000 Mg	1 x Main_Engine	0.500 kN	Aero_Ascent_SixDOF
3	20.00 s - 56.57 s D = 36.57 s	1 x Payload 1 x **Body_Nose_Tail**	0.0208 Mg	0.0000 Mg	0.0000 Mg	-	0.000 kN	Aero_Ascent_SixDOF

1) vehicle component **BOLD** = with active tank, *ITALIC* = will be jettisoned

Dynamic System and Constraints

P	Dynamic System	Attitude Control	Boundary Constraints[1,2]	Path Constraints[1]	Parameter Constraints[1]
1	Accelerate_Flightpath_State RANGE DRAG_LOSS GRAVITY_LOSS	EULER_ANGLES_L_FULL Yaw Angle (L): Constant Law Pitch Angle (L): Constant Law Roll Angle (L): Constant Law	**Initial_Fuel_PROP_TANK@Body_Nose_Tail $_i$ = 0.000 kg** Residual_Propellant_PROP_TANK@Body_Nose_Tail >= 0.000 kg	-	**Virtual_Ignition_Time@Main_Engine_Constraint = 0.000 s**
2	Inertial_Vel_Euler_6DOF_State RANGE DRAG_LOSS GRAVITY_LOSS	EULER_ANGLES_L_UNCONTROLLED Uncontrolled Euler Angles	Residual_Propellant_PROP_TANK@Body_Nose_Tail >= 0.000 kg	-	-
3	Inertial_Vel_Euler_6DOF_State RANGE DRAG_LOSS GRAVITY_LOSS	EULER_ANGLES_L_UNCONTROLLED Uncontrolled Euler Angles	**Residual_Propellant_PROP_TANK@Body_Nose_Tail >= 0.000 kg**	-	-

1) **constraint** = enforced, 2) index i = initial boundary constraint

Model Properties

Vehicle Properties

Name	Type	Ass. Propulsion	Properties
Payload	Payload	-	Nominal Mass = 0.20 kg Scaling = 1.00 Total Mass = 0.20 kg
Body_Nose_Tail	Basic_Vehicle_Stage	Main_Engine	Structural Mass = 20.560 kg Propellant Mass = 5.000 kg

Propulsion Properties

Name	Type	Properties
Main_Engine	Profile Rocket_Type	Engine Length = 3.000000 m Ae = 0.00 m^2 Mass flow = 0.25 kg/s Tvac = 500.00 N

Aerodynamic Properties

Name	Type	Properties
Aero_Drogue_SixDOF	Trim_6dof	CD : Interpol.: LINEAR Vars.: MACH CL : Interpol.: LINEAR Vars.: MACH Reference_Diameter = 1.08 m Reference_Area = 0.91 m^2 Q=CONVECTIVE.SUPERSONIC(C=5.00E-1, m=1.0, n=3.00)
Aero_Main_SixDOF	Trim_6dof	CD : Interpol.: LINEAR Vars.: MACH CL : Interpol.: LINEAR Vars.: MACH Reference_Diameter = 1.97 m Reference_Area = 3.03 m^2 Q=CONVECTIVE.SUPERSONIC(C=5.00E-1, m=1.0, n=3.00)
Aero_Ascent_SixDOF	Trim_6dof	CA : Interpol.: LINEAR Vars.: REYNOLDS CN_Alpha : Interpol.: LINEAR Vars.: MACH CY_Beta : Interpol.: LINEAR Vars.: MACH CM_Q : Interpol.: LINEAR Vars.: MACH CLN_R : Interpol.: LINEAR Vars.: MACH Reference_Diameter = 0.12 m Reference_Area = 0.01 m^2 Q=CONVECTIVE.SUPERSONIC(C=5.00E-1, m=1.0, n=3.00)

Environment Properties

Celestial Bodies

Name	Type	Properties
Earth	spherical/sphere	Sidereal Time of Ini. Passage of Asc. Node 280.415 ° UTC at Sidereal Time of Ini. Passage of Asc. Node = 2000-01-01 12:00:00.00 UTC Equatorial Radius = 6371009.000 m Polar Radius = 6371009.000 m Gravity Constant = 3.98600E+14 m^3/s^2

Atmospheres

Name	Type	Properties
Atm_76	US_Standard	-

Winds

Name	Type	Properties
windnord	Standard	-
nowind	Standard	-
windeast	Standard	-